China Geology 8 (2025) 806−842

China Geology

Journal homepage: http://chinageology.cgs.cn
https://www.sciencedirect.com/journal/china-geology

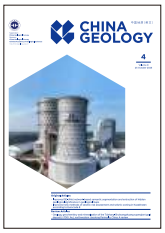

Metallogenic characteristics and mineralization of supergiant gold deposits (223 t) in the northeastern margin of the Jiaolai Basin, Shandong Province: A review

Jun-wei Bo[a, b, c, d], Zheng-jiang Ding[a, c, d,*], Jun Deng[e], Feng-yue Sun[a], Kun-feng Qiu[e], Ming-chun Song[f]

[a] *College of Earth Science Jilin University, Changchun* 130061, *China*
[b] *Shandong Provincial No.* 3 *Exploration Institute of Geology and Mineral Resources, Yantai* 264004, *China*
[c] *Shandong Engineering Research Center of Application and Development of Big Data for Deep Gold Exploration, Ministry of Natural Resources Technology Innovation Center for Deep Gold Resources Exploration and Mining, Shandong Provincial No.* 6 *Exploration Institute of Geology and Mineral Resources, Weihai* 264209, *China*
[d] *State Key Laboratory of Geological Processes and Mineral Resources, China University of Geosciences, Wuhan* 430074, *China*
[e] *China University of Geosciences (Beijing), Beijing* 100083, *China*
[f] *Hebei GEO University, Shijiazhuang* 050031, *China*

ARTICLE INFO

Article history:
Received 25 November 2023
Received in revised form 16 April 2024
Accepted 19 April 2024
Available online 30 August 2024

Keywords:
Supergiant gold deposit
Pyrite-bearing carbonate vein-type
Altered rock type
CO_2-NaCl-H_2O fluid system
C-H-O, S, and Pbisotopes
Mantle fluids
Metallogenic characteristics
Mineralization
Mineral exploration engineering
Jiaolai Basin
Shandong Province

ABSTRACT

Since the first discovery of gold deposits on the northeastern margin of the Jiaolai Basin in Shandong Province at the end of the 20th century, seven medium-sized to large/super-large gold deposits have been identified in this region, with cumulative proven gold resources of 223 t. This study reviewed the metallogenic and geochemical characteristics of various gold deposits in this region, examined the sources of their ore-forming fluids and materials, as well as their gold metallogenic epochs and processes, and developed a gold metallogenic model. The gold deposits in this region are governed by both dense fractures and detachment structural systems along basin margins, primarily categorized into the altered rock type and the pyrite-bearing carbonate vein type. The latter type, a recently discovered mineralization type in the Jiaodong Peninsula, enjoys high gold grade, a large scale, and high gold mineral fineness, suggesting considerable prospecting potential. Both types of gold deposits show metallogenic epochs ranging from 116 Ma to 119 Ma. Their ore-forming fluids are identified as a CO_2-NaCl-H_2O fluid system characterized by moderate to low temperatures, moderate to low salinity, and low density, with the pyrite-bearing carbonate vein-type gold deposits manifesting slightly higher salinity. The C-H-O, S, and Pb isotopes of hydrothermal minerals reveal that the ore-forming fluids and materials are characteristic of crust-mantle mixing. Specifically, they were derived from mantle fluids in the early stages, mixed with stratum water and meteoric water in the later stages for mineralization. The gold metallogenic process is identified as follows: During the Early Cretaceous, the subduction of the Pacific Plate and the destruction of the North China Craton led to asthenospheric upwelling. The resulting fluids, after metasomatizing the enriched mantle, differentiated and evolved into C-H-O ore-bearing fluids, which were then mixed with crustal fluids. The mixed fluids migrated to the shallow crust, where they mingled with stratum water and meteoric water. Then, the fluids underwent unloading and final mineralization in detachment fault tectonic systems on basin margins. Due to differences in mixed crustal materials or the surrounding rocks involved in water-rock interactions, altered rock- and pyrite-bearing carbonate vein-type gold deposits were formed in acidic and alkaline fluid environments, respectively.

1. Introduction

The Jiaodong Peninsula, a celebrated gold metallogenic province in China, hosts gold deposits primarily in gold metallogenic regions (belts) of Jiaoxibei, Qixia-Penglai-Fushan, Muping-Rushan, and the northeastern margin of the Jiaolai Basin, with proven gold reserves of above 5000 t (Song MC et al., 2021). The northeastern margin of the Jiaolai Basin, a gold metallogenic region newly discovered since the 1990s, is the home of seven medium-sized to large/super-large gold deposits, i.e., the Pengjiakuang, Songjiagou, Guocheng (including Longkou, Dongliujia, Tudui, Shawang,

First author: *E-mail address*: bojunwei@126.com (Jun-wei Bo).
* Corresponding author: *E-mail address*: ytdzhj@126.com (Zheng-jiang Ding).

Literary editor: Li-qiong Jia
doi:10.31035/cg2023122
2096-5192/© 2025 China Geology Editorial Office.

and Houkuang; Table 1), Xijingkou, Liaoshang, Xilaokou (including the No. 18 Xilaokou vein; Table 1), and Qianchuiliu deposits, and four gold ore occurrences, i.e., Nandikou, Nanguozi, Daligou, and Mashidian. This gold metallogenic region has achieved cumulative proven gold resources of over 223 t (Table 2), comprising over 82 t and 141 t from altered rock- and pyrite-bearing carbonate vein-type gold deposits, respectively. This region has experienced two stages of gold exploration: (1) Shallow gold exploration prior to 2010, primarily discovering altered rock-type gold deposits; and (2) deep prospecting post-2010, principally revealing pyrite-bearing carbonate vein-type gold deposits. From 1989 to 1997, the 3rd Exploration Institute of Geology and Mineral Resources of Shandong Province (also referred to as the Institute) discovered the first large altered rock-type gold deposit at Pengjiakuang in this region, instigating gold exploration in this region and substantiating the considerable potential for the prospecting of large gold deposits on the northeastern margin of the Jiaolai Basin. In 2002, the Institute discovered the first large altered conglomerate-type gold deposit at Songjiagou, further enriching gold mineralization types in the Jiaolai Basin. From 2010 to 2014, this region witnessed a breakthrough in deep prospecting as the Institute discovered a new type of super-large (69 t) gold deposit in eastern Jiaodong for the first time —the Liaoshang pyrite-bearing carbonate vein-type gold deposit. Subsequently, the

Table 1. Major gold deposits on the northeastern margin of the Jiaolai Basin.

Type		Name	Comments
Altered rock type	Altered conglomerate type	Deposit: Songjiagou Ore occurrence: Daligou	(1) The Songjiagou gold deposit is also referred to as the Fayunkuang gold deposit. (2) The Longkou, Dongliujia, Tudui, Shawang, and Houkuang gold deposits, distributed in areas with the same exploration right, are collectively referred to as the Guocheng or Tudui-Shawang gold deposit. (3) The Pengjiakuang gold deposit, a deposit of the altered breccia type primarily, is categorized as an independent type of deposit—the Pengjiakuang altered breccia-type gold deposit. (4) The Xilaokou mining area contains two gold mineralization types: The pyrite-bearing carbonate vein type and the altered rock type. In this study, the pyrite-bearing carbonate vein-type gold deposit is referred to as the Xilaokou gold deposit, and the altered rock-type gold deposit is referred to as the No. 18 Xilaokou vein.
	Fracture-zone altered rock type	Deposit: Pengjiakuang, Xijingkou, the No. 18 Xilaokou vein, Longkou, Dongliujia, Tudui, and Shawang Ore occurrence: Nanguozi, and Nandikou	
Pyrite-bearing carbonate vein type		Deposit: Liaoshang, Xilaokou, Qianchuiliu, and Houkuang Ore occurrence: Mashidian	

Table 2. Mineral resources of gold deposits/ore occurrences on the northeastern margin of the Jiaolai Basin.

Gold deposit	Mineral resource/t	Mineral resource type	Ore type	Comments
Songjiagou	21.8	Indicated + inferred	Altered conglomerate type	Gold resources exceed 50 t based on the cut-off grade (0.5 g /t) of open-pit mining.
Daligou	0.9	Indicated + inferred	Altered conglomerate type	Ore occurrence
Pengjiakuang	22.6	Indicated + inferred	Fracture-zone altered rock type	
Xijingkou	11.0	Indicated + inferred	Fracture-zone altered rock type	
No. 18 Xilaokou vein	8.6	Indicated + inferred	Fracture-zone altered rock type	
Longkou	3.0	Indicated + inferred	Fracture-zone altered rock type	
Dongliujia	1.7	Indicated + inferred	Fracture-zone altered rock type	
Tudui	6.5	Indicated + inferred	Fracture-zone altered rock type	
Shawang	6.1	Indicated + inferred	Fracture-zone altered rock type	
Nanguozi	To be estimated	−	Fracture-zone altered rock type	Ore occurrence
Nandikou	To be estimated	−	Fracture-zone altered rock type	Ore occurrence
Liaoshang	77.0	Measured + indicated + inferred	Pyrite-bearing carbonate vein type	Shallow + deep
Xilaokou	46.0	Indicated + inferred	Pyrite-bearing carbonate vein type	
Qianchuiliu	13.5	Inferred	Pyrite-bearing carbonate vein type	Duan LA et al., 2021; Preliminary estimates have reached 27.5 t (China Geological Survey's top 10 geological surveys in 2023)
Houkuang	4.3	Indicated + inferred	Pyrite-bearing carbonate vein type	
Mashidian	To be estimated	−	Pyrite-bearing carbonate vein type	Ore occurrence

Note: The gold resources include the estimated resources of low-grade ores. Values are corrected to one decimal place using the rounding-off method.

Xilaokou large and Qianchuiliu medium-sized pyrite-bearing carbonate vein-type gold deposits were discovered successively at the periphery of Liaoshang (Duan LA et al., 2021).

Since the discovery of the Pengjiakuang gold deposit, the northeastern margin of the Jiaolai Basin has garnered considerable attention from geologists. Specifically, extensive studies have been conducted on the geological characteristics of deposits (Qi JJ et al., 2009; Wang ZJ et al., 2009; Zou WL et al., 2010; Li HM et al., 2010; Yang CF, 2010; Liu JF et al., 2011; Zhang ZC et al., 2012; Yang LQ et al., 2014; Ji P et al., 2016), the sources of ore-forming fluids and materials (Zhao YL et al., 2000; Yang JZ et al., 2001; Li MQ et al., 2001; Liu XH et al., 2002; Zeng QD et al., 2002; Mao JW et al., 2005; Liu JY et al., 2012; Wang DR et al., 2015; Wang M et al., 2016), the characteristics of ore-controlling structures (Liu YW et al., 2002; Gao YJ et al., 2006; Men YK et al., 2013), metallogenic regularity and prospecting direction (Liu YQ et al., 2000; Liu JY et al., 2006; Zhang HQ et al., 2006; Duan LA et al., 2009; Zhang PJ et al., 2015; Li GH et al., 2016), and diagenetic and metallogenic epochs (Zhang LC et al., 2002a; Shen YC et al., 2002; Hou ML et al., 2006; Li J et al., 2012). These studies, together with those on pyrite-bearing carbonate vein-type gold deposits (Ji P et al., 2016; Li GH et al., 2016, 2017; Wang ZX et al., 2017; Bo JW et al., 2021), contribute substantially to the promotion of gold mineralization theories and the breakthroughs in ore prospecting in this region. Gold deposits occur from both the margins and interior of the basin within the metallogenic region. However, since previous research merely focused on isolated gold deposits, there is a lack of exploration of the internal and spatial relationships of gold mineralization. Most especially, the metallogenic model previously proposed failed to account for the metallogenic processes of pyrite-bearing carbonate vein-type gold deposits, newly discovered in deep strata, leading to a biased understanding of their origin and prospecting modes. This puts certain constraints on the exploration of deep gold deposits. It is necessary to further investigate the complexity and diversity of gold mineralization in this region. This study reviewed the prospecting achievements, characteristics, and geochemical characteristics of gold deposits on the northeastern margin of the Jiaolai Basin, investigated the sources of ore-forming fluids and materials, metallogenic epochs, and metallogenic tectonic setting, and established a new metallogenic model. This study holds great significance for deeply understanding the Mesozoic gold metallogenic characteristics and their formation mechanisms on basin margins and can serve as a guide for gold exploration.

2. Regional geological setting

The Jiaodong Peninsula, hosting the gold metallogenic region on the northeastern margin of the Jiaolai Basin, is situated at the junction of the Paleo-Asian and circum-Pacific metallogenic domains. During the Mesozoic, the collision between the Yangtze and the North China plates and the subduction of the Pacific Plate led to the Cretaceous lithosphere thinning and the upwelling of asthenospheric materials. They were accompanied by strong crust-mantle interactions and frequent tectono-magmatic activity, leading to explosive Cretaceous gold mineralization in the Jiaodong Peninsula (Song MC et al., 2013; Deng J et al., 2015a, 2018). The Jiaodong Peninsula, primarily comprising the Precambrian metamorphic basement, Mesozoic intrusions, and Meso-Cenozoic volcanic sedimentary rocks, can be divided into two parts by the Muping-Jimo fault zone: The Jiaobei terrane in the west and the Sulu terrane in the east (Fig. 1a; Yang LQ et al., 2014).

2.1. Basement metamorphic rocks

The Jiaobei terrane is located on the southern margin of the North China plate. Its Precambrian metamorphic basement comprises Meso- to Neoarchean and Meso- to Neoproterozoic metamorphic rocks (Fig. 1b). The former consists primarily of a tonalite-trondhjemite-granodiorite (TTG) gneiss suites that have undergone amphibolite facies metamorphism, with a scant presence of magnetite quartzites, biotite leptynites, and amphibolite enclaves of the Tangjiazhuang and Jiaodong groups subjected to leptynite-amphibolite facies metamorphism occurring in the TTG gneiss suites. The Paleoproterozoic Jingshan and Fanzishan groups are a set of khondalite-like series composed of high-alumina schists, leptynites, diopsides, marbles, and graphite-bearing rocks (Wang SJ et al., 2009). Their protoliths are dominated by feldspathic quartz siltstones and clay-rich feldspathic quartz graywackes, mingled with claystones, marlstones, and carbonate rocks, formed in a neritic environment at approximately 2100 Ma (Liu PH et al., 2011a). The Jingshan Group experienced high-pressure granulite facies metamorphism from 1900 Ma to 1850 Ma (Wan YS et al., 2006; Zhou XW et al., 2008; Tam PY et al., 2011; Liu PH et al., 2011a, 2011b, 2011c; Liu JH et al., 2011) and amphibolite facies retrogressive metamorphism from 1840 Ma to 1820 Ma (Liu PH et al., 2011b, 2011c). In contrast, the Fenzishan Group experienced high greenschist facies-low amphibolite facies metamorphism. The Mesoproterozoic Zhifu Group consists of quartzites and K-feldspar quartzites interbedded with magnetite layers. Its protoliths are a set of terrigenous clastics interbedded with carbonate sedimentary suites, subjected to low amphibolite facies metamorphism. Its feldspar quartzites exhibit detrital zircon U-Pb isotope ages of 1664 ± 34 Ma (Wang HC et al., 2022). The Neoproterozoic Penglai Group principally encompasses phyllites, slates, quartzites, crystalline limestones, and marbles. Its protoliths are aluminum- and calcium-rich argillaceous-carbonate sedimentary rocks (Deng YH et al., 1984; Zhu G et al., 1994; Li XH et al., 2007; Chu H et al., 2011). The Sulu terrane on the northeastern margin of the Sulu orogenic belt is composed primarily of Neoproterozoic granitic gneisses, with diagenetic epochs ranging from 780–700 Ma and ultrahigh-pressure

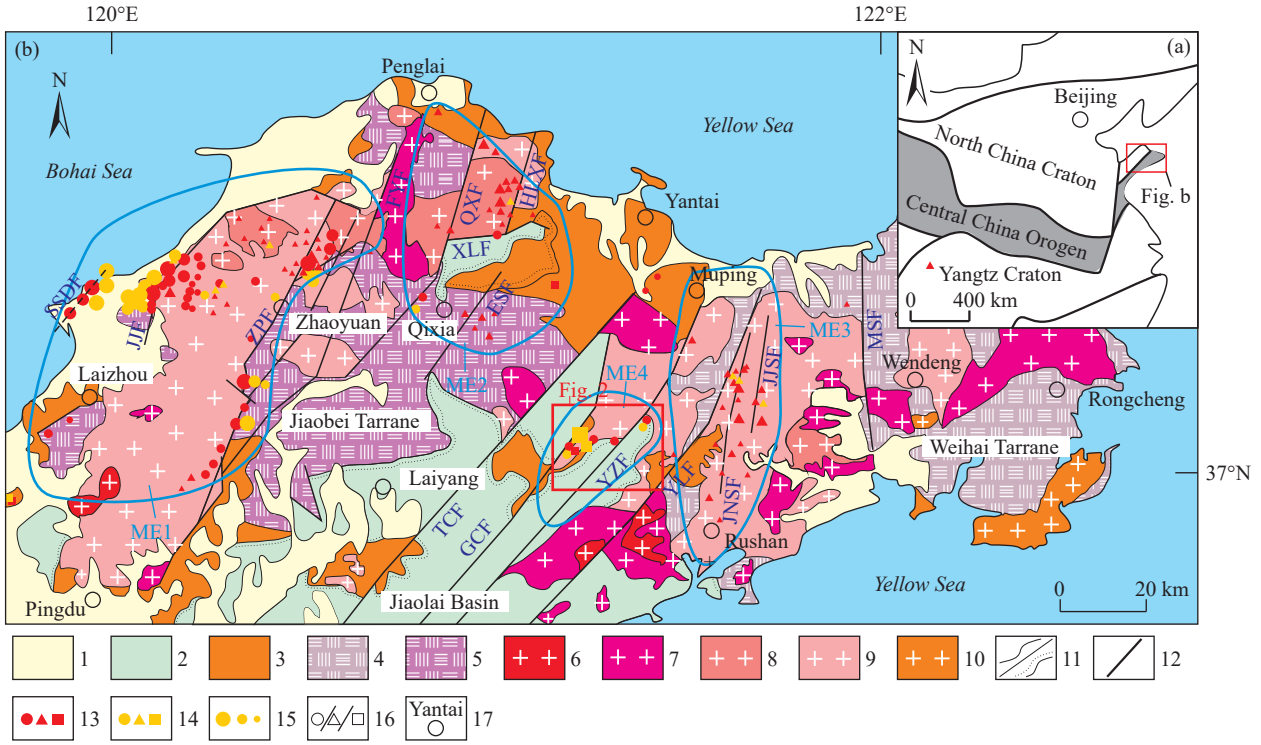

Fig. 1. Regional geological sketch map and gold deposit distribution of the Jiaodong Peninsula (after Song MC et al., 2021). 1–Quaternary; 2–Cretaceous; 3–Paleoproterozoic and Neoproterozoic; 4–Neoproterozoic eclogite granitic gneiss; 5–Archean granite-greenstone belt; 6–Cretaceous Laoshan-type granite; 7–Cretaceous Weideshanian granite; 8–Cretaceous Guojialingian granite; 9–Jurassic granitoid; 10–Triassic granitoid; 11–geological conformity/unconformity; 12–fault; 13–shallow gold deposit; 14–deep gold deposit; 15–super-large and large/medium-sized/small; 16–altered rock-type/quartz vein-type/pyrite carbonate vein-type gold deposit; 17–place name; ME1–Jiaoxibei gold metallogenetic sub-region; ME2–Qixia-Penglai-Fushan gold metallogenetic region; ME3–Muping-Rushan gold metallogenetic sub-region; ME4–Gold metallogenetic sub-region on the northeastern margin of the Jiaolai Basin; SSDF–Sanshandao fault; JJF–Jiaojia fault; ZPF–Zhaoping fault; FYF–Fengyi fault; QXF–Qixia fault; XLF–Xilin fault; HLXF–Huluxian fault; ESF–E'shan fault; TCF–Taocun fault; GCF–Guocheng fault; YZF–Yazi fault; YLF–Yuli fault; JNSF–Jinniushan fault; JJSF–Jiangjunshi fault; MSF–Mishan fault.

metamorphic ages between 240 Ma and 220 Ma (Tang J et al., 2004; Xu ZQ et al., 2006; Wang HC et al., 2022). Besides, it hosts some Paleoproterozoic Jingshan Group metamorphic strata, Mesoproterozoic mafic-ultramafic intrusions (meta-pyroxene peridotites), and Triassic ultrahigh-pressure metamorphic rocks (eclogites).

2.2. Mesozoic intrusions

The Mesozoic intrusions, widespread in the Jiaodong Peninsula, consist primarily of the Triassic, Late Jurassic, and Early Cretaceous intrusions (Fig. 1b). The Triassic intrusions in the Sulu terrane primarily encompass the Ningjinsuo pluton comprising porphyritic pyroxene syenites, hornblende syenites, and quartz syenites and the Chashan pluton consisting of fine-, medium-, and coarse-grained syenogranites, with diagenetic epochs concentrated between 225 Ma and 205 Ma (Chen JF et al., 2003; Guo JH et al., 2005; Yang JH et al., 2005; Chen JZ et al., 2011; Wang LM et al., 2021). The Late Jurassic intrusions, the most extensively distributed in Jiaodong, serve as the major ore-hosting surrounding rocks of gold deposits, with the Jiaobei and Sulu terranes represented by the Linglong and Kunyushan plutons, respectively. They are predominantly composed of fine-, medium-, and coarse-grained monzogranites, which generally contain garnets and are S-type granites formed by crustal remelting, with diagenetic epochs ranging from 160–140 Ma (Guo JH et al., 2005; Zhang T et al., 2007; Wang SJ et al., 2009; Wang B et al., 2021; Wang LM et al., 2021). The Early Cretaceous Guojialingian granites in the Jiaobei terrane are composed of medium-grained monzodiorites, porphyritic quartz monzonites, porphyritic granodiorites, and porphyritic monzogranites. They are intrusions formed by crust-derived anatectic magmas mixed with some mantle-derived magmas, with diagenetic epochs ranging from 135 Ma to 125 Ma (Chen GJ et al., 2014; Liu Y et al., 2014; Luo XD et al., 2014; Geng K et al., 2016; Shen YK et al., 2016; Li HK et al., 2017; Wang LM et al., 2021). These granites correlate closely with gold mineralization in time and space. The Early Cretaceous Weideshanian granites, distributed in both Jiaobei and Sulu terranes, are composed of fine-grained hornblende diorites, medium-grained monzodiorites, porphyritic quartz monzonites, and porphyritic monzogranites. They are granites with crust-mantle mixing sources, with diagenetic epochs ranging from 125 Ma to 110 Ma (Guo JH et al., 2005; Ding ZJ et al., 2013; Geng K et al., 2020; Ren TL et al., 2021; Wang LM et al., 2021), aligning with partial gold mineralization in the Jiaodong Peninsula. The Early Cretaceous Laoshanian granites are primarily distributed in the Sulu terrane, with a minor presence in the Jiaobei terrane.

They comprise miarolitic monzogranites, syenogranites, and alkali feldspar granites, standing out as A-type granites, with diagenetic epochs ranging from 118 Ma to 108 Ma (Zhang T et al., 2007; Wang SJ et al., 2010; Wang LM et al., 2021).

2.3. Meso-Cenozoic continental volcanic sedimentary rocks

The Meso-Cenozoic continental volcanic sedimentary rocks, distributed within the Jiaolai, Zangjiazhuang, and Lidao basins (Fig. 1b), consist primarily of the Mesozoic Cretaceous Laiyang, Qingshan, and Wangshi groups and the Cenozoic Linqu Group. The Laiyang Group comprises conglomerates, conglomeratic gritstones, gritstones, fine sandstones, and lentoid argillaceous siltstones, with sedimentary epochs ranging from 135 Ma to 123 Ma as inferred from the U-Pb ages of detrital zircon and the zircon of intrusions that cut through strata (Zhang YQ et al., 2007, 2008; Xie SW et al., 2012; Huo TF et al., 2015; Zhou JB et al., 2016). The Qingshan Group is a set of continental volcanic rocks composed of acidic - intermediate-mafic - acidic - slightly alkaline volcanic and pyroclastic rocks, with mafic magma eruptions occurring at roughly 122–113 Ma and acidic magma eruptions at 110–98 Ma (Ling WL et al., 2006; Kuang YS et al., 2012; Zhou JB et al., 2016; Kong XC et al., 2022). The Wangshi Group is composed of variegated clastics and a minor quantity of marls interbedded with mafic volcanic rocks, with a sedimentary epoch at about 90 Ma as inferred from the U-Pb ages of detrital zircon and the Ar-Ar dating results of basalt interlayers (Yan J et al., 2005; Meng FC et al., 2006; An W et al., 2016; Zhou YQ et al., 2018; Yang Y et al., 2021; Zhang LX et al., 2021). The Linqu Group in the Jiaobei terrane comprises a suite of extrusive facies olivine basalt - olivine nephelinite - nepheline picrite basalt assemblages.

2.4. Structures

The Jiaodong Peninsula has experienced multistage tectonic activity, resulting in the formation of a network of crisscrossed structures. Its basement structure appears as a nearly-EW-directed structural line composed of the schistosity, gneissosity, ductile deformation zone, and fold axis of the Precambrian metamorphic rocks. Since the Mesozoic, a fault structure system dominated by NE-NNE-trending faults has been superimposed on the basement structure (Fig. 1b), governing both the spatial locations of regional magmatic rocks and the distributions of gold and polymetallic deposits in the Jiaodong Peninsula (Ding ZJ et al., 2015). From west to east, dominant faults in Jiaodong include the Sanshandao, Jiaojia, Zhaoping, Qixia, Muping-Jimo, Jinniushan, and Mishan. The former four faults, situated in western Jiaodong, are generally NE-trending, whereas the latter two, located in eastern Jiaodong, generally have a nearly SN strike. The Muping-Jimo fault is generally NE-trending, serving as a dividing line between eastern and western Jiaodong. Different gold mineralization types occur in faults with different mechanical properties, resulting in the formation of a series of gold mineralization types that align with the structural characteristics. The uplift zone of Jiaodong hosts fracture-zone altered rock- and quartz vein-type gold deposits. The former is governed by regional transpressive faults with gentle dip angles, such as Sanshandao, Jiaojia, and Zhaoping. The wide tectonic fracture zones of these faults provide pathways for fluid activity and also serve as the destination for the accumulation and precipitation of ore-forming materials, with mineralization dominated by metasomatism. By contrast, the quartz vein-type gold deposits are influenced d by steeply dipping tensional faults such as Jinniushan, with mineralization dominated by filling. The extensional space inside these faults is filled with sulfide-bearing quartz veins. Detachment fault systems are found on basin margins, with gold deposits occurring within the dominant detachment fault zones and the secondary tectonic zones in their hanging walls.

2.5. Geological setting of the northeastern margin of the Jiaolai Basin

The metallogenic region on the northeastern margin of the Jiaolai Basin, situated in central Jiaodong, spans across the Jiaobei and Sulu terranes, with the Yetou and Douya formations of the Jingshan Group in this region (Fig. 2) acting as partial ore-hosting surrounding rocks. The Yetou Formation consists of a leptynite section as its lower part and a marble section as its upper part. The lower leptynite section is composed of biotite-plagioclase gneisses, tremolite leptynites, and amphibolites interbedded with marbles. In contrast, the upper marble section comprises calcite marbles, dolomitic marbles, and ophicalcites interbedded with diopsides. The Douya Formation is dominated by graphite-bearing rocks, consisting of graphite-biotite-plagioclase gneisses, biotite leptynites interbedded with graphite marbles, and diopsides, hosting crystalline graphite-bearing ores. The Laiyang Group primarily comprises the Linsishan Formation conglomerates and the Zhifengzhuang Formation sandstones. The Linsishan Formation has a NE strike, a dip direction of SE, and dip angles ranging from 20° to 50°, serving as the primary ore-hosting surrounding rocks of the altered conglomerate-type gold deposits. The volcanic rocks of the Qingshan Group are principally composed of the Bamudi and the Shiqianzhuang formations. The Bamudi Formation is a set of intermediate-mafic pyroclastic rock pyroclastic rocks interbedded with intermediate-mafic lavas, whereas the Shiqianzhuang Formation is a set of intermediate-acidic to acidic pyroclastic rocks and lavas (Ding ZJ et al., 2015). The intrusions in this region are dominated by the Late Jurassic Linglongian garnet-bearing weakly gneissic monzogranites (the Queshan pluton, 152–160 Ma; Sun FY et al., 1995; Ding ZJ et al., 2015), serving as primary ore-hosting surrounding rocks. Additionally, the Cretaceous monzonite porphyry - diorite porphyrite - lamprophyre vein swarm (114–116 Ma; Tan J, 2009) is found in this region. Moreover, this region hosts well-developed fault structures, including NE-trending regional transcrustal faults Guocheng and Yazi, which govern

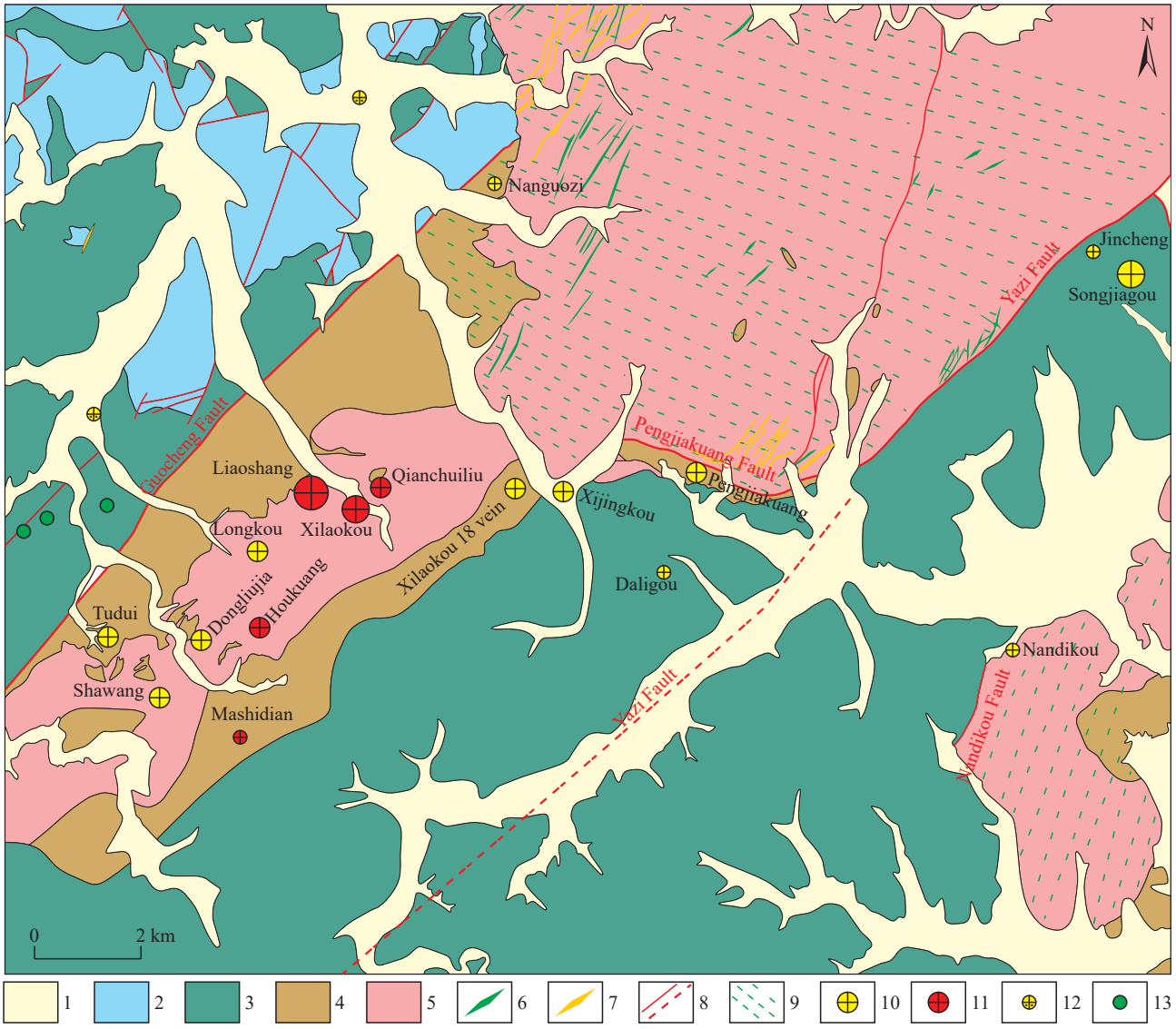

Fig. 2. Geological sketch map showing the metallogenic region on the northeastern margin of the Jiaolai Basin (after Bo JW et al., 2021). 1–Quaternary; 2–Cretaceous Qingshan Group; 3–Cretaceous Laiyang Group; 4–Paleoproterozoic Jingshan Group; 5–late Jurassic Linglong-type granite; 6–Mesozoic mafic vein; 7–Mesozoic acidic vein; 8–fault; 9–ductile shear zone; 10–altered rock-type gold deposit (ore occurrence); 11–pyrite-bearing carbonate vein-type gold deposit (ore occurrence); 12–gold placer; 13–copper nodule.

the formation and evolution of the Jiaolai Basin as boundary faults.

3. Geological characteristics of gold deposits

The gold deposits on the northeastern margin of the Jiaolai Basin can be divided into the altered rock type (including the altered conglomerate type and the fracture-zone altered rock type) and the pyrite-bearing carbonate vein type (Table 1). Focusing on the Songjiagou, Pengjiakuang, and Liaoshang deposits, this study elaborated on the geological characteristics of various types of typical gold deposits in this region.

3.1. Altered conglomerate-type gold deposits (Songjiagou-type)

The Songjiagou gold deposit is the only gold deposit with the potential for commercial exploitation in the sedimentary strata of the Jiaolai Basin. Its orebodies are found in the terrigenous clastic sedimentary rocks of the Cretaceous Laiyang Group's Linsishan Formation, composed of grayish-white conglomerates. Its strata have strikes ranging from 20° to 70° NE, dip direction from 110° to 160°, and dip angles from 20°–40°. Its orebodies are governed by dense fracture zones (F4, F5; Fig. 3a), exhibiting strikes ranging from 45° to 80° NE, a dip direction of SE, and dip angles from 45° to 80°. The dip angles of the fractures are steep generally and gentle locally, less than 30° (Fig. 3b). The dense fracture zones have a length of about 1200 m and a width of about 400 m, with single-fracture widths varying only between 1 cm and 10 cm and fractured rocks within and on both sides of fractures. Additionally, beresitization, phyllic alteration, and kaolinization are developed in the dense fracture zones.

A total of 35 gold orebodies have been delineated in the Songjiagou gold deposit, consisting of 21 in the southern ore

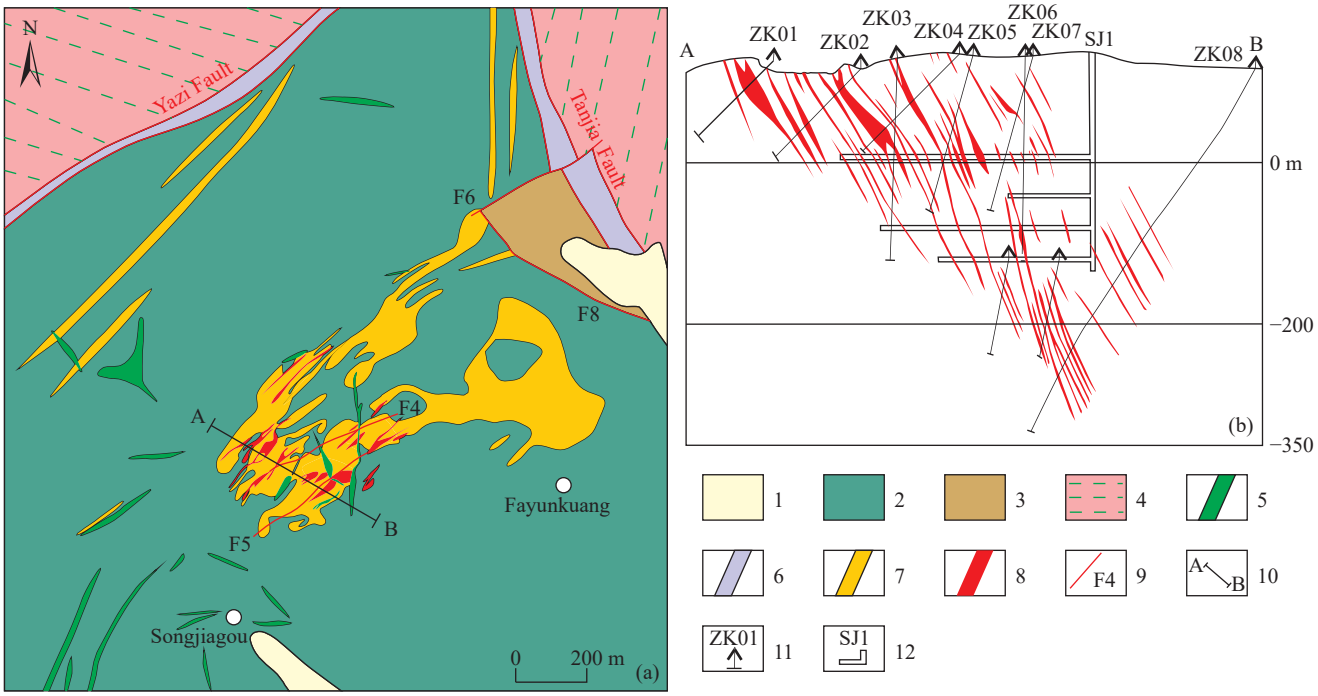

Fig. 3. Geological sketch map (a) and exploration line profile (b) of the Songjiagou gold deposit (after Chen Y, 2014). 1–Quaternary; 2–Laiyang Group conglomerate; 3–Jingshan Group graphite plagioclase gneiss with biotite metamorphic rock; 4–Late Jurassic weakly gneissic fine- to medium-grained pomegranate monzogranite; 5–mafic-ultramafic vein (e.g., diorite porphyrite, diabase porphyrite, and lamprophyre); 6–tectonic breccia zone; 7–conglomerate with beresitization; 8–gold orebody; 9–fault and its number; 10–profile location; 11–borehole and its number; 12–exploration and mining engineering using shafts, along veins, and through vein, etc.

block and 14 in the northern ore block. These orebodies show complex morphologies, distributed as irregular veins and lenses (Fig. 4). The orebodies in the southern ore block are subject to open-pit and underground mining, with lengths of individual orebodies ranging from 30 m to 540 m, maximum depths along their dip directions from 25 m to 240 m, and occurrence elevations from +145 m to −402 m. These orebodies have burial depths ranging from 0 m to 535 m, strikes from 35° to 50° NE, a dip direction of SE, dip angles from 35°–87°, and thicknesses between 0.90 m and 8.81 m (average: 6.01 m). Additionally, they manifest ore grades ranging from 0.62 g/t to 6.03 g/t, with an average of 1.18 g/t. In contrast, the orebodies in the northern ore block are subject to underground mining, with lengths of individual orebodies ranging from 60 m to 330 m, maximum depths along their dip directions from 25 m to 240 m, and occurrence elevations from +102 m to −195 m. These orebodies present burial depths ranging from 0 m to 283 m, strikes from 35° to 50° NE, a dip direction of SE, dip angles from 30° to 71°, and thicknesses from 0.92 m to 8.00 m (average: 3.72 m). Additionally, they manifest ore grades ranging from 1.03 g/t to 5.39 g/t, with an average of 2.40 g/t.

Conglomerates with beresitization emerge as the primary ores in the Songjiagou gold deposit (Fig. 5c), with pyrite content ranging from 2% to 15% and distributed within the matrix and on conglomerate edges as lumpy, disseminated, and irregular veins. They show relatively simple mineral compositions. Specifically, the gangue minerals consist primarily of feldspar and quartz, with minor amounts of K-feldspar, muscovite, clay, and carbonate minerals. Most of them have been recrystallized into sericite and calcite. The ore minerals primarily comprise electrum, native gold, and pyrite, with a minor presence of chalcopyrite, sphalerite, galena, magnetite, and limonite. The gold minerals are dominated by native gold and electrum. Native gold is golden yellow and xenomorphic granular, with sizes ranging from 0.05 mm to 0.1 mm generally, from 0.1 mm to 0.15 mm partially, and from 0.02 mm to 0.05 mm in a trace amount. The gold minerals occur as interstitial, inclusion, and fissure gold (Figs. 5d–e), with interstitial gold primarily occurring within the interstices of pyrite and gangue minerals, inclusion gold principally within pyrite, and fissure gold within pyrite fissures. The gold minerals display fineness ranging from 723‰ to 768‰, with an average of 745‰.

The ore textures are dominated by the idiomorphic-hypidiomorphic-xenomorphic granular textures (e.g., pyrite, chalcopyrite, galena, and sphalerite), cataclastic textures (e.g., pyrite undergoing fracturing or crushing), and interstitial textures (chalcopyrite, sphalerite, quartz, and calcite exhibiting interstitial distributions in pyrite fissures), succeeded by metasomatic and poikilitic textures. The ore structures commonly include lumpy structures (mineral aggregates such as pyrite occurring as uneven lumps), veined structures (pyrite veinlets forming stockwork and veinlet structures after experiencing filling along fissures), disseminated structures (pyrite manifesting an uneven dotted distribution within breccias and their cements), and brecciated structures (brecciated fractured protoliths being filled and cemented by later minerals like pyrite, forming brecciated structures).

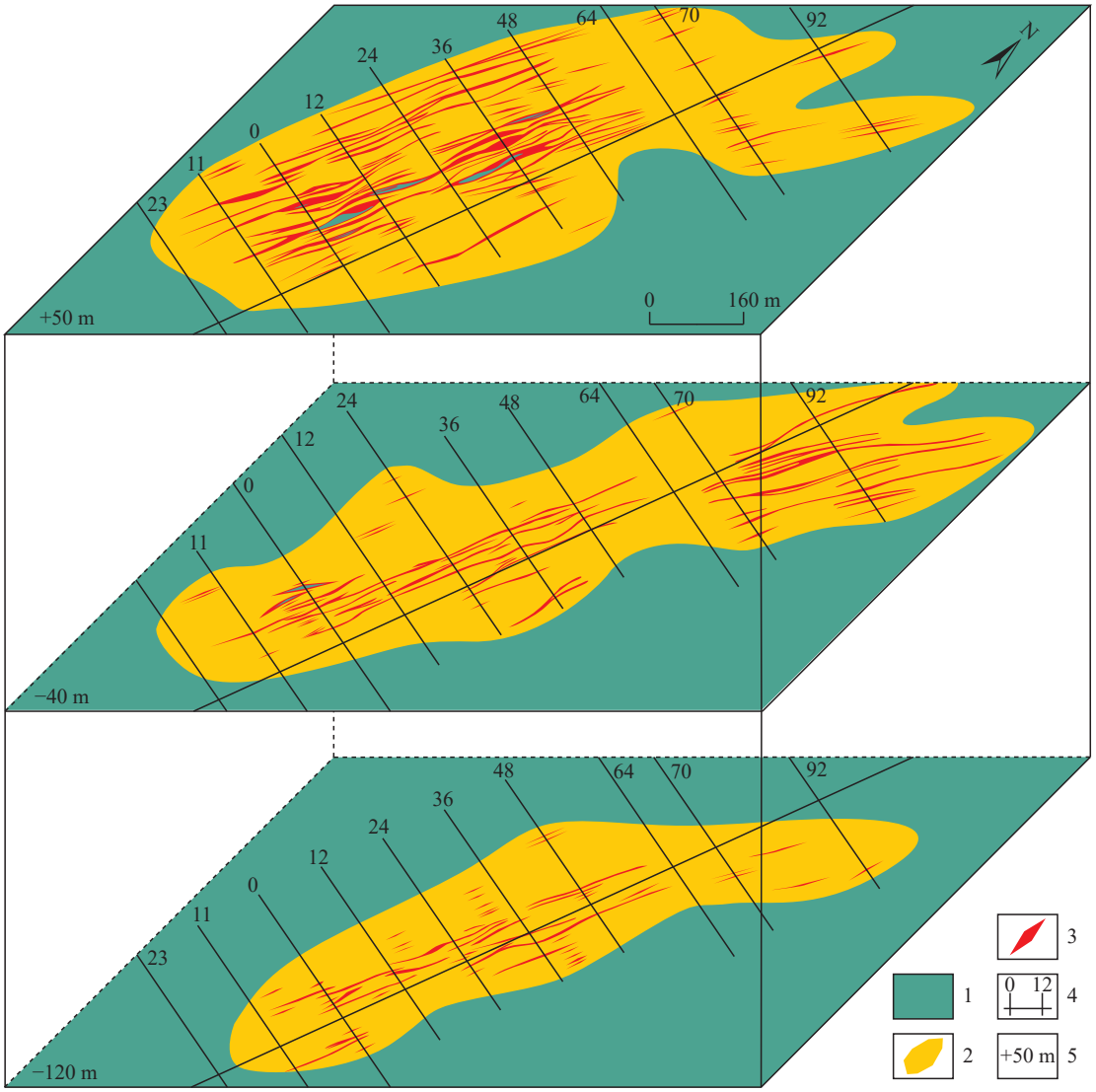

Fig. 4. Schematic maps showing the middle section of orebodies in the Songjiagou gold deposit (after Chen Y, 2014). 1–Laiyang Group conglomerate; 2–conglomerate with beresitization; 3–gold orebody; 4–exploration line and its number; 5–elevation.

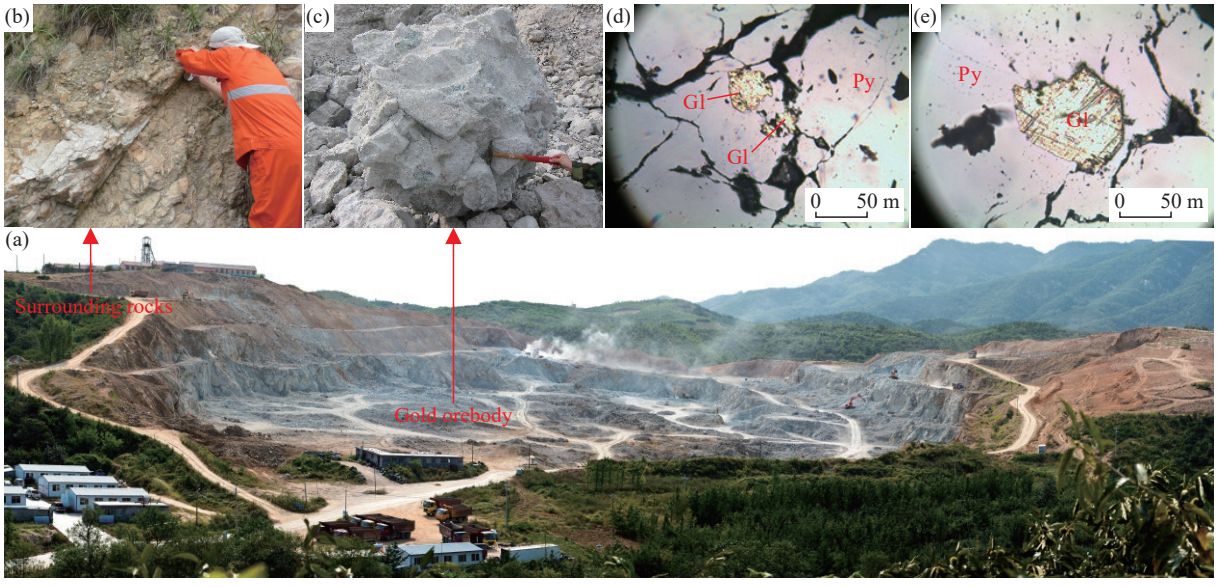

Fig. 5. Characteristics of ores in the Songjiagou gold deposit. a–Panorama of open-pit mining; b–hoary conglomerates (ore-bearing surrounding rocks); c–ores of the conglomerate type with beresitization; d–e–inclusion gold in pyrite. Gl–Native gold; Py–Pyrite.

The alterations of surrounding rocks in the Songjiagou gold deposit primarily include beresitization, silicification, potassic alteration, and carbonatization. The former two alterations correlate closely with gold mineralization, serving as significant indicators for the prospecting of gold orebodies. Gold ore shoots tend to occur in parts with intense beresitization and silicification.

The Songjiagou gold deposit underwent four hydrothermal metallogenic stages: (1) The quartz-pyrite stage (stage I). This stage exhibited extremely weak gold mineralization, with resulting minerals dominated by quartz and pyrite; (2) the quartz-sericite-pyrite stage (stage II). This stage witnessed extensive pyritization and phyllic alteration, forming conglomerates with beresitization; (3) the gold-quartz-polymetallic sulfide stage (stage III). In this stage, polymetallic sulfides like chalcopyrite, sphalerite, and galena were formed. These polymetallic sulfides, together with gold minerals, are mostly distributed in fissures or interstices of pyrite; (4) the carbonate stage (stage IV). This stage is a late metallogenic stage characterized by the presence of carbonate veinlets, with a lack of gold mineralization. Among them, stages II and III are the major gold metallogenic stages.

3.2. Fracture-zone altered rock-type gold deposits (Pengjiakuang type)

The Pengjiakuang gold deposit, located in the central segment of the Pengjiakuang fault (F1), is controlled by the Pengjiakuang fault —a nearly-EW-directed basin-margin decollement structure near the contact zone between the Late Jurassic monzogranites and the Jingshan Group metamorphic rocks (Fig. 6). This fault exhibits an exposed length of approximately 4 km, widths ranging from 15 m to 280 m, a dip direction of S, and dip angles of 5°–50°. It presents a listric distribution pattern consisting of a steep upper part and a gentle lower part on the profile and a gently wavy distribution pattern in the plan. The upper portion of the fault zone is composed of graphite-bearing plagiogneissic tectonic breccias, significantly fractured. Its lower part comprises felsic tectonic breccias interbedded with felsic cataclasites, with the breccias mostly rounded and cemented by fault gouge. Its central portion consists of pyritized felsic tectonic breccias and felsic cataclasites, exhibiting intensive pyritization and phyllic alteration. This portion is a main ore-hosting destination, hosting orebodies Ⅰ-1 and Ⅰ-2.

A total of 14 gold orebodies have been delineated in the Pengjiakuang gold deposit, with the primary orebodies including Ⅰ-1, Ⅱ-1, and Ⅰ-2. The largest Ⅰ-1 orebody, under the strict control of the Pengjiakuang fault, exhibits a length of 300 m, widths ranging from 1.50 m to 25.00 m, thicknesses between 0.64 m and 41.92 m, occurrence elevations from +95 m to −107 m, and a maximum depth along its dip direction of 490 m (unclosed in deep strata). The orebodies in the deposit have relatively simple morphologies, occurring as veins primarily, with branching and recombination occurring locally. They generally show a gently wavy distribution pattern consisting of a steep upper part and a gentle lower part along their strikes and dip directions, with morphologies strictly governed by nearly-EW-trending faults (Fig. 7). They have an overall strike of

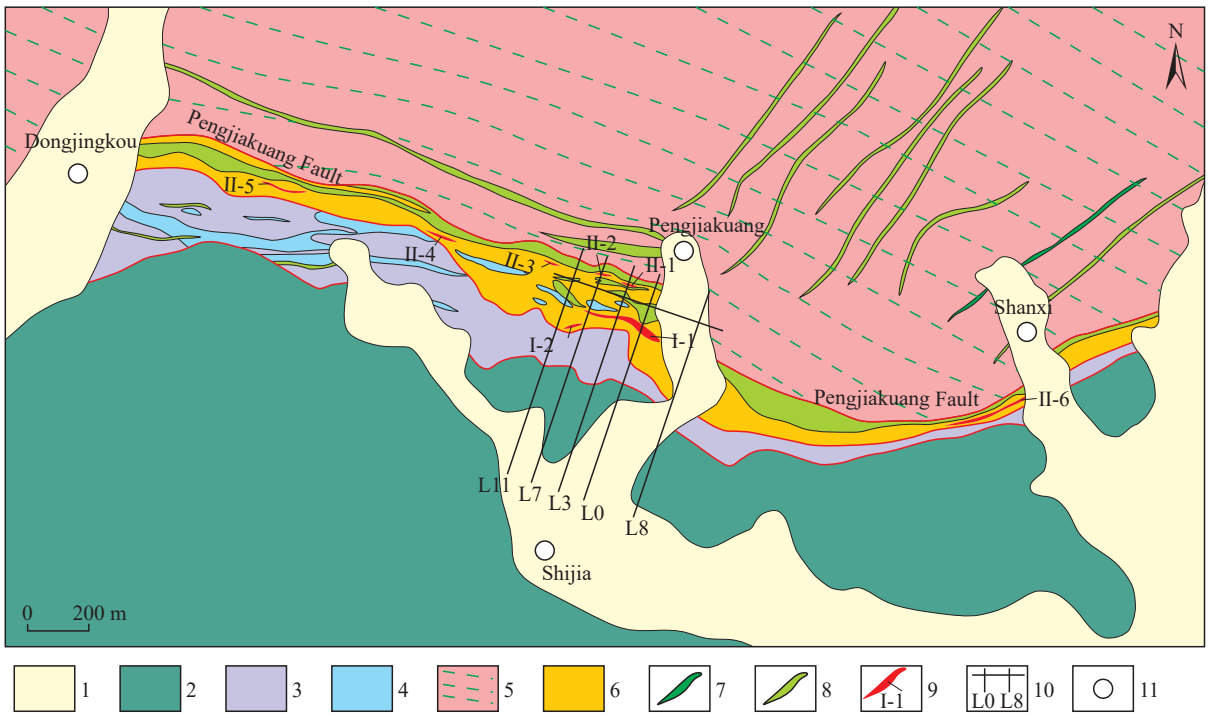

Fig. 6. Geological sketch map of the Pengjiakuang gold deposit (after Ding ZJ, 2022). 1–Quaternary; 2–Laiyang Group conglomerate; 3–Jingshan Group biotite-plagioclase gneiss; 4–Jingshan Group marble; 5–Late Jurassic weakly gneissic fine- to medium-grained pomegranate monzogranite; 6–Pyritized and silicified tectonic breccia; 7–lamprophyre; 8–diorite; 9–gold orebody and its number; 10–exploration line and its number; 11–village.

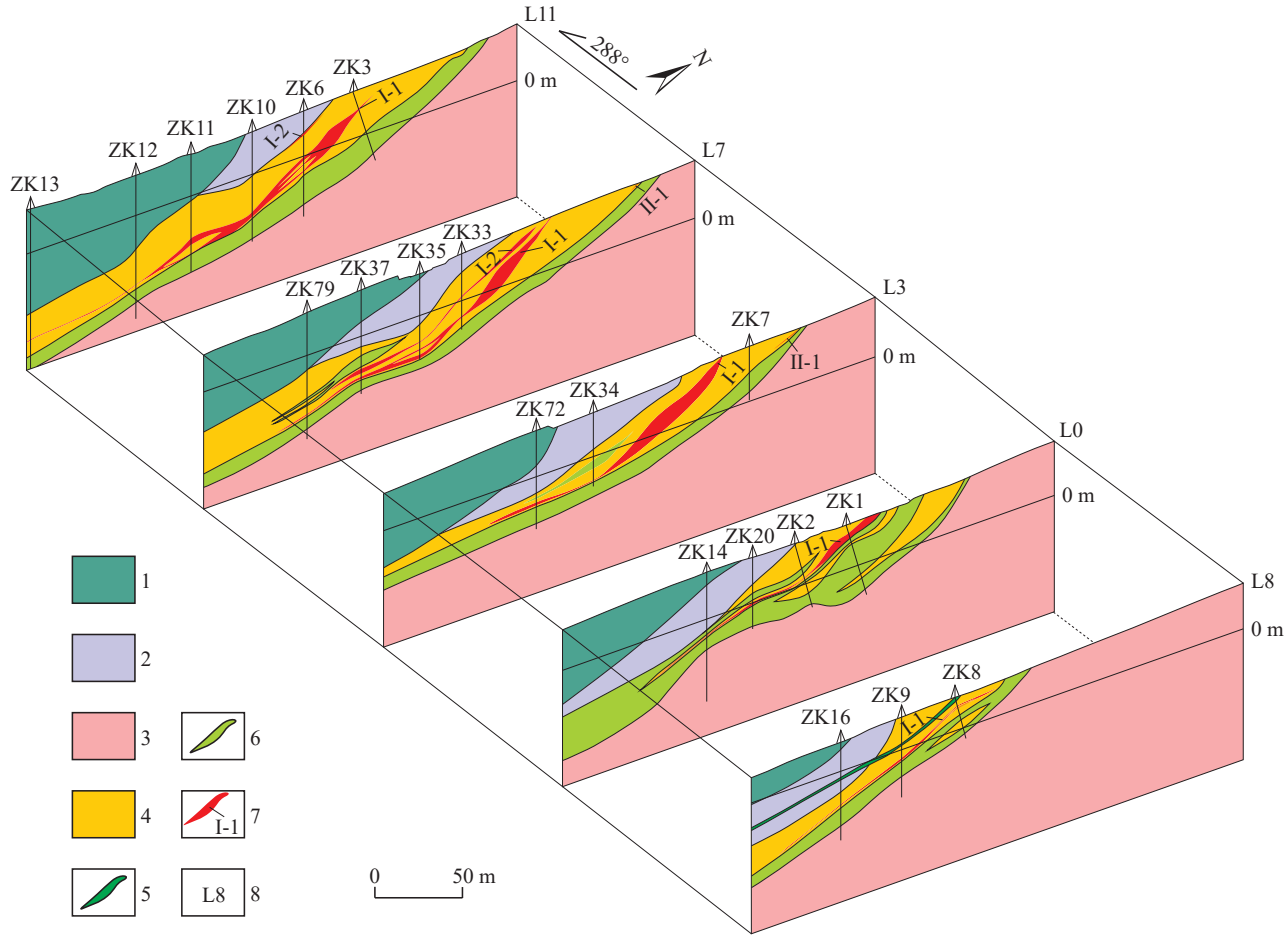

Fig. 7. Composite profile of the exploration lines in the Pengjiakuang gold deposit. 1–Laiyang Group conglomerate; 2–Jingshan Group biotite-plagioclase gneiss; 3–Late Jurassic weakly gneissic fine- to medium-grained pomegranate monzogranite; 4–breccia of a pyrite silicide structure; 5–dioritic porphyrite; 6–diorite; 7–gold orebody and its number; 8–exploration line number.

nearly EW (290°), a dip direction of S, and dip angles ranging from 30° to 50° in the shallow part and from 5° to 25° in the deep part. Their thicknesses vary significantly from 0.64 m to 41.92 m (average: 10.28 m), presenting a wide top and a narrow bottom; the gold grades of the orebodies range from 1.00 g/t to 8.48 g/t, with an average of 3.24 g/t.

The alteration range and intensity of surrounding rocks within the deposit are primarily influenced by the scale, attitudes, and fragmentation's degree of detachment fault zones. Their predominant alterations include potassic alteration, phyllic alteration, silicification, sericitization, carbonatization, illitization, and chloritization. Among them, silicification, phyllic alteration, and sericitization are the most closely associated with gold mineralization. In contrast, carbonatization, occurring in the late stage of hydrothermal activity, shows a minor correlation with gold mineralization. The surrounding rock alterations show a zoning pattern, with silicification, sericitization, carbonatization, and illitization primarily occurring in detachment fault zones and silicification and local K-feldspar alteration in the mylonite zone in the dominant fault's footwall. Additionally, argillization and carbonatization are principally found on the ground surface, gradually transitioning to silicification and sericitization toward deep parts. The X-ray diffraction analysis shows that the surface argillization zone is primarily composed of illite, quartz, calcite, and iron-manganese carbonates (Sun LW, 2015).

The ores in the Pengjiakuang gold deposit, primarily categorized as fracture-zone altered rocks, encompass pyritized felsic tectonic breccias, pyritized felsic cataclasites, and pyritized cataclastic dolomite dacites (Fig. 8). The former two are the main ore types of the Ⅰ-1 orebody, exhibiting relatively low gold grades, while the latter is the major ore type of the Ⅰ-2 orebody, manifesting a high gold grade. The ore minerals consist primarily of pyrite and electrum, followed by galena, sphalerite, and chalcopyrite. The gangue minerals are dominated by quartz, plagioclase, and calcite, succeeded by K-feldspar, muscovite, and sericite. The predominant ore textures include cataclastic and idiomorphic-hypidiomorphic textures. Pyrite is mostly crushed into powders and debris. The cubic and pentagonal dodecahedral pyrite grains can be observed. With sizes mostly between 0.5 mm and 2.0 mm, they are significantly finer than those in other gold deposits in the Jiaodong Peninsula. Additionally, the ore structures principally include disseminated, brecciated, and blocky structures.

Gold minerals in the Pengjiakuang deposit are dominated by electrum, followed by native gold. They are bright

yellowish-white or bright yellow, with fineness determined at 805‰–943‰, with an average of 860‰. They are angular granular and flaky in shape (accounting for 75%), followed by wheat-shaped, long angular granular, and linear morphologies. Their grain sizes are generally 2–16 μm, with a minimum and maximum of 1×3 μm and 10×34 μm, respectively. Accordingly, they are primarily micro- to fine-grained gold, with a scant distribution of medium-grained gold. They predominantly occur as inclusion gold (44%), followed by fissure gold and a minor amount of intergranular gold. The inclusion gold occurs primarily in pyrite and gangue (Figs. 9a–d), the fissure gold, together with gangue minerals, is mainly filled in pyrite fissures (Fig. 9d), and the intergranular gold occurs among the grains of pyrite and gangue minerals (Figs. 9e–g).

Based on the crosscutting relationships of veins, as well as

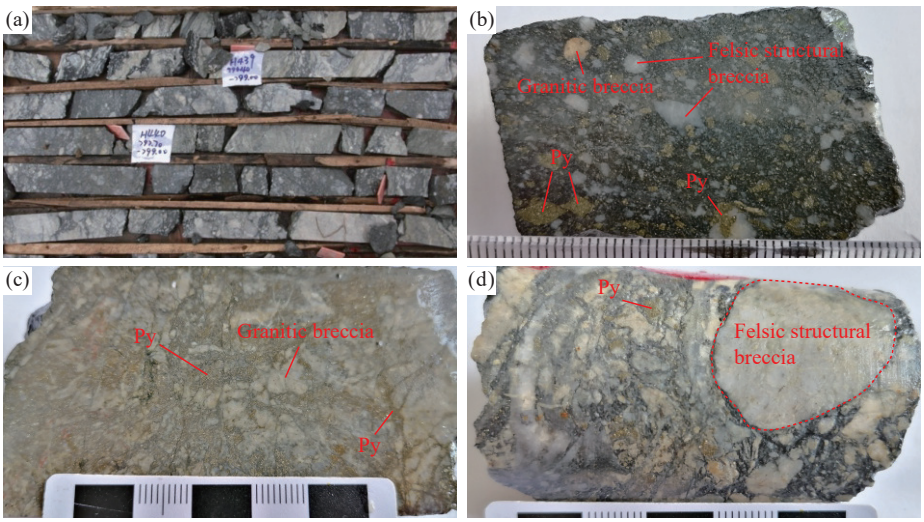

Fig. 8. Characteristics of ores in the Pengjiakuang deposit. a–basin-margin decollement structure-hosted breccia; b–pyrite aggregates in altered breccia; c–pyrite veinlets in tectonic fractures; d–disseminated pyrite in altered breccia.

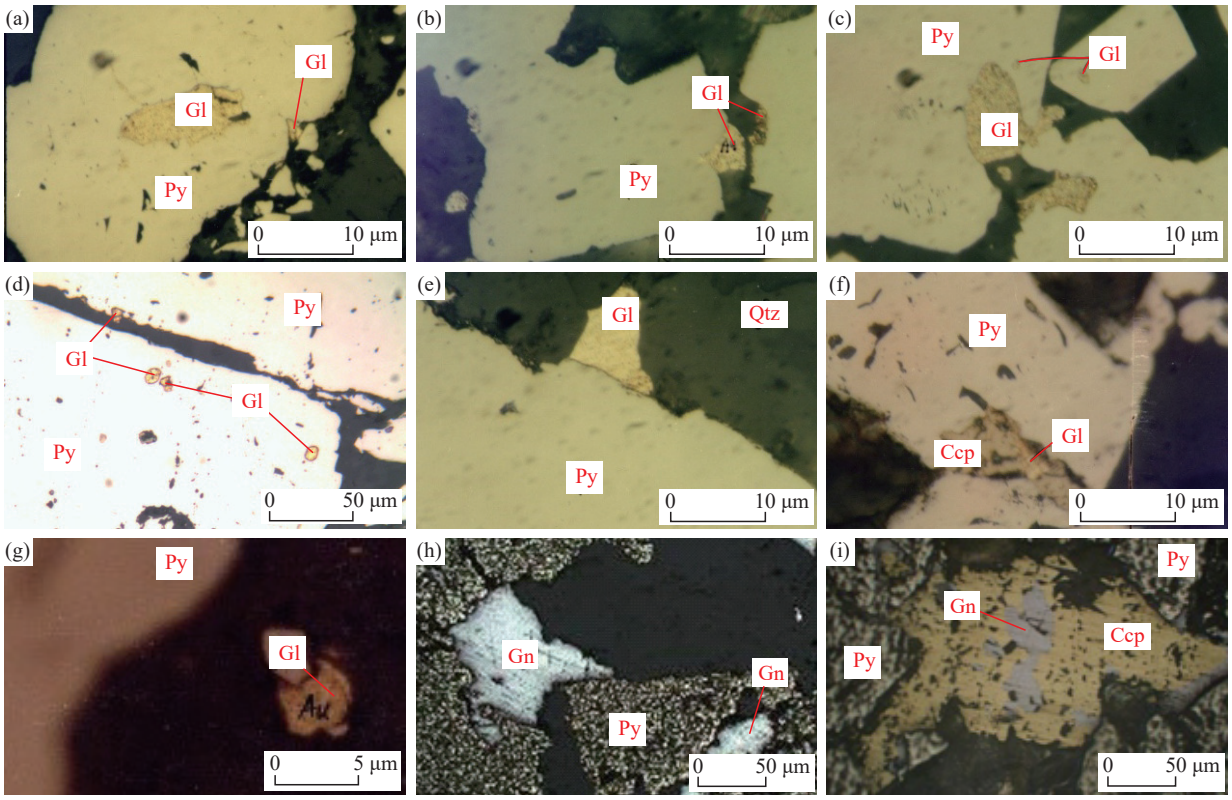

Fig. 9. Characteristics of ore minerals in the Pengjiakuang gold deposit. a–gold ores encapsulated in pyrite; b–gold ores occurring between pyrite grains or enclosed in quartz; c–gold ores occurring between pyrite and quartz grains or encapsulated in pyrite; d–gold ores encapsulated in pyrite; e–gold ores occurring between pyrite and quartz grains; f–gold minerals and chalcopyrite co-occurring between pyrite grains; g–gold ores distributed in gangue minerals; h–galena-metasomatized pyrite; i–chalcopyrite and galena-metasomatized pyrite. Gl–native gold; Py–pyrite; Gn–galena; Ccp–chalcopyrite; Qtz–quartz.

the paragenetic association and formation sequence of ore minerals, it can be inferred that the Pengjiakuang gold deposit experienced metallogenic stages in chronological order: The quartz-pyrite stage (stage I), the gold-bearing quartz (sericite)-pyrite stage (stage II), the quartz-polymetallic sulfide stage (stage III), and the quartz-carbonate stage (stage IV) (Sun LW, 2015). Among them, stages II and III are major stages for gold enrichment (Figs. 9f, h–i), whereas no ores were formed in stage IV.

3.3. The Pyrite-bearing carbonate vein-type (Liaoshang-type) gold deposit

The ore-hosting surrounding rocks of the Liaoshang gold deposit principally consist of Jingshan Group marbles and leptynites, Late Jurassic monzogranites, and a small number of Late Yanshanian veins (Fig. 10a). The orebodies of the deposit are significantly governed by fault structures, while not selectively occurring within certain surrounding rocks. The ore-controlling faults have a NE strike and a dip direction of SE, with dip angles becoming gradually gentle from upper to lower segments. They occur near the contact zone between the Jingshan Group and the Late Jurassic monzogranites, composed of several subparallel fault alteration zones (Fig. 10b).

Fault alteration zone III: This fault alteration zone has an exposed length of approximately 960 m and widths between 1 m and 14 m. It exhibits a gently wavy distribution pattern along both its strike and dip direction, with an overall strike of 50° ±, a dip direction of SE, and a dip angle of 42°. It widens and thickens from an elevation of −300 m downwards, with a maximum engineering-controlled thickness of up to 285 m (Fig. 10b). Various alterations are found in its shallow part, primarily including pyritization and carbonatization, as well as minor amounts of silicification and phyllic, K-feldspar, and chlorite alterations. A gradual transition is observed between this alteration zone and the surrounding rocks, with no significant boundary. In contrast, in the deep part of this alteration zone, pyritization and carbonatization are primarily found.

Fault alteration zone IV: This fault alteration zone is located in the hanging wall of fault alteration zone III. Both alteration zones are roughly parallel, with distances ranging from 100 m to 150 m (Fig. 10b). It has an intermittently exposed length of approximately 980 m and widths between 1 m and 10 m. It slightly widens and thickens from an elevation of −200 m toward deep parts. It has overall strikes ranging from 40° to 56°, a dip direction of SE, and dip angles between 23° and 58°. It shares roughly the same alteration characteristics with fault alteration zone III, except for slightly reduced mineralization intensity.

Four major and three secondary gold orebodies have been primarily discovered at elevations ranging from −500 m to −1000 m in the deposit (unclosed downwards, extending to the Xilaokou deposit; Fig. 10b). The orebodies are mostly lentoid, stratoid, veined, wedge-shaped, and saddle-shaped, with an overall strike of 37°, a dip direction of SE, and dip angles varying between 5° and 55° (mostly 10° to 40°). Besides, they extend for 80–550 m horizontally and 42–271 m laterally, with thicknesses ranging between 1.36 m and 42.93 m and ore grades from 1.36 g/t to 22.68 g/t.

Actually, the Xilaokou large gold deposit and the Qianchuiliu gold deposit, at the periphery of the Liaoshang gold deposit, are the Liaoshang gold deposit's extensions along its strike and dip direction. The three deposits, controlled by the same fault alteration zone, constitute different ore blocks of the same super-large gold deposit.

The Liaoshang-type gold deposits experienced

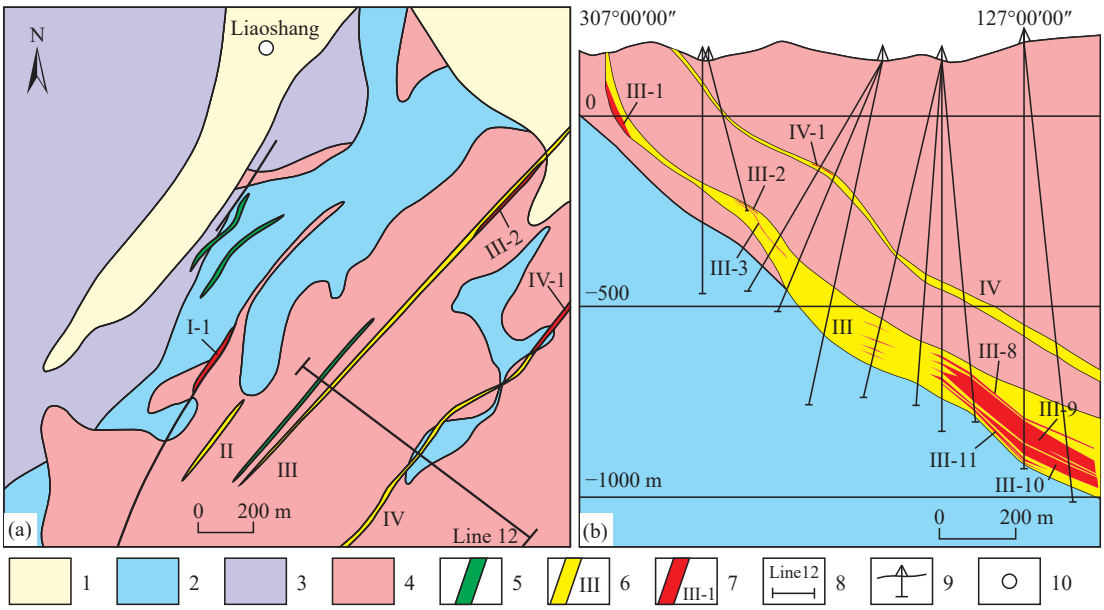

Fig. 10. Geological map (a) of the Liaoshang gold deposit and the and profile of the No. 12 exploration line (b) (after Bo JW et al., 2021). 1–Quaternary; 2–Jingshan Group marble; 3–Jingshan Group leptynite; 4–late Jurassic weakly gneissic fine- to medium-grained pomegranate monzogranite; 5–lamprophyre; 6–a mineralized alteration zone and its number; 7–gold orebody and its number; 8–exploration line and its number; 9–borehole location; 10–village.

mineralization dominated by filling. Their pyrite-bearing carbonate veins/veinlets containing gold are filled along the fractures of surrounding rocks (granites or metamorphic rocks), while not selectively occurring in certain surrounding rocks. These veins/veinlets have widths ranging from 1.0 cm to 5.0 cm primarily, from 0.2 cm to 0.5 cm partially, and up to 80 cm in a small number. The Liaoshang-type gold deposits host three ore types (Bo JW et al., 2021): Granites of pyrite-bearing carbonate veins (Figs. 11a–c), metamorphic rocks of pyrite-bearing carbonate veins (Fig. 11d), and large pyrite-carbonate veins (Fig. 11e). For the former two types, there is a positive correlation between their gold content and the number of their pyrite-bearing carbonate veinlets. The last type shows the highest gold grade, with visible gold formed locally (Fig. 11f). The pyrite-bearing carbonate veins are composed primarily of pyrites and dolomites (Figs. 11g–i).

In Liaoshang-type gold deposits, ores of the pyrite-bearing carbonate veins consist primarily of native gold, pyrite, and dolomite, along with minor amounts of calcite, chalcopyrite, galena, and sphalerite. Among these minerals, pyrite (Figs. 12a–b) and dolomite (Figs. 12c–d) serve as gold-bearing minerals. The gold minerals principally comprise yellow-to-light-yellow electrum and golden-yellow native gold. They were lighter in color with an increase in silver content. With xenomorphic irregular granular textures, they are closely associated with pyrite and dolomite. The gold minerals are angular granular, flaky, dotted, round granular, and branched in shape, dominated by the former two morphologies. Their grain sizes vary from 5 μm to 350 μm, mostly concentrated in a range of 20–50 μm. They primarily occur as inclusion, interstitial, fissure, and intergranular gold. Specifically, gold minerals that are distributed in pyrite as irregular fine-grained textures constitute inclusion gold (Figs. 12a–b), those filled in dolomite interstices form interstitial gold (Figs. 12c–d), those filled along the pyrite fissures form fissure gold (Fig. 12e), and those occurring between pyrite grains form intergranular gold (Fig. 12f). The gold minerals display fineness ranging from 805‰ to 940‰, with an average of 912‰.

The paragenetic association and formation sequence of minerals reveal that the Liaoshang-type gold deposits underwent three metallogenic stages (Bo JW et al., 2021): (1) The gold - coarse-grained pyrite - carbonatization stage (stage I). In this stage, coarse-grained pyrite (grain sizes: 0.5 mm to 5 mm and 20 mm partially, correlating positively with the width of pyrite-bearing carbonate veins) were formed, with high automorphic degree, cubic and pentagonal dodecahedral morphologies, and wide veins (1.0 cm to 5.0 cm, and 80 cm partially). Much native gold with large grain sizes can be observed in pyrite or dolomite; (2) the gold - fine-grained pyrite - polymetallic sulfide - carbonatization

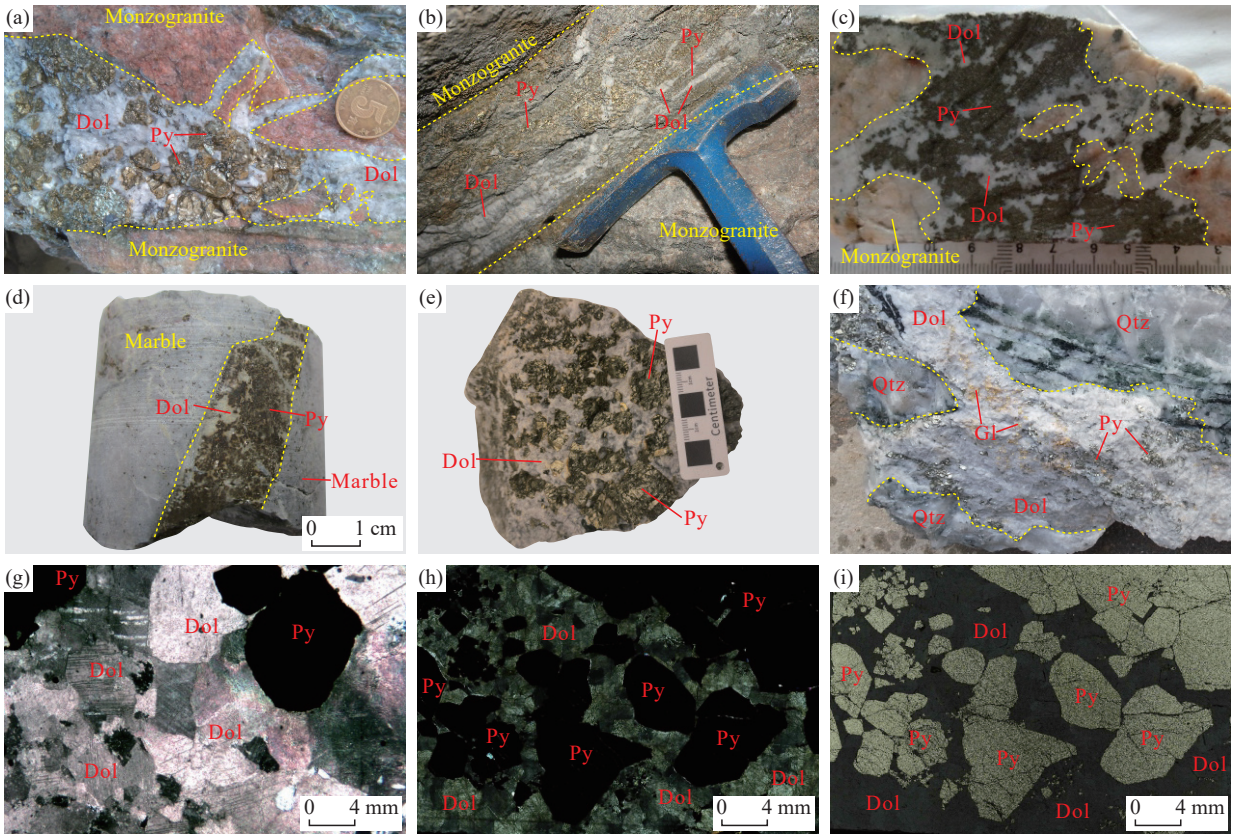

Fig. 11. Ore characteristics of Liaoshang-type gold deposits. a–granites of a pyrite-bearing carbonate vein in the Liaoshang gold deposit; b–granites of a pyrite-bearing carbonate vein in the Houkuang gold deposit; c–granites of a pyrite-bearing carbonate vein from the Xilaokou gold deposit; d–metamorphic rocks of a pyrite-bearing carbonate vein; e–large pyrite-bearing carbonate vein; f–native gold in ores of a pyrite-bearing carbonate vein; g–h–micrographs of a pyrite-bearing carbonate vein under transmitted light (+); i–micrograph of a pyrite-bearing carbonate vein under reflected light (-). Dol–dolomite; Py–pyrite; Gl–native gold.

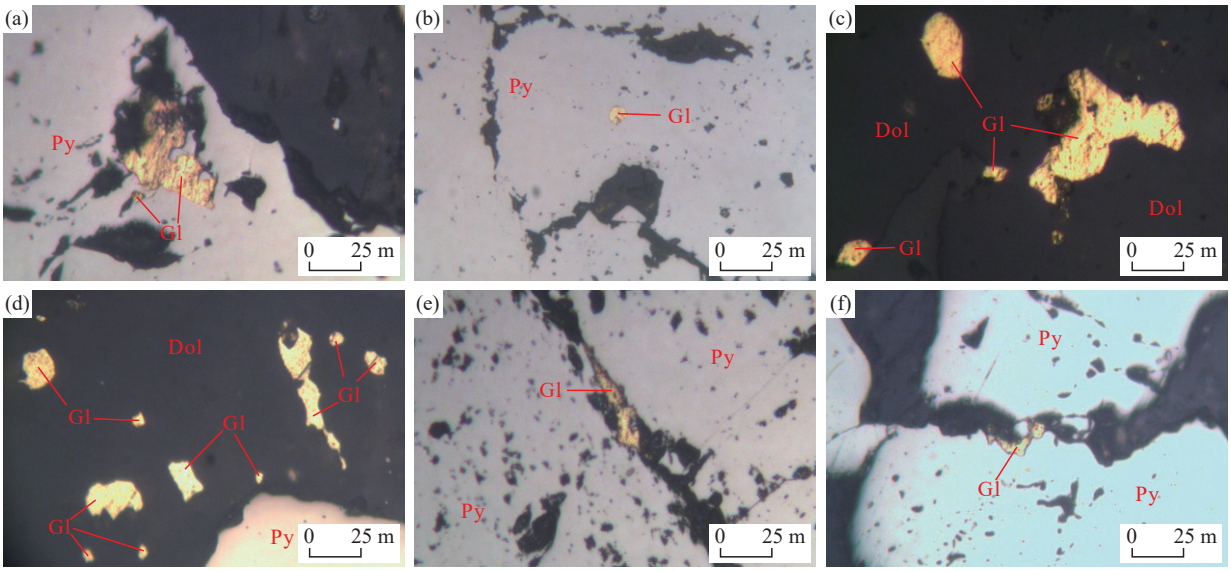

Fig. 12. Gold mineral characteristics of the Liaoshang gold deposit. a–b–inclusion gold in pyrite; c–d–gold ores in dolomite; e–gold ores filled in a pyrite fissure; f–intergranular gold between pyrite grains. Dol-dolomite; Py-pyrite; Gl-native gold.

stage (stage II). This stage witnessed the filling of pyrite and dolomite along fissures, forming veinlets (widths: 0.2 cm to 0.5 cm). The pyrite was hypidiomorphic and fine-grained (0.02 mm to 0.3 mm, and 1.0 mm to 3.5 mm partially). Additionally, minor amounts of chalcopyrite, pyrrhotite, and galena occurred in this stage. Gold minerals precipitated and were enriched in large quantities with the crystallization of dolomite and pyrite; (3) the carbonatization stage (stage III). In this stage, minerals occur as veinlets with widths ranging from 0.1 cm to 0.5 cm. No significant pyritization or only a minor amount of micro-fine-sized pyrite (< 0.02 mm) was identified, with no gold formed.

4. Geochemical characteristics of gold deposits

4.1. Fluid inclusions

In both the Songjiagou and Pengjiakuang gold deposits, fluid inclusions in quartz can be categorized into three types (Sun LW, 2015; Chen Y, 2015): Gas-liquid two-phase inclusions (type I), pure CO_2 inclusions (type II), and CO_2-bearing three-phase inclusions (type III), exhibiting roughly the same characteristics (Figs. 13a–f). In the Songjiagou gold deposit, the type-I inclusions (Figs. 13a–b) show the largest number, consisting of primary and secondary inclusions. The primary inclusions of type I show sizes ranging from 5 μm to 12 μm and gas-liquid ratios between 20% and 50%. They are elliptical and are distributed in clusters mostly, with some spreading directionally along mineral growth zones. The secondary inclusions of type I manifest sizes ranging from 3 μm to 10 μm and gas-liquid ratios between 10% and 30%. They are elliptical, elongated, and irregular mostly and scatter in a bead-like pattern along fissures. The type-II inclusions (Fig. 13b), composed of CO_2 in liquid and gas phases, are found in a small number. They are elliptical mostly, followed by irregularly polygonal morphologies locally, with sizes ranging from 6 μm to 10 μm and gas-liquid ratios from 15% and 40%. The type-III inclusions (Fig. 13c) are composed of gas- and liquid-phase CO_2 and liquid-phase H_2O, with CO_2 accounting for 30% to 60% of the total volume and gas-phase CO_2 accounting for 30% to 90% of the total volume of gas- and liquid-phase CO_2. They are elliptical and circular mostly and irregularly polygonal marginally, with sizes ranging from 6 μm to 12 μm. In the Liaoshang gold deposit, fluid inclusions within the dolomite primarily include liquid-phase inclusions and gas-liquid two-phase inclusions, with tiny CO_2-bearing three-phase inclusions locally visible (Ji P, 2016). Among them, the gas-liquid two-phase inclusions are elliptical, elongated, and irregular mostly, with sizes ranging from 3 μm to 7 μm. Their gas-liquid ratios range between 10% and 35%, concentrated in a range of 20%–25% (Figs. 13g–i). The pure liquid-phase inclusions tend to be distributed in clusters. Most of them are circular and elliptical, with sizes less than 3 μm.

In the Songjiagou gold deposit, the temperatures of the type-I and -III inclusions range from 175.8°C to 251.3°C (200–220°C mostly) and from 208.3°C to 262.8°C (220–240°C mostly), respectively. Their densities range from 0.88 g/cm^3 to 0.98 g/cm^3 (0.92–0.96 g/cm^3 mostly) and from 0.63 g/cm^3 to 0.71 g/cm^3 (0.64–0.68 g/cm^3 mostly), respectively. Furthermore, their salinities range from 8.67 wt% to 14.42 wt% (peaks concentrated in 10–12 wt%) and from 4.14 wt% to 10.73 wt% (peaks concentrated in 5–7 wt%), respectively, suggesting typical low-salinity characteristics (Fig. 14a). In the Pengjiakuang gold deposit, the temperatures of the type-I and -III inclusions range from 147.6°C to 375.3°C (concentrated within 195–260°C and 273–350°C) and from 248.5°C to 350.6°C (260–325°Cmostly), respectively. Their densities vary from 0.553–0.969 g/cm^3 (0.7–0.95 g/cm^3 mostly) and from 0.28 g/cm^3 to 0.77 g/cm^3 (0.60–0.75 g/cm^3 mostly), respectively. Moreover, their salinities (w(NaCl)) range from 1.22 wt% to 13.77 wt% (4–9 wt% mostly) and from 2.62 wt% to 12.63 wt% (5–9 wt% mostly), also suggesting typical low-salinity characteristics (Fig. 14b). In

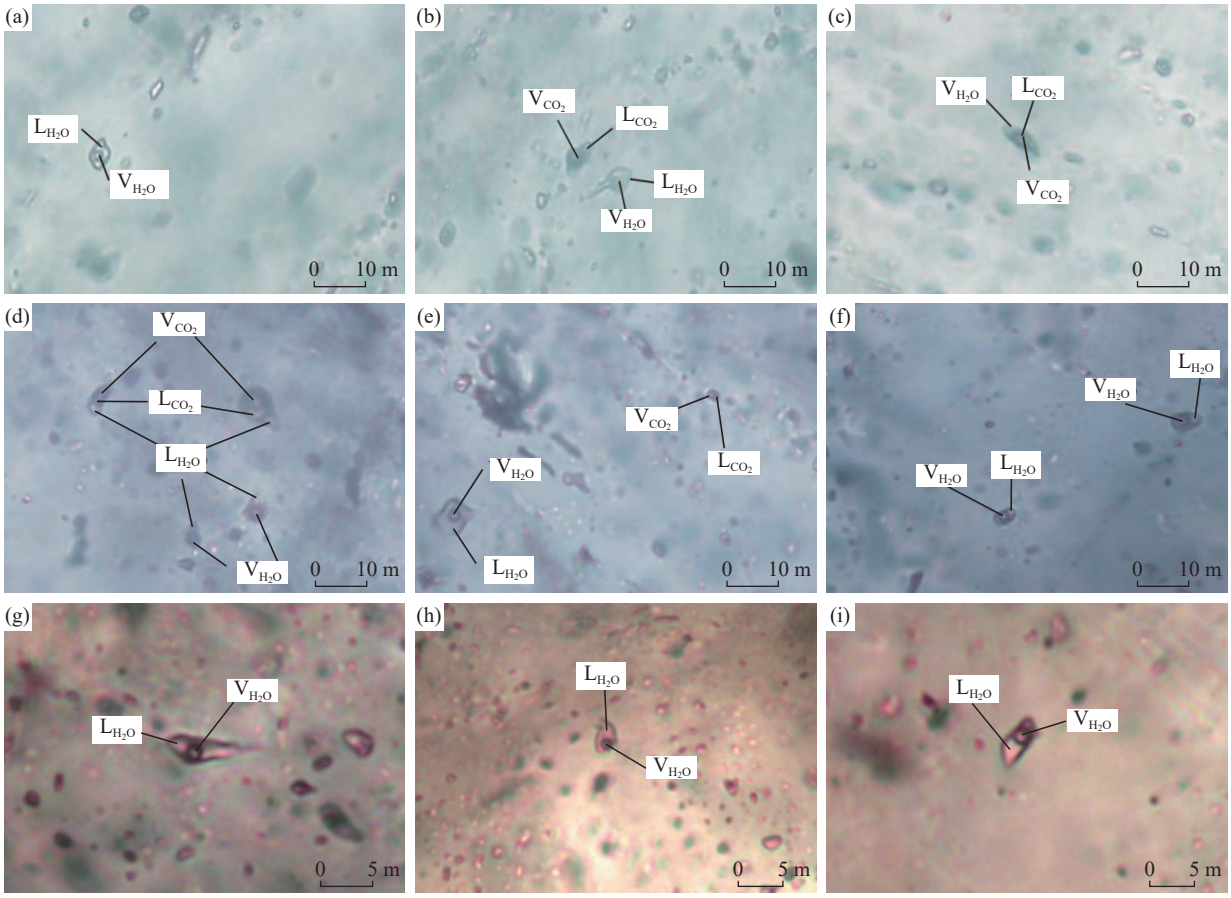

Fig. 13. Fluid inclusion characteristics of gold deposits on the northeastern margin of the Jiaolai Basin. a–c–Songjiagou gold deposit (after Chen Y, 2015); d–f–Pengjiakuang gold deposit (after Sun LW, 2015); g–i–Liaoshang gold deposit. a–gas-liquid two-phase fluid inclusion; b–gas-liquid two-phase and pure CO_2 fluid inclusions; c–CO_2-bearing three-phase fluid inclusion; d–gas-liquid two-phase and CO_2-bearing three-phase fluid inclusions; e–gas-liquid two-phase and pure CO_2 fluid inclusions; f–gas-liquid two-phase fluid inclusion; g–i–gas-liquid two-phase fluid inclusion.

the Liaoshang gold deposit, the type-I inclusions exhibit homogenization temperatures from 199.8°C to 247.1°C, densities from 0.80 g/cm^3 to 0.87 g/cm^3, and salinities from 10.11 wt% to 12.31 wt%, suggesting moderate to slightly low temperatures, moderate salinity, and low density (Fig. 14c; Ji P, 2016; Liang H et al., 2022). The laser Raman spectroscopy analyses indicate that the fluid inclusions in the Pengjiakuang, Songjiagou, and Liaoshang gold deposits contained rich H_2O, common CO_2, and a minor amount of N_2, suggesting CO_2-NaCl-H_2O fluid systems (Sun LW, 2015; Chen Y, 2015; Liang H et al., 2022).

4.2. Hydrogen-oxygen isotope characteristics

For the altered rock-type gold deposits on the northeastern margin of the Jiaolai Basin, hydrothermally altered minerals such as quartz and sericite exhibit $\delta^{18}O_{H2O}$ values ranging from 0.59‰ to 7.70‰, with an average of 2.43‰, and δD values from −105.8‰ to −47.1‰, with an average of −75.1‰ (n=33; Table 3).

4.3. Carbon-oxygen isotope characteristics

For the gold deposits on the northeastern margin of the Jiaolai Basin, hydrothermal minerals like calcite, dolomite, and siderite manifest $\delta^{13}C_{PDB}$ values ranging from −6.0‰ to 1.70‰, with an average of −3.7‰, and $\delta^{18}O_{V\text{-}SMOW}$ values concentrated in a range of 6.9‰–16.6‰, averaging 10.3‰ (n=41; Table 4). These values slightly differ among different types of gold deposits. Specifically, for altered rock-type gold deposits, calcite and siderite show $\delta^{13}C_{PDB}$ values ranging from −5.6‰ to 1.7‰, with an average of −1.9‰, and $\delta^{18}O_{V\text{-}SMOW}$ values concentrated in a range from 8.2‰ from 6.6‰, averaging 11.5‰ (n=10). For the pyrite-bearing carbonate vein-type gold deposits, dolomite displays $\delta^{13}C_{PDB}$ values ranging from −6.0‰ to −2.9‰, with an average of −4.3‰, and $\delta^{18}O_{V\text{-}SMOW}$ values concentrated in a range of 6.9‰–10.6‰, averaging 9.8‰ (n=31).

4.4. Sulfur isotope characteristics

For the gold deposits on the northeastern margin of the Jiaolai Basin, pyrite or pyrrhotite display $\delta^{34}S$ values significantly varying from +3.4‰ to +16.2‰, with an average of 9.6‰ (n= 124; Table 5). For the altered rock-type gold deposits, pyrite or pyrrhotite exhibits $\delta^{34}S$ values ranging from +3.5‰ to +16.2‰, with an average of 9.5‰ (n=72). In contrast, for the pyrite-bearing carbonate vein-type gold deposits, pyrite manifests $\delta^{34}S$ values ranging from +3.4‰ to

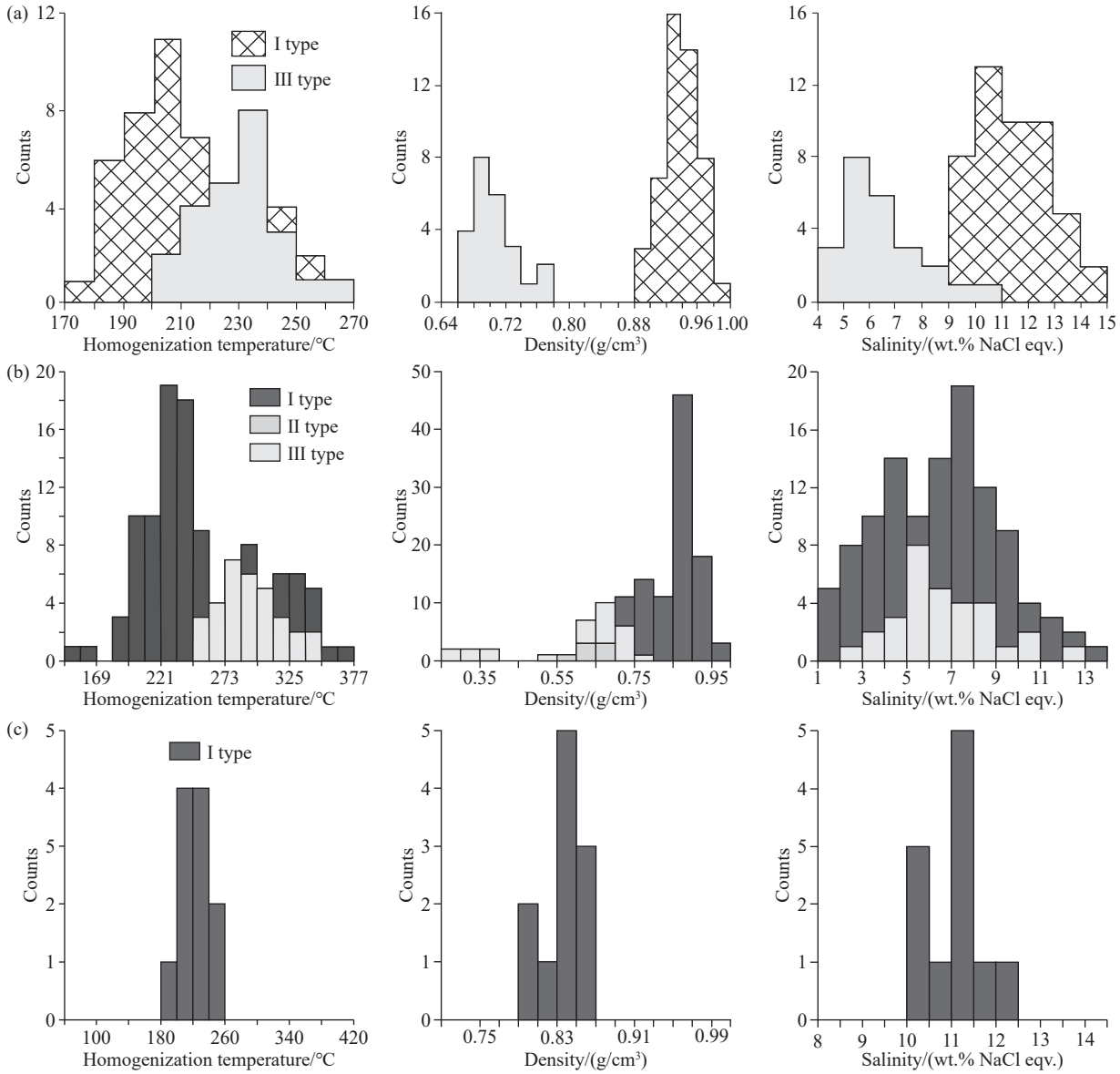

Fig. 14. Histograms showing the homogenization temperature, density, and salinity of fluid inclusions from gold deposits on the northeastern margin of the Jiaolai Basin. (a)–Songjiagou gold deposit (after Chen Y, 2015); (b)–Pengjiakuang gold deposit (after Sun LW, 2015); (c)–Liaoshang gold deposit (after Ji P, 2016).

+12.6‰, with an average of 9.6‰ (n=52). Hence, the two types of deposits show roughly consistent $\delta^{34}S$ values except for some different extreme values.

4.5. Lead isotope characteristics

For gold deposits on the northeastern margin of the Jiaolai Basin, pyrite or pyrrhotite exhibits $^{206}Pb/^{204}Pb$, $^{207}Pb/^{204}Pb$, and $^{208}Pb/^{204}Pb$ values ranging from 16.920 to 18.886 (average: 17.354), from 15.307 to 15.677 (average: 15.474), and from 37.359 to 40.073 (average: 37.998), respectively (n=105; Table 6). For the altered rock-type gold deposits, pyrite or pyrrhotite exhibit $^{206}Pb/^{204}Pb$, $^{207}Pb/^{204}Pb$, and $^{208}Pb/^{204}Pb$ values ranging from 16.920 to 17.862 (average: 17.221), from 15.307 to 15.627 (average: 15.450), and from 37.359 to 38.596 (average: 37.831), respectively (n=58). For the pyrite-bearing carbonate vein-type gold deposits, pyrite manifests $^{206}Pb/^{204}Pb$, $^{207}Pb/^{204}Pb$, and $^{208}Pb/^{204}Pb$ values ranging from 17.027 to 18.886 (average: 17.518), from 15.435 to 15.677 (average: 15.504), and from 37.706 to 40.073 (average: 38.204), respectively (n=47).

4.6. Helium-argon isotope characteristics

For the gold deposits on the northeastern margin of the Jiaolai Basin, pyrite-hosted fluid inclusions display ^{3}He, ^{4}He, ^{40}Ar, and $^{40}Ar^{*}$ contents ranging from 0.12×10^{-13} cm^3STP/g to 34.05×10^{-13} cm^3STP/g, from 0.12×10^{-7} cm^3STP/g to 22.93×10^{-7} cm^3STP/g, from 0.54×10^{-7} cm^3STP/g to 64.29×10^{-7} cm^3STP/g, and from 0.06×10^{-7} cm^3STP/g to 40.78×10^{-7} cm^3STP/g, respectively, with $^{3}He/^{4}He$, R/Ra, and $^{40}Ar/^{36}Ar$ ratios varying from 0.17×10^{-6} to 2.39×10^{-6}, from 0.12 to 1.71, and from 328.50 to 2112.00, respectively (n=26; Table 7). For the altered rock-type gold deposits, pyrite-

Table 3. Hydrogen-oxygen isotopic compositions of gold deposits on the northeastern margin of the Jiaolai Basin.

Gold deposit	Sample	δD_{SMOW}/‰	$\delta^{18}O_{SMOW}$/‰	$\delta^{18}O_{H2O}$/‰	Reference
Songjiagou	Quartz	−92.0	−	1.02	Yang JZ et al., 2001
Pengjiakuang	−	−89.5	−	4.03	Sun FY et al., 1995
	−	−89.9	6.9	0.61	Zhao YL et al., 2000
	−	−92.0	7.8	0.85	
	−	−97.9	6.2	0.59	
	−	−96.6	8.7	1.02	
	Sericite	−58.0	4.3	1.15	Mao JW et al., 2005
	Sericite	−59.0	5.1	1.95	
	Sericite	−64.0	5.3	2.15	
Dongliujia	Quartz	−81.5	9.7	3.49	Li HM et al., 2010
	Quartz	−82.7	9.9	3.73	
Shawang	Quartz	−72.8	6.0	1.96	
	Quartz	−105.8	13.4	6.50	Chen CX, 2015
No. 18 Xilaokou vein	Quartz	−90.0	6.9	0.60	Sun XL, 2013
	Quartz	−92.0	7.8	1.00	
	Quartz	−98.0	6.2	0.60	
	Quartz	−97.0	8.7	0.90	
Dongliujia	Dolomite	−47.1	9.6	2.50	Shui P, 2019
	Dolomite	−48.3	9.9	2.80	
	Dolomite	−49.5	9.6	2.50	
Longkou	Dolomite	−50.6	9.8	2.06	
	Dolomite	−51.7	9.7	1.96	
	Dolomite	−52.8	9.7	1.96	
Tudui	Dolomite	−53.9	12.7	4.96	
Liaoshang	Dolomite	−65.1	10.1	2.85	
	Dolomite	−66.8	10.2	2.95	
	Dolomite	−68.0	9.6	2.35	
Shawang	Quartz	−73.0	6.0	0.60	Tan J et al., 2015
Dongliujia	Quartz	−83.0	9.9	3.70	
	Quartz	−82.0	9.7	3.50	
	Quartz	−86.0	10.7	3.80	
Liaoshang	Quartz	−69.0	8.3	1.90	
	Quartz	−74.0	14.8	7.70	

Table 4. Carbon-oxygen isotopic compositions of gold deposits on the northeastern margin of the Jiaolai Basin.

Deposit type	Gold deposit	Sample	Mineral	$\delta^{13}C_{V\text{-}PDB}$/‰	$\delta^{18}O_{V\text{-}PDB}$/‰	$\delta^{18}O_{V\text{-}SMOW}$/‰	Reference
Alteration type	Dongjingkou	Jan-64	Calcite	−1.7	−18.0	12.3	Zhao YL et al., 2000
	Pengjiakuang	99-43	Calcite	−0.9	−22.0	8.2	
		99-56	Calcite	1.7	−13.8	16.6	
		−	Calcite	−5.6	−	9.9	Li ZP, 1992
		−	Siderite	−4.5	−	9.4	
		−	Calcite	−3.6	−	10.5	Sun FY et al., 1995
		−	Calcite	−3.9	−	11.4	
		−	Calcite	1.7	−13.7	16.6	Zhang LC et al., 2002b
		−	Calcite	−1.7	−18.0	12.3	
		−	Calcite	−0.9	−22.0	8.2	
Pyrite-bearing carbonate vein type	Liaoshang	SD101B3	Dolomite	−4.4	−	10.0	Li JJ et al., 2020
		SD101B4	Dolomite	−6.0	−	10.0	
		SD101B8	Dolomite	−3.8	−	10.1	
		SD101B11	Dolomite	−4.2	−	10.4	
		SD101B12	Dolomite	−4.1	−	10.2	
		SD101B13	Dolomite	−5.2	−	10.3	
		2015LS-01	Dolomite	−4.5	−20.5	9.7	Bo JW et al., 2021
		2015LS-02	Dolomite	−4.4	−20.3	9.9	
		2015LS-03	Dolomite	−4.5	−20.2	10.1	
		2015LS-04	Dolomite	−4.1	−20.5	9.7	

Table 4. (*Continued*)

Deposit type	Gold deposit	Sample	Mineral	$\delta^{13}C_{V\text{-}PDB}$/‰	$\delta^{18}O_{V\text{-}PDB}$/‰	$\delta^{18}O_{V\text{-}SMOW}$/‰	Reference
		2015LS-05	Dolomite	−3.7	−20.0	10.2	
		2015LS-06	Dolomite	−4.5	−20.4	9.8	
		LS-07	Dolomite	−4.5	−19.7	10.6	
		LS-08	Dolomite	−4.4	−19.8	10.4	
		LS-09	Dolomite	−4.5	−19.8	10.5	
		LS-10	Dolomite	−4.3	−19.9	10.4	
		LS-11	Dolomite	−4.4	−20.1	10.2	
		LS-12	Dolomite	−4.1	−19.8	10.5	
		6474	Dolomite	−3.6	−20.5	9.8	
		H179	Dolomite	−4.2	−20.4	9.9	
		H173	Dolomite	−4.6	−20.6	9.6	
		17B25	Dolomite	−3.8	−20.0	10.3	
		B23	Dolomite	−3.8	−19.9	10.4	
		17B26	Dolomite	−4.0	−20.0	10.2	
		LS-5	Dolomite	−4.1	−20.8	9.4	Liang H et al., 2022
		LS-6	Dolomite	−4.4	−20.9	9.4	
		LS-9	Dolomite	−4.7	−20.7	9.6	
	Xilaokou	XL74ZK1-4	Dolomite	−2.9	−23.3	6.9	
		XL74ZK1-7	Dolomite	−4.4	−21.1	9.1	
		XLK-1	Dolomite	−3.7	−21.9	8.3	
		XLK-2	Dolomite	−4.3	−21.0	9.3	

Table 5. Sulfur isotopic compositions of gold deposits on the northeastern margin of the Jiaolai Basin.

Deposit type	Gold deposit	Sample	Mineral	$\delta^{34}S_{V\text{-}CDT}$/‰	References
Alteration type	Songjiagou	Fa52	Pyrite	12.6	Zeng QD et al., 2002
		F8	Pyrite	13.0	
		Fa9	Pyrite	13.6	
		Fa9-2	Pyrite	12.9	
		Fa9-5	Pyrite	12.8	
		Faw	Pyrite	10.4	
		Fy-1	Pyrite	10.4	
		Fy-2	Pyrite	10.4	
		Fy-4	Pyrite	10.1	
		09FYK-1	Pyrite	9.0	Sun XL, 2013
		09FYK-3	Pyrite	8.5	
		09FYK-4	Pyrite	8.6	
		SJG-1	Pyrite	8.6	Chen Y, 2015
		SJG-2	Pyrite	7.7	
		SJG-3	Pyrite	8.7	
	Pengjiakuang	−	Pyrite	13.0	Zhao YL et al., 2000
		−	Pyrite	12.7	
		−	Pyrite	11.6	
		−	Pyrite	10.6	
		−	Pyrite	10.9	
		4-11	Pyrite	9.7	Zhang ZR et al., 1999
		4-12	Pyrite	10.4	
		4-7	Pyrite	10.3	
		4-4	Pyrite	10.7	
		4-1	Pyrite	11.3	
		−	Pyrite	10.9	Sun FY et al., 1995
		−	Pyrite	11.5	
		−	Pyrite	11.2	
		PJK-1	Pyrite	6.2	Sun LW, 2015
		PJK-2	Pyrite	7.5	
		PJK-3	Pyrite	8.3	

Table 5. (*Continued*)

Deposit type	Gold deposit	Sample	Mineral	$\delta^{34}S_{V\text{-}CDT}$/‰	References
		09PJK-8	Pyrite	3.5	Sun XL, 2013
		09PJK-10	Pyrite	7.5	
		09PJK-17	Pyrite	7.7	
		09PJK-18	Pyrite	7.9	
	Tudui-Shawang	TD-1	Pyrite	8.2	Chen CX, 2015
		TD-2	Pyrite	8.0	
		SW-1	Pyrite	7.2	
		SW-2	Pyrite	8.0	
		SW-3	Pyrite	10.3	
		TK1	Pyrrhotite	9.7	Li HM et al., 2010
		TK4	Pyrrhotite	10.6	
		K2	Pyrite	8.5	
		K3	Pyrite	9.1	
		SK1	Pyrite	9.1	
		SK3	Pyrite	10.8	
		SK4	Pyrite	10.0	
		SK5	Pyrite	12.7	
		09TD-5	Pyrite	8.0	Sun XL, 2013
		09TD-6	Pyrite	8.2	
		09TD-8	Pyrite	6.2	
		09TD-9	Pyrite	7.0	
		09TD-15	Pyrite	8.0	
		09TD-19	Pyrite	7.5	
		09SW-1	Pyrite	8.2	
		09SW-4	Pyrite	9.6	
		09SW-5	Pyrite	7.9	
		09SW-8	Pyrite	8.5	
		09SW-10	Pyrite	8.4	
	No. 18 Xilaokou vein	B21	Pyrite	7.8	
		B04	Pyrite	7.6	
		B42	Pyrite	8.8	
		B48	Pyrite	8.7	
		B49	Pyrite	8.6	
		B36	Pyrite	9.0	
		B30	Pyrite	8.9	
		B31	Pyrite	9.4	
		B39	Pyrite	9.5	
		B40	Pyrite	9.5	
		B11	Pyrite	16.2	
		B12	Pyrite	15.4	
		B47	Pyrite	7.6	
Pyrite-bearing carbonate vein type	Liaoshang	09LS-2	Pyrite	8.2	
		09LS-4	Pyrite	8.3	
		09LS-5	Pyrite	8.3	
		SD17-28B101	Pyrite	8.2	Li JJ et al., 2020
		SD17-28B102	Pyrite	8.6	
		SD17-28B103	Pyrite	8.1	
		SD17-28B104	Pyrite	7.6	
		SD17-28B105	Pyrite	8.1	
		SD17-28B106	Pyrite	8.5	
		SD17-28B107	Pyrite	8.4	
		SD17-28B108	Pyrite	8.3	
		SD17-28B109	Pyrite	8.5	
		SD17-28B110	Pyrite	8.4	
		SD17-28B111	Pyrite	8.6	
		SD17-28B112	Pyrite	9.2	

Table 5. (*Continued*)

Deposit type	Gold deposit	Sample	Mineral	$\delta^{34}S_{V\text{-}CDT}$/‰	References
		LS-01	Pyrite	8.0	Bo JW et al., 2021
		LS-02	Pyrite	9.4	
		LS-03	Pyrite	8.4	
		LS-04	Pyrite	7.7	
		LS-05	Pyrite	9.1	
		LS-06	Pyrite	7.3	
		LS-1	Pyrite	3.4	
		LS-2	Pyrite	7.4	
		LS-1	Pyrite	10.7	Liang H et al., 2022
		LS-3	Pyrite	10.7	
		LS-4	Pyrite	10.2	
		LS-5	Pyrite	9.8	
		LS-6	Pyrite	10.3	
		LS-9	Pyrite	9.8	
	Xilaokou	XL74ZK1-4	Pyrite	11.2	
		XL74ZK1-7	Pyrite	11.2	
		XLK-1	Pyrite	11.0	
		XLK-2	Pyrite	11.4	
		XLK-5	Pyrite	9.8	
		XLK-6	Pyrite	12.6	
	Qianchuiliu	ZK3201-64	Pyrite	11.2	Han XM et al., 2023
		ZK3201-97	Pyrite	11.2	
		ZK3201-128	Pyrite	10.3	
		ZK3201-131	Pyrite	12.4	
		ZK3201-338	Pyrite	11.5	
		ZK3201-340	Pyrite	10.1	
		ZK3201-343	Pyrite	10.9	
		ZK1603-391	Pyrite	10.8	
		ZK1603-393	Pyrite	10.8	
		ZK1603-395	Pyrite	10.6	
		ZK1603-401	Pyrite	10.3	
		ZK1603-403	Pyrite	11.1	
		ZK1603-405	Pyrite	10.9	
		ZK1603-407	Pyrite	11.1	
		ZK1603-409	Pyrite	11.2	
		ZK1603-411	Pyrite	11.4	
		ZK1603-413	Pyrite	10.9	

hosted fluid inclusions exhibit ^{3}He, ^{4}He, ^{40}Ar, and $^{40}Ar^{*}$ contents ranging from 0.97×10^{-1} cm^3STP/g to 34.05×10^{-13} cm^3STP/g, from 0.89×10^{-7} cm^3STP/g to 22.93×10^{-7} cm^3STP/g, from 3.35×10^{-7} cm^3STP/g to 64.29×10^{-7} cm^3STP/g, and from 1.69×10^{-7} cm^3STP/g to 40.78×10^{-7} cm^3STP/g, respectively, with $^{3}He/^{4}He$, R/Ra, and $^{40}Ar/^{36}Ar$ ratios varying from 0.43×10^{-6} to 2.39×10^{-6}, from 0.31 to 1.71, and from 367.00 to 2112.00, sequentially (n=16). For the pyrite-bearing carbonate vein-type gold deposits, pyrite-hosted fluid inclusions manifest ^{3}He, ^{4}He, ^{40}Ar, and $^{40}Ar^{*}$ contents ranging from 0.12×10^{-13} cm^3STP/g to 5.71×10^{-13} cm^3STP/g, from 0.12×10^{-7} cm^3STP/g to 6.07×10^{-7} cm^3STP/g, from 0.54×10^{-7} cm^3STP/g to 14.79×10^{-7} cm^3STP/g, and from 0.06×10^{-7} cm^3STP/g to 7.15×10^{-7} cm^3STP/g, respectively, with $^{3}He/^{4}He$, R/Ra, and $^{40}Ar/^{36}Ar$ ratios varying from 0.17×10^{-6} to 1.75×10^{-6}, from 0.12 to 1.25, and from 328.50 to 929.00, respectively (n=10).

5. Discussion

5.1. Comparison between altered rock- and pyrite-bearing carbonate vein-type gold deposits

The northeastern margin of the Jiaolai Basin hosts relatively complex geological structures. The Cretaceous sedimentary strata in this region, along with the adjacent basement metamorphic rocks, Jurassic Queshan pluton, Cretaceous Yuangezhuang pluton, and related fault structures, jointly constitute the Queshan metamorphic core complex. This metamorphic core complex exhibits a three-layer structure consisting hanging wall, footwall, and the portion between them, typical of Cordilleran metamorphic core complexes. Specifically, the hanging wall of the Queshan metamorphic core complex is composed of Cretaceous sedimentary strata and Paleoproterozoic basement, its

Table 6. Lead isotopic composition of gold deposits on the northeastern margin of the Jiaolai Basin.

Deposit type	Gold deposit	Sample	Mineral	$^{206}Pb/^{204}Pb$	$^{207}Pb/^{204}Pb$	$^{208}Pb/^{204}Pb$	References
Alteration type	Songjiagou (Fayunkuang)	Fa5	Pyrite	17.312	15.558	37.974	Zeng QD et al., 2002
		F8	Pyrite	17.249	15.506	37.890	
		Fa9	Pyrite	17.404	15.513	38.120	
		Fa9-2	Pyrite	17.088	15.405	37.544	
		Fa9-5	Pyrite	17.325	15.627	38.243	
		Faw	Pyrite	17.190	15.447	37.754	
		Fy-1	Pyrite	17.123	15.422	37.724	
		Fy-2	Pyrite	17.225	15.492	37.851	
		Fy-4	Pyrite	16.987	15.307	37.406	
		Fa52	Pyrite	17.122	15.381	37.526	Zhang LC et al., 2001
		Fa8	Pyrite	17.159	15.412	37.621	
		Fa9	Pyrite	17.175	15.429	37.673	
		Fa9-2	Pyrite	17.183	15.437	37.702	
		Fa9-5	Pyrite	17.170	15.437	37.725	
		09FYK-1	Pyrite	17.186	15.450	37.750	Sun XL, 2013
		09FYK-4	Pyrite	17.196	15.433	37.807	
		09FYK-7	Pyrite	17.222	15.474	37.895	
	Pengjiakuang	−	Pyrite	17.147	15.442	37.765	Zhang LC et al., 2002b
		−	Pyrite	17.125	15.402	37.678	
		−	Pyrite	17.198	15.376	37.447	
		−	Pyrite	16.953	15.348	37.359	
		−	Pyrite	17.142	15.426	37.740	
		−	Pyrite	16.920	15.350	37.430	Sun FY et al., 1995
		−	Pyrite	17.259	15.613	38.020	
		09PJK-8	Pyrite	17.201	15.455	37.806	Sun XL, 2013
		09PJK-10	Pyrite	17.178	15.454	37.773	
		09PJK-17	Pyrite	17.176	15.468	37.798	
		09PJK-18	Pyrite	17.175	15.454	37.755	
	Tudui-Shawang	TK1	Pyrrhotite	17.242	15.454	37.878	Li HM et al., 2010
		TK4	Pyrrhotite	17.862	15.451	37.704	
		K2	Pyrite	17.124	15.413	37.616	
		K3	Pyrite	17.155	15.447	37.755	
		SK1	Pyrite	17.079	15.359	37.552	
		SK3	Pyrite	17.248	15.433	37.877	
		SK4	Pyrite	17.197	15.417	37.785	
		SK5	Pyrite	17.232	15.431	37.858	
		09TD-5	Pyrite	17.176	15.471	37.840	Sun XL, 2013
		09TD-6	Pyrite	17.194	15.464	37.871	
		09TD-8	Pyrite	17.159	15.447	37.654	
		09TD-9	Pyrite	17.172	15.454	37.769	
		09TD-15	Pyrite	17.163	15.458	37.776	
		09TD-19	Pyrite	17.159	15.449	37.778	
		09SW-1	Pyrite	17.204	15.444	37.829	
		09SW-4	Pyrite	17.246	15.463	37.989	
		09SW-5	Pyrite	17.243	15.452	37.831	
		09SW-8	Pyrite	17.282	15.455	37.947	
		09SW-10	Pyrite	17.446	15.475	38.122	
	No. 18 Xilaokou vein	B04	Pyrite	17.193	15.439	37.816	
		B21	Pyrite	17.202	15.456	37.726	
		B30	Pyrite	17.235	15.461	37.845	
		B31	Pyrite	17.161	15.446	37.797	
		B36	Pyrite	17.342	15.484	38.117	
		B39	Pyrite	17.343	15.463	38.099	
		B40	Pyrite	17.353	15.470	38.152	
		B42	Pyrite	17.456	15.504	38.563	
		B47	Pyrite	17.324	15.462	38.280	

Table 6. (*Continued*)

Deposit type	Gold deposit	Sample	Mineral	$^{206}Pb/^{204}Pb$	$^{207}Pb/^{204}Pb$	$^{208}Pb/^{204}Pb$	References
		B48	Pyrite	17.458	15.479	38.596	
		B49	Pyrite	17.359	15.479	37.995	
Pyrite-bearing carbonate vein type	Liaoshang	09LS-2	Pyrite	17.157	15.459	37.842	
		09LS-4	Pyrite	17.125	15.467	37.786	
		09LS-5	Pyrite	17.248	15.455	37.904	
		SD17-28B1	Pyrite	17.159	15.442	37.900	Li JJ et al., 2020
		SD17-29B1-1	Pyrite	17.182	15.441	38.099	
		SD17-29B1-1a	Pyrite	17.183	15.444	38.089	
		SD17-29B1-2	Pyrite	17.187	15.466	38.190	Bo JW et al., 2021
		SD17-30B1	Pyrite	17.394	15.474	38.447	
		LS-01	Pyrite	17.316	15.475	37.883	
		LS-02	Pyrite	17.576	15.503	38.205	
		LS-03	Pyrite	17.106	15.435	37.750	
		LS-04	Pyrite	17.260	15.465	37.827	
		LS-05	Pyrite	17.317	15.486	38.013	
		LS-06	Pyrite	17.282	15.460	37.910	
		6474	Pyrite	17.156	15.449	37.819	
		H179	Pyrite	17.137	15.443	37.794	
		H173	Pyrite	17.222	15.470	37.947	
		17B25	Pyrite	17.100	15.441	37.798	
		B23	Pyrite	17.027	15.454	37.706	
		17B26	Pyrite	17.151	15.498	38.017	
		LS-1	Pyrite	17.319	15.496	37.999	Liang H et al., 2022
		LS-3	Pyrite	17.426	15.483	38.240	
		LS-4	Pyrite	17.253	15.465	37.729	
		LS-5	Pyrite	17.658	15.516	38.341	
		LS-6	Pyrite	17.202	15.472	37.840	
		LS-9	Pyrite	17.955	15.540	38.171	
	Xilaokou	XL74ZK1-4	Pyrite	17.261	15.478	37.993	
		XL74ZK1-7	Pyrite	17.224	15.479	37.844	
		XLK-1	Pyrite	17.206	15.457	37.783	
		XLK-2	Pyrite	17.427	15.498	37.886	
		XLK-5	Pyrite	17.240	15.474	37.777	
		XLK-6	Pyrite	17.798	15.577	38.304	
	Qianchuiliu	ZK1603-391	Pyrite	17.149	15.482	37.860	Han XM et al., 2023
		ZK1603-392	Pyrite	17.178	15.498	37.917	
		ZK1603-393	Pyrite	17.941	15.540	38.432	
		ZK1603-394	Pyrite	17.544	15.515	38.000	
		ZK1603-395	Pyrite	17.390	15.497	37.995	
		ZK1603-399	Pyrite	18.625	15.618	38.626	
		ZK1603-401	Pyrite	17.753	15.535	38.227	
		ZK1603-402	Pyrite	17.953	15.555	38.488	
		ZK1603-403	Pyrite	18.886	15.677	39.676	
		ZK1603-404	Pyrite	18.797	15.645	39.185	
		ZK1603-407	Pyrite	18.019	15.566	38.600	
		ZK1603-408	Pyrite	18.059	15.566	39.527	
		ZK1603-411	Pyrite	18.474	15.644	40.073	
		ZK1603-412	Pyrite	17.790	15.562	38.756	
		ZK1603-413	Pyrite	18.552	15.613	39.395	

footwall consists of Jurassic intrusions, and the portion between them is a dominant detachment fault (Sun FY et al., 1995). All gold deposits discovered in this region occur within the dominant detachment fault zone and its secondary tectonic zones in the hanging wall, with no gold deposits having been identified in the footwall. The gold deposits occurring in various tectonic positions and surrounding rocks show different ore characteristics. Based on this finding, previous researchers have proposed various mineralization types and deposit types, such as fracture-zone altered rock-type gold deposits (Pengjiakuang type) occurring within a dominant detachment fault (the Pengjiakuang fault), altered

Table 7. Helium-argon isotopic compositions of gold deposits on the northeastern margin of the Jiaolai Basin.

Gold deposit	Mineral	$^4He/\times10^{-7}$	$^3He/\times10^{-13}$	$^3He/^4He/\times10^{-6}$	$^{40}Ar/\times10^{-7}$	$^{36}Ar/\times10^{-7}$	$^{40}Ar^*/\times10^{-7}$	$^{40}Ar/^{36}Ar$	R/Ra	References
Tudui	Pyrite	5.48	11.95	2.18	14.84	0.019	9.28	796.00	1.56	Tan J et al., 2018
	Pyrite	5.57	4.51	0.81	31.20	0.064	12.07	486.00	0.58	
	Pyrite	1.27	2.67	2.10	3.35	0.006	1.69	604.00	1.50	
	Pyrite	5.80	5.22	0.90	8.92	0.013	5.02	682.00	0.64	
Shawang	Pyrite	19.07	8.20	0.43	12.40	0.014	8.20	880.00	0.31	
	Pyrite	5.37	6.55	1.22	15.99	0.044	3.02	367.00	0.87	
	Pyrite	3.84	9.18	2.39	11.50	0.010	8.54	1158.00	1.71	
	Pyrite	1.31	2.08	1.59	6.17	0.010	3.32	645.00	1.14	
Dongliujia	Pyrite	12.02	6.25	0.52	10.52	0.010	7.53	1048.00	0.37	
	Pyrite	5.93	5.57	0.94	16.13	0.017	11.11	958.00	0.67	
	Pyrite	13.58	8.28	0.61	13.43	0.013	9.53	1025.00	0.44	
	Pyrite	22.93	16.97	0.74	22.91	0.021	16.54	1072.00	0.53	
	Pyrite	17.55	34.05	1.94	64.29	0.079	40.78	815.00	1.39	
Longkou	Pyrite	0.89	0.97	1.09	7.33	0.013	3.38	553.00	0.78	
	Pyrite	10.05	11.66	1.16	30.27	0.014	26.00	2112.00	0.83	
	Pyrite	10.40	8.01	0.77	14.93	0.027	6.85	551.00	0.55	
Liaoshang	Pyrite	2.98	4.68	1.57	7.57	0.008	5.14	929.00	1.12	
	Pyrite	3.26	5.71	1.75	14.79	0.026	7.15	577.00	1.25	
	Pyrite	1.85	1.81	0.98	5.74	0.012	2.11	471.00	0.70	
	Pyrite	6.07	2.49	0.41	4.94	0.009	2.40	581.00	0.29	
	Pyrite	0.12	0.12	0.97	0.54	0.002	0.06	331.30	0.70	Xu YW et al., 2023
	Pyrite	3.24	0.54	0.17	1.13	0.002	0.46	495.80	0.12	
	Pyrite	0.15	0.17	1.14	0.61	0.002	0.06	328.50	0.81	
	Pyrite	0.17	0.17	1.00	0.69	0.002	0.12	358.10	0.71	
	Pyrite	1.28	0.48	0.38	1.04	0.002	0.39	474.50	0.27	
	Pyrite	1.69	0.87	0.51	1.87	0.004	0.79	511.30	0.37	

Note: $R = {}^3He/{}^4He$ ratio; Ra = atmospheric $^3He/^4He$ ratio; 1 Ra = 1.4×10^{-6}; $^{40}Ar^*$ = radiogenic excess Ar after deducting ^{40}Ar; mHe (%) is the mantle-derived He isotope value; $mHe(\%) = (R_{sample}-R_{crust})/(R_{mantle}-R_{crust})$, R_{mantle} = 6.5 Ra, R_{crust} = 0.02 Ra; $^{40}Ar^*(\%) = [(^{40}Ar/^{36}Ar)_{sample}-295.5]/(^{40}Ar/^{36}Ar)_{sample}\times100$ (Stuart FM et al., 1995); unit: cm^3STP/g.

conglomerate-type gold deposits (Songjiagou type) occurring in secondary tectonic zones in the hanging wall of a dominant detachment fault, and pyrite-bearing carbonate vein-type gold deposits (Liaoshang type). Both the altered conglomerate- and the fracture-zone altered rock-type gold deposits are characterized as the altered rock type, with mineralization dominated by metasomatism. Their hydrothermal alterations associated with gold mineralization are represented by pyritization, silicification, and phyllic alteration, suggesting acidic fluid environments. Their gold-bearing minerals include pyrite (pyrrhotite for the Tudui deposit) and quartz, and their gold minerals are dominated by electrum. The altered conglomerate-type gold deposits exhibit extensive mineralized alterations but small single-orebody scales, low gold grades, and low fineness. In contrast, the fracture-zone altered rock-type gold deposits manifest large alteration zones and moderate orebody scales, gold grades, and fineness. For the pyrite-bearing carbonate vein-type gold deposits, their mineralization is dominated by filling. Their hydrothermal alterations associated with gold mineralization comprise pyritization and carbonatization, suggesting alkaline fluid environments. Their gold-bearing minerals consist of pyrite and dolomite, and their gold minerals are dominated by electrum. Their orebodies display large sizes, high gold grades, and high fineness (Table 8). The pyrite-bearing carbonate vein type is identified as the most significant type of gold deposits on the northeastern margin of the Jiaolai Basin. Since the discovery of the Liaoshang super-large gold deposit in 2014, the Xilaokou large and Qianchuiliu medium-sized gold deposits have been discovered successively, with cumulative proven gold resources exceeding 141 t, which account for above 60% of the total proved gold resources in this region (Fig. 15), signifying a breakthrough in ore prospecting in a short period. As a result, the pyrite-bearing carbonate vein-type gold deposits have considerable potential for the prospecting of super-large gold deposits following the fracture-zone altered rock-type (Jiaojia-type) gold deposits and the quartz vein-type (Linglong type) gold deposits in Jiaodong.

5.2. Metallogenic epochs

Using different methods, previous studies conducted isotopic dating on altered minerals or post-mineralization intermediate-mafic veins in different gold deposits on the northeastern margin of the Jiaolai Basin (Table 9), determining that the hydrothermal minerals were formed at 128.49–100.59 Ma, specifically at 119–116 Ma (Fig. 16). Due to significantly varying isotopic age results, the gold metallogenic epochs remain debated. As per the younger isotopic ages of the Liaoshang, Pengjiakuang, and Tudui gold

Table 8. Primary geological characteristics of different types of gold deposits on the northeastern margin of the Jiaolai basin.

Item	Altered conglomerate type	Fracture-zone altered rock type	Pyrite-bearing carbonate vein type
Deposit name	Songjiagou	Pengjiakuang	Liaoshang
Structural type	Dense fracture zone	Nearly EW-directed strike-slip structure	NE-directed strike-slip structure
Ore-bearing surrounding rocks	Conglomerates dominated by feldspar gravels such as variegated rocks, plagioclase gneisses, amphibolites, and monzogranites	Monzogranites in the footwall and dolomitic marbles in the hanging wall	Dolomitic marbles in the footwall and monzogranites in the hanging wall
Ore type	Altered conglomerates	Altered tectonic breccias, and fracture-zone altered rocks	Pyrite-bearing carbonate veins
Mineralization mode	Metasomatism	Metasomatism	Filling
Alteration	Silicification, beresitization	Silicification, beresitization	Carbonation
Fluid property	Acidic fluids	Acidic fluids	Alkaline fluids
Gold-bearing mineral	Pyrite, quartz	Pyrite, quartz	Pyrite, dolomite
Average gold grade	Low	Medium	High
Gold fineness	745	860	912
Thickness	Small and unstable	Medium and highly variable	Large and stable
Single-orebody scale	Small	Medium	Large
Deposit size	Large	Large	Giant
Deposit type	Songjiagou type	Pengjiakuang type	Liaoshang type

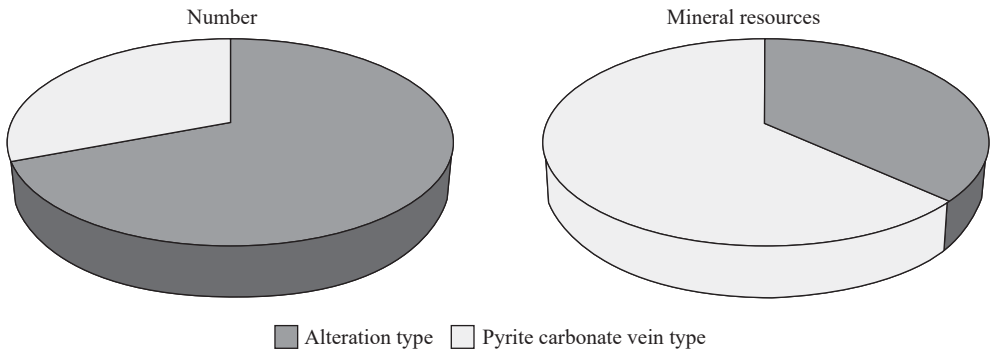

Fig. 15. Numbers and resources of gold deposits on the northeastern margin of the Jiaolai Basin (numbers of deposits refer to the gold deposits participating in the resource statistics).

Table 9. Metallogenic ages of gold deposits on the northeastern margin of the Jiaolai Basin.

Deposit	Mineral	Method	Age/Ma	Reference
Songjiagou	Pyrite	Rb-Sr	128.49±7.2	Zhang LC et al., 2002a
Pengjiakuang	Quartz in the main metallogenic stage	^{39}Ar-^{40}Ar	117.39	Zhang LC et al., 2002a
Pengjiakuang	Alteration mineral sericite	K-Ar	100.59±1.96	Zhang LC et al., 2002a
No. 18 Xilaokou vein	Alteration mineral sericite	^{39}Ar-^{40}Ar	116.54±0.61	Sun XL, 2013
Guocheng	Pyrite	Rb-Sr	119±2	Li J et al., 2020
Tudui-Shawang	Quartz-hosted fluid inclusions of gold ore	Rb-Sr	119±5	Li HM et al., 2010
Guocheng	Quartz-hosted fluid inclusions of gold ore	Rb-Sr	116.2±2.4	Tan J et al., 2015
Houkuang	Dolomite in pyrite-bearing carbonate veins	Sm-Nd	119±4.7	Ding ZJ et al., 2019
Houkuang	Pyrite in pyrite-bearing carbonate veins	Rb-Sr	118.6±3.8	Ding ZJ et al., 2019
Liaoshang	Pyrite in pyrite-bearing carbonate veins	Rb-Sr	105.5±9.0	Li JJ et al., 2020
Liaoshang	Dolomite in pyrite-bearing carbonate veins	Sm-Nd	119.0±1.2	Ding ZJ et al., 2021
Liaoshang	Pyrite in pyrite-bearing carbonate veins	Rb-Sr	117.9±2.4	Ding ZJ et al., 2021
Guocheng	Zircon in post-mineralization diorite porphyrite veins	U-Pb	116±1	Tan J et al., 2008
Guocheng	Zircon in post-mineralization monzonite porphyry veins	U-Pb	114±2	Tan J et al., 2008

deposits, some researchers considered that these gold deposits were formed at approximately 100–110 Ma (Sun FY et al., 1995; Yang JZ et al., 2001; Zhang PP et al., 2018; Li JJ et al.，2020), significantly younger than the gold deposits in the Jiaoxibei area. Some other researchers posited that the metallogenic epochs of gold deposits on the northeastern

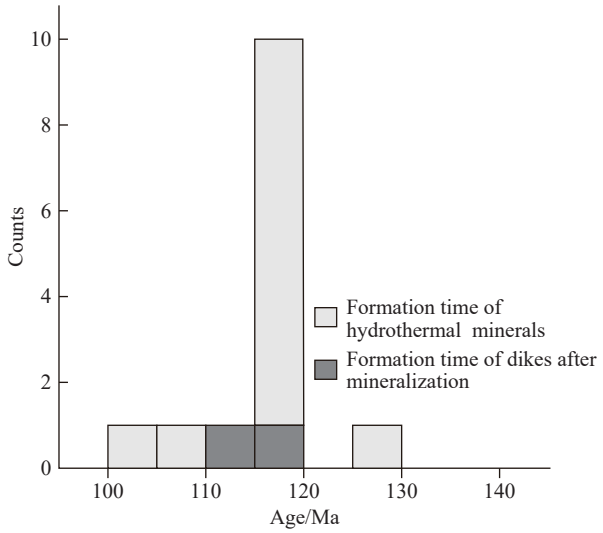

Fig. 16. Formation epochs of hydrothermal minerals and post-mineralization veins in gold deposits on the northeastern margin of the Jiaolai Basin.

margin of the Jiaolai Basin is generally consistent with those (120±10 Ma) in the Jiaodong Peninsula (Zhang LC et al., 2003; Tan J et al., 2015). Given that the low accuracy of K-Ar dating and the prolonged existence of pyrite pose challenges to the selection of accurate minerals in the metallogenic stage for age testing, this study held that the previously tested ages of carbonate minerals, sericite Ar-Ar, and quartz inclusions in metallogenic stages can indicate the gold metallogenic epoch, that is from 119 Ma to 116 Ma. Tan J et al. (2008) performed zircon U-Pb dating of post-mineralization diorite porphyrites and monzonite porphyries in the Guocheng gold deposit, concluding that veins in the deposit were formed at 114–116 Ma. This result constrains the lower limit of the gold metallogenic epochs and is consistent with the tested lower limit of altered minerals' ages in the gold deposits. Therefore, it can be inferred that the metallogenic epochs of gold deposits on the northeastern margin of the Jiaolai Basin are 116–119 Ma, which is consistent with the formation epochs (concentrated at 120±5 Ma) of the Sanshandao (Hu FF et al., 2013), Jiaojia (Chen YJ et al., 2004; Fan HR et al., 2005), Dayingezhuang (Liu XD et al., 2022), and Daliuhang (Feng K et al., 2020) gold deposits in the Jiaoxibei metallogenic region (Zhai MG, et al., 2004; Song MC et al., 2023). With the continued enhancement of testing techniques, some researchers have limited the metallogenic epochs of gold deposits in the Jiaoxibei area to 120±2 Ma using *in situ* U-Pb dating of hydrothermal monazite in gold mineralized alteration zones (Deng J et al., 2020a; Zhang L et al., 2020). Based on a comprehensive analysis, this study concluded that the metallogenic epochs of gold deposits on the northeastern margin of the Jiaolai Basin are contemporaneous with or slightly later than that in the Jiaoxibei area. Their metallogenic epochs are consistent with those of the Weideshanian intrusions with a crust-mantle mixing origin (Zhang T et al., 2007; Zhou JB et al., 2016; He DY et al., 2020; Song MC et al., 2015, 2020a), such as 117.7±2.9 Ma for the Yashan pluton in Qixia (Zhang T et al., 2007), 118.10±0.66 to 118.80±0.67 Ma for the Yuangezhuang pluton in Muping (Zou J et al., 2021), and 119±1 Ma for the Haiyang pluton (Ren TL et al., 2021) on the northeastern margin of the Jiaolai Basin. Moreover, their metallogenic epochs align with those of the Qingshan Group volcanic rocks with the same origin in this region (123.6±3.1 Ma to 98.0±1.0 Ma, Kuang YS et al., 2012; Song MC et al., 2018; He DY et al., 2020). These results suggest that the gold mineralization of these deposits occurred under the background of crust-mantle interactions.

5.3. Sources of ore-forming fluids and materials

Extensive studies have been conducted on the sources of ore-forming fluids in gold deposits in Jiaodong. Many researchers considered that the ore-forming fluids were dominated by mantle-derived mafic magmatic water during the mineralization, mixed with meteoric or formation water in the late metallogenic stage (Fan HR et al., 2005; Mao JW et al., 2008; Deng J et al., 2015b; Wen BJ et al., 2016; Liu JC et al., 2017; Cai YC et al., 2018; Yu XF et al., 2019). Some held that the ore-forming fluids were composed primarily of metamorphic water, potentially mixed with magmatic and meteoric water (Yang LQ et al., 2014; Chai P et al., 2017; Wei YJ et al., 2019; Guo LN et al., 2020). Deng J et al. (2023) pointed out that during the Early Cretaceous, the Jiaolai Basin, under continuous sedimentation, did not experience significant regional metamorphic activity and thus could not produce metamorphic fluids. Moreover, the Precambrian high-grade metamorphism and the Triassic ultrahigh-pressure metamorphism, occurring much earlier than gold mineralization, were difficult to provide metamorphic fluids. The hydrogen-oxygen isotopes of samples of hydrothermally altered minerals like quartz, sericite, and dolomite, collected from the gold deposits on the northeastern margin of the Jiaolai Basin, reveal that the ore-forming fluids' sources have multiple origins and complexity. As illustrated by the H-O isotopic composition diagram, except for some samples falling into the zones of primary magmatic water and primary mantle water, most of them fell between the zones of formation water, primary mantle water, and meteoric water, aligning toward the primary magmatic water zone or the primary mantle water zone (Fig. 17). The transition of the data points' linear arrangement from primary magmatic water zone toward the formation water zone suggests that basin formation water involved in the metallogenic process on the northeastern margin of the Jiaolai Basin. Therefore, the metallogenic fluids in this region are basin-affinity.

For the gold deposits on the northeastern margin of the Jiaolai Basin, the carbon-oxygen isotopic compositions of hydrothermal minerals like calcite, dolomite, and siderite exhibit $\delta^{13}C_{PDB}$ values ranging from −6.0‰ to 1.70‰ (average: −3.7‰), suggesting overall $\delta^{13}C$ depletion. The altered rock- and pyrite-bearing carbonate vein-type gold deposits present some differences in carbon isotopic

composition, displaying $\delta^{13}C_{PDB}$ values significantly ranging from −5.6‰ to 1.7‰ (average: −1.9‰) and from −6.0‰ to −2.9‰ (average: −4.3‰; serious $\delta^{13}C$ depletion), respectively. Overall, the carbon isotopic composition of gold deposits in this region fell within the carbon isotopic composition ranges of a magmatic system's total carbon (−9‰ to −3‰ and −5‰ to +2‰; Hoefs J, 1997), mantle-derived Mengyin diamonds (−6.4‰–−0.4‰; Zhang HF et al., 2009), and marbles (−5.7‰ to +3.8‰; Luo ZK et al., 2002) (Fig. 18). Compared to the Jingshan Group marbles with marine carbonate characteristics (0.24‰–1.70‰; Yang MZ et al., 1996; Zhang LC et al., 2002b), the gold deposits in the region are depleted in $\delta^{13}C$. The gold deposits in the region showed $\delta^{18}O_{V\text{-}SMOW}$ values ranging from 6.9‰ to 11.4 ‰ (n=37) primarily and from 12.3‰ to 16.6‰ partially (n=4), close to those of magmatic carbonate rocks (5.5‰ to 14.5‰; Deines P et al., 1973). However, they show $\delta^{18}O$ depletion to varying degrees compared to the Jingshan Group marbles (11.93‰ to 16.6‰; Zhang LC et al., 2002b). As illustrated by the $\delta^{13}C$-$\delta^{18}O$ diagram (Fig. 19), the samples from gold deposits on the northeastern margin of the Jiaolai Basin were concentrated in the magmatic rock zone, suggesting that the carbon sources of the ore-forming fluids are primarily associated with deep magmatic-hydrothermal fluids. The $^3He/^4He$ ratios of the pyrite-hosted fluid inclusions range from 0.17 Ra to 2.39 Ra, higher than the characteristic values of

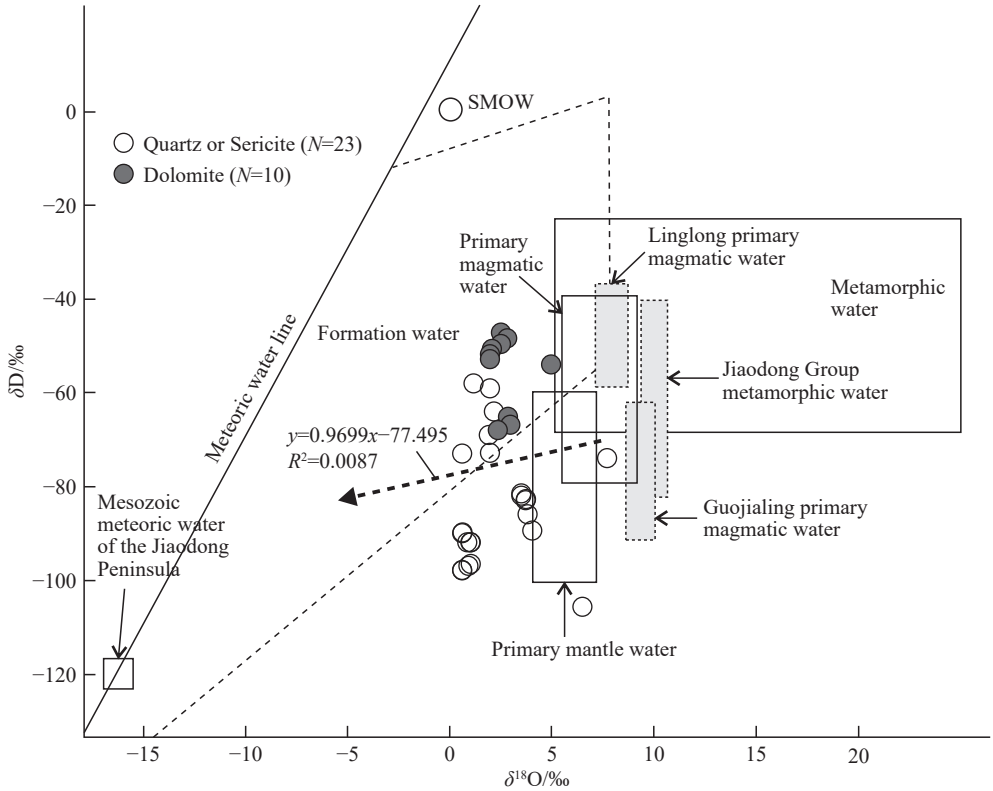

Fig. 17. δD *vs.* $\pm^{18}O$ diagram of ore-forming fluids in gold deposits on the northeastern margin of the Jiaolai Basin.

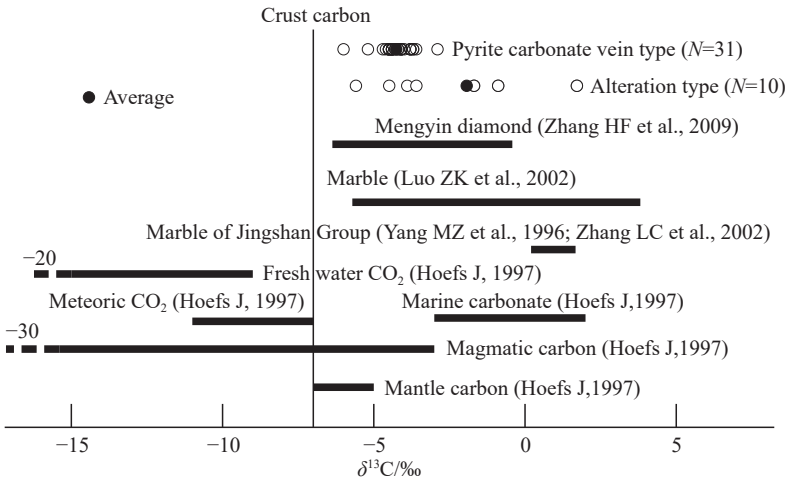

Fig. 18. Plot showing the $\delta^{13}C$ values of gold deposits on the northeastern margin of the Jiaolai Basin and associated carbon reservoirs.

continental crustal fluids (0.01 Ra to 0.05 Ra; Stuart FM et al., 1994, 1995) but lower than those of the mantle (6 Ra to 9 Ra; Dunai TJ and Porcelli D, 2002), implying a mixed mantle-crustal composition. As shown in Fig. 20, the He-Ar isotope data all fell between the mantle and crustal fluid zones, presenting a trend of evolution from mantle helium (He) to crustal He. Based on the binary model for crust-mantle mixing (Stuart FM et al., 1995), it was calculated that the mantle-derived He accounted for 1.56%–26.35% (average: 11.82%; n=26) of pyrite in the gold deposits on the northeastern margin of the Jiaolai Basin. This suggests that a large quantity of mantle-derived fluids involved in the metallogenic process and that the gold mineralization was associated with crust-mantle interactions.

In sum, the ore-forming fluids of the gold deposits on the northeastern margin of the Jiaolai Basin and those in the basement uplift zone of Jiaodong (Mao JW et al., 2008; Yan YT, 2012; Zhang YQ et al., 2012; Xue JL et al., 2013; Shen JF et al., 2013) share similar characteristics, all originating from mixed sources. In the early stage, all of them were derived from magmatic water sourcing from crust-mantle interactions. In the early stages, they were mixed with meteoric water in the basement uplift zone and a large amount of basin formation water on the northeastern margin of the Jiaolai Basin. Hence, the ore-forming fluids of gold deposits on the northeastern margin of the Jiaolai Basin are significantly basin-affinity.

The gold deposits on the northeastern margin of the Jiaolai Basin showed significantly varying sulfur isotope values. Their δ^{34}S values range from +3.4‰ to +16.2‰ (average: 9.6‰), concentrated between +7.5‰ and +11.5‰ (Fig. 21) and higher than those of meteorites and basalts (Hoefs, 1997). The altered rock- and pyrite-bearing carbonate vein-type gold deposits share almost the same sulfur isotope characteristics (Fig. 22). Their δ^{34}S values resemble those of the Jingshan Group metamorphic rocks (Zhang ZR et al., 1999), Linglong granites (Huang DY, 1994), Guojialing granites (Li ZL et al., 1993), and intermediate-mafic veins in Jiaodong (Huang DY, 1994) and slightly exceed those of the Sanshandao (Guo CY, 2009; Jiang XH et al., 2011) and Jinqingding gold deposits (Ying HL, 1994; Hu FF, 2006; Li XF, 2011) in the basement uplift zones. The sulfur isotope characteristics indicate that sulfur in the gold deposits on the northeastern margin of the Jiaolai Basin and even in Jiaodong possibly originated from the deep magmatic-hydrothermal fluids. The mixing with large quantities of crustal materials caused the fractionation of sulfur isotopes, ultimately leading to high δ^{34}S values. For gold deposits on the northeastern margin of the Jiaolai Basin, their ore-hosting surrounding rocks comprise the Jingshan Group with high δ^{34}S values. In contrast, for the gold deposits in the basement uplift zone, their ore-hosting surrounding rocks contain Jiaodong Group metamorphic rocks with low δ^{34}S values. Therefore, the former has higher δ^{34}S values than the latter.

As shown in the ^{207}Pb/^{204}Pb *vs.* ^{206}Pb/^{204}Pb diagram of sulfides for tectonic setting discrimination (Fig. 23), the distribution of samples' projected points suggests the characteristics of crust-mantle mixing-derived lead, which are similar to the lead isotope characteristics of gold deposits and lamprophyres in Jiaodong (Hou ML et al., 2006). It can be inferred that the lead in the gold deposits on the northeastern margin of the Jiaolai Basin stemmed from crust-mantle mixing, correlating closely with deep magmatic activity

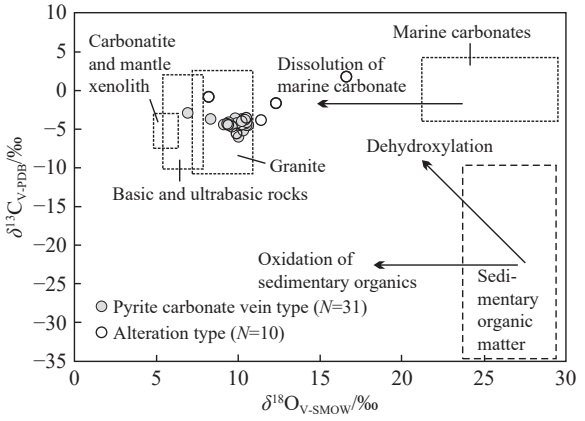

Fig. 19. $\delta^{13}C_{V\text{-}PDB}$ *vs.* $\delta^{18}O_{V\text{-}SMOW}$ diagram of ore-forming fluids of gold deposits on the northeastern margin of the Jiaolai Basin (after Liu JM et al., 1997).

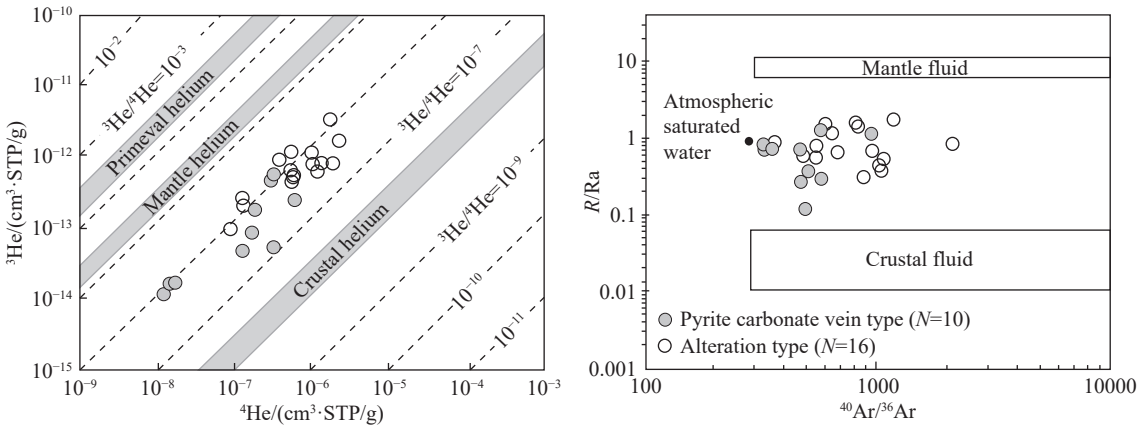

Fig. 20. He-Ar isotopic compositions of hydrothermal pyrite-hosted fluid inclusions of gold deposits on the northeastern margin of the Jiaolai Basin (fluid sources of major reservoirs after Mamyrin and Tolstikhin, 1984).

(Yang JZ et al., 2001; Li HM et al., 2010; Tan J et al., 2012; Yang QY et al., 2015). The distribution of Pb isotopes' projected points differed between the gold deposits of the altered rock type and the pyrite-bearing carbonate vein type. Specifically, the projected points of the former type were extensively distributed, beyond the part between the lower and upper crust evolutionary line, while those of the latter type were concentrated between the mantle and upper crust evolutionary lines. This difference may be attributed to the different metallogenic models of both types. The altered rock-type gold deposits primarily experienced metasomatic replacement of ore-hosting surrounding rocks by ore-forming fluids, resulting in the mixing of many crustal materials. In contrast, the mineralization of the pyrite-bearing carbonate vein-type gold deposits is dominated by filling, lacking metasomatic replacement of ore-hosting surrounding rocks. As a result, only a few crustal materials were mixed.

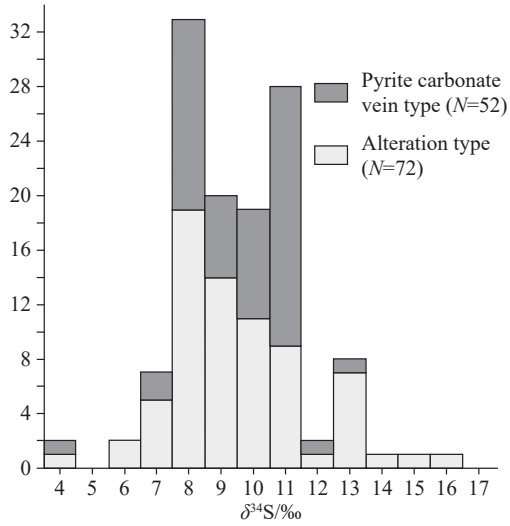

Fig. 21. Sulfur isotope histogram of gold deposits on the northeastern margin of the Jiaolai Basin.

The sources of ore-forming materials in gold deposits in Jiaodong are highly controversial. Some researchers posited that the Jiaodong Group metamorphic rocks serve as the material source of gold (Zhu FS, 1980; Yang MZ et al., 1996; Li SX et al., 2007), with partial ore-forming materials derived from deep-seated magmas (Wang YW et al., 2002; Yang LQ et al., 2014; Zhang C et al., 2014; Zhang RZ et al., 2016). Some scholars considered that it was difficult for the Precambrian metamorphic basement in Jiaodong to provide enormous ore-forming materials (Wang ZC et al., 2020, 2021). Instead, they correlated the sources of ore-forming materials with deep crust-mantle interactions, holding the prevalence of mantle sources (Sun FY et al., 1995; Li SR et al., 2014) or deep crust-mantle mixing sources (Fan HR et al., 2003; Mao JW et al., 2008; Deng J et al., 2015b, 2019, 2020a; Wang CM et al., 2015; Jiang YH et al., 2020; Li J et al., 2022). A third standpoint underscores that the underplating of mantle-derived mafic magmas led to the formation of gold sulfide cumulates in the lower crust (Xiong L et al., 2020; Wang QF et al., 2022; Dong LL et al., 2023) or that the enriched lithospheric mantle of the North China Craton, subject to subduction and metasomatism, formed reservoirs with high gold content (Deng J et al., 2020b, 2020c, 2023). As indicated by the comprehensive analysis in this study, the Pb isotopes of the gold deposits on the northeastern margin of the Jiaolai Basin exhibit crust-mantle mixing characteristics, and their high $\delta^{34}S$ values, similar to those of the ore-hosting surrounding rocks, primarily result from the contamination by crustal materials (Deng J et al., 2023). In other words, the ore-forming materials of the gold deposits partially originated from the mantle, mixed with crustal materials during fluid ascent and the metasomatic replacement of surrounding rocks. This process was coupled with the strong magmatism resulting from crust-mantle mixing in Jiaodong during the

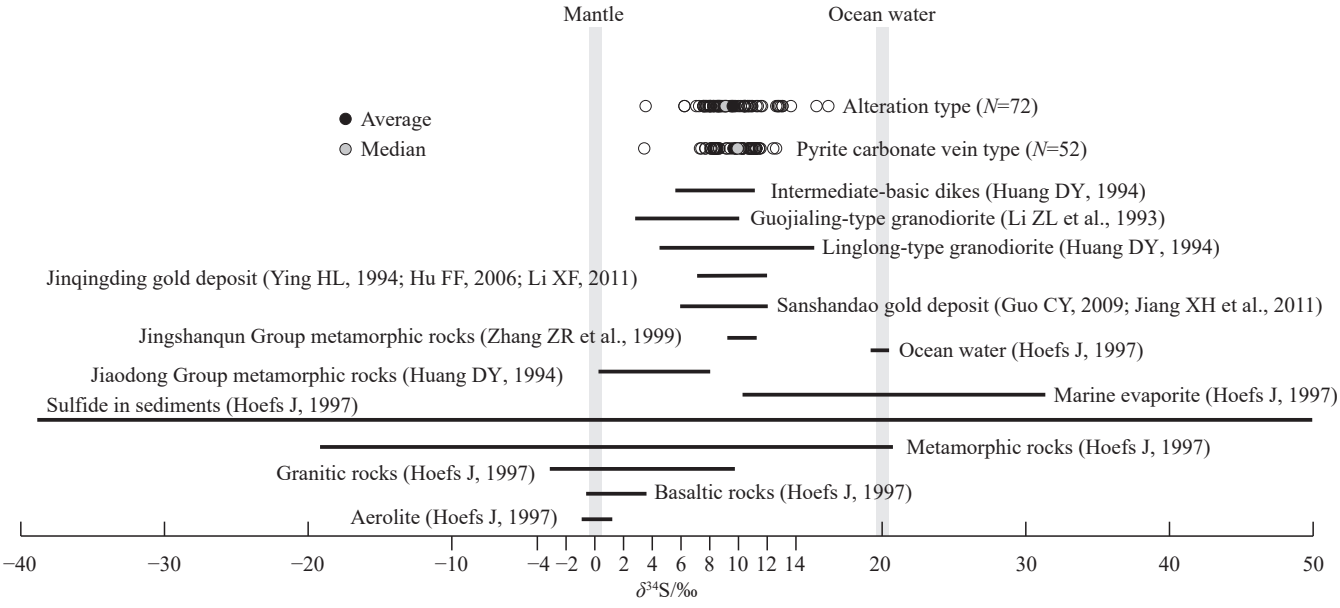

Fig. 22. Comparison of sulfur isotopic compositions between the gold deposits on the northeastern margin of the Jiaolai Basin and other gold deposits or different rocks.

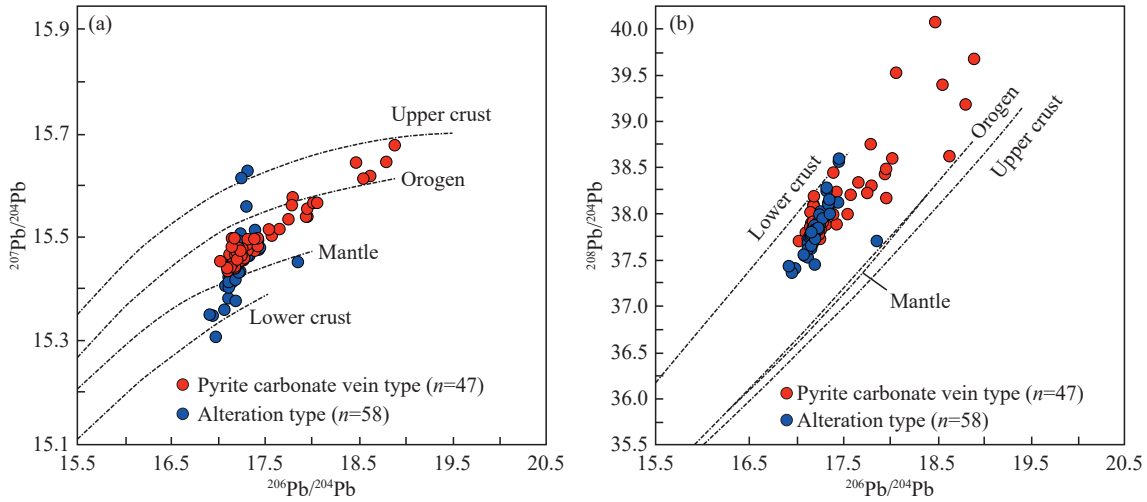

Fig. 23. $^{207}Pb/^{204}Pb$ *vs.* $^{206}Pb/^{204}Pb$ (a) and $^{208}Pb/^{204}Pb$ *vs.* $^{206}Pb/^{204}Pb$ (b) diagrams showing the lead isotopic compositions of gold deposits on the northeastern margin of the Jiaolai Basin (after Zartman RE and Doe BR, 1981).

Early Cretaceous (Zhou JB et al., 2016; He DY et al., 2020; Song MC et al., 2023), also suggesting that the formation of the gold deposits on the northeastern margin of the Jiaolai Basin is associated with crust-mantle interactions.

5.4. Mineralization modes

The gold deposits on the northeastern margin of the Jiaolai Basin were formed in the context of asthenospheric upwelling and extensive lithospheric thinning in eastern China during the Early Cretaceous. From 125 Ma to 115 Ma, the subduction direction of the Pacific Plate shifted from SEE to NWW, and the tectonic regime of the North China Craton underwent a major transition characterized by large-scale asthenospheric upwelling, lithospheric delamination and thinning, and intense crust-mantle interactions (Zhai MG et al., 2003; Wu FY et al., 2003; Deng JF et al., 2003; Xu WL et al., 2004; Xu YG et al., 2004; Zhou XH, 2006; Yan J and Chen JF, 2007; Ma L et al., 2014; Fan HR et al., 2016). In the Jiaodong Peninsula, asthenospheric upwelling caused the partial melting of the enriched mantle, producing mafic magmas and C-H-O fluids (Sun FY et al., 1995). Deep heat drove magmas and fluids to migrate upward and differentiate, leading to the formation of high-magnesium diorites (Song MC et al., 2020b), mafic veins, and mafic volcanic rocks (the Qingshan Group). As mantle-derived magmas ascended to the crustal floor, underplating occurred, inducing the partial melting of lower crustal materials. Then, crustal and mantle magmas were mixed, forming Weideshanian granites. Concurrently, the mantle-derived C-H-O fluids were mixed with the crust-derived fluids and materials during their ascent, forming the ore-forming fluids with the characteristics of crust-mantle mixing. During the Cretaceous, rapid magma uplift resulted in the formation of extensional structures including metamorphic core complexes (e.g., Queshan) and faulted basins in the shallow crust. Meanwhile, detachment faults emerged along the margin of the Jiaolai Basin and weak structural zones such as consolidated Jurassic granites and Paleoproterozoic Jingshan Group. As a result, a thermal uplifting-extension structural system was formed (Song MC et al., 2023). Driven by magmatic heat, the ore-forming fluids with the characteristics of crust-mantle mixing migrated to the shallow crust, where they were mixed with the basin formation water and some meteoric water, forming multi-source mixed ore-forming fluids. After migrating to the basin-margin detachment fault structural system, the ore-forming fluids accumulated and underwent mineralization. As revealed by the He isotopes of gold deposits on the northeastern margin of the Jiaolai Basin, mantle-derived He account for 4.50%–26.35% (average: 13.21%; n=16) of the altered rock-type gold deposits and 1.56%–19.21% (average: 9.60%; n=10) of the pyrite-bearing carbonate vein-type gold deposits. This suggests that more crustal materials were mixed into the ore-forming fluids of the pyrite-bearing carbonate vein-type gold deposits during crust-mantle interactions or ore-forming fluids ascending, Moreover, the Mg isotopes of dolomite in the pyrite-bearing carbonate vein-type gold deposits (Ji P, 2016) were principally derived from the Jingshan Group marbles. Therefore, the authors of this study hold that during the metallogenic process, the pyrite-bearing carbonate vein-type gold deposits might have received more components from the Jingshan Group marbles, leading to the formation of acidic fluids. In contrast, the altered rock-type gold deposits might have received more crustal sialic components, contributing to the formation of alkaline fluids. The differentiated gold mineralization between the two types of gold deposits was primarily attributable to the differences in the crustal components mixed into the ore-forming fluids under crustal-mantle interactions or those in surrounding rocks involved in water-rock reactions during the ascent of ore-forming fluids. Different ore-forming fluid environments created conditions for two different mineralization of both types of gold deposits, also leading to varying fineness of gold minerals (Fig. 24).

6. Conclusions

(i) The gold deposits on the northeastern margin of the

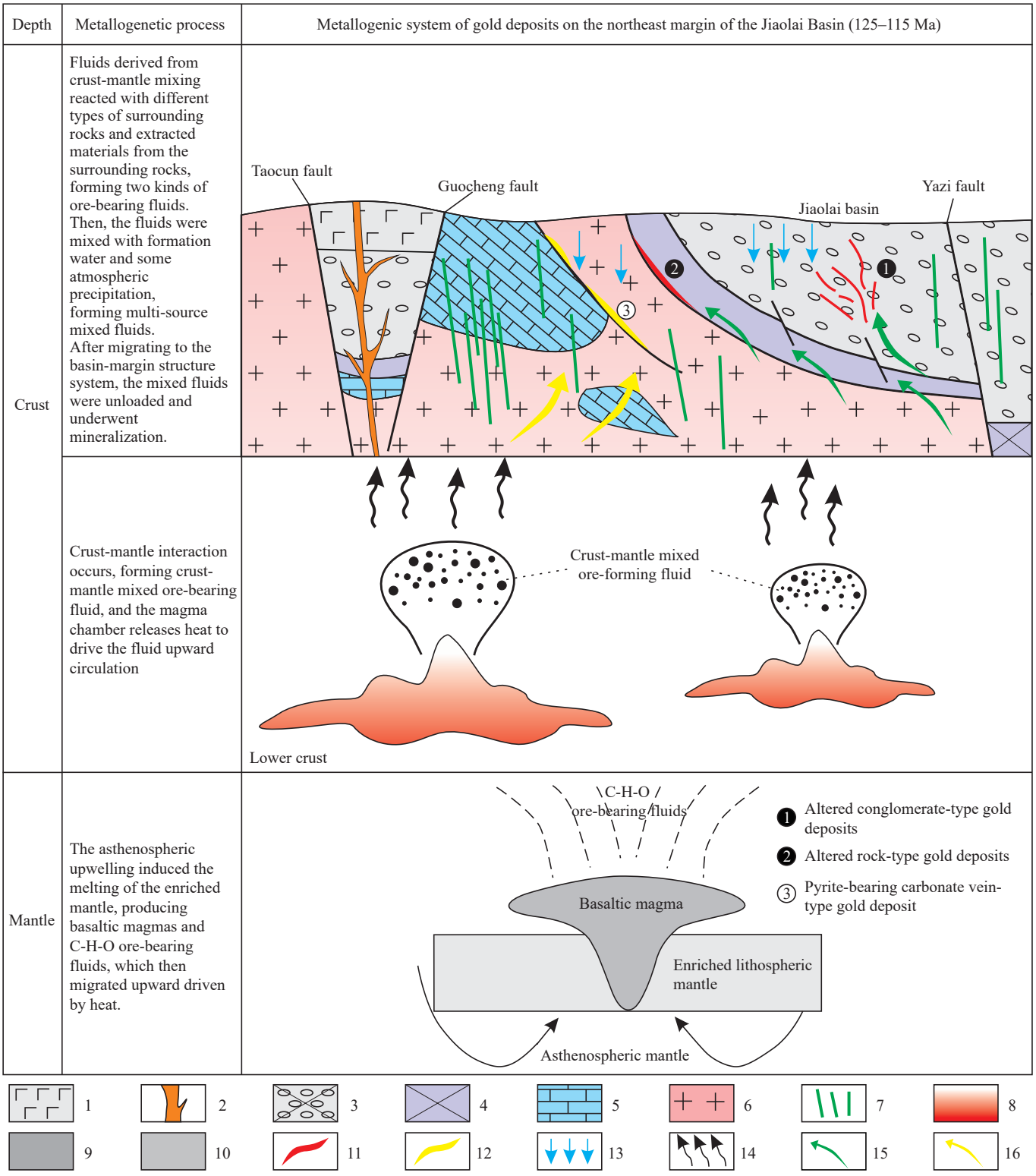

Fig. 24. Mineralization modes of gold deposits on the northeastern margin of the Jiaolai Basin. 1–Qingshan Group volcanic rock; 2–volcanic system; 3–Laiyang Group conglomerate; 4–Jingshan Group metamorphic granite and amphibolite; 5–Jingshan Group marble; 6–late Jurassic monzogranite; 7–intermediate-mafic vein; 8–magma chamber; 9–basaltic magma; 10–enriched lithospheric mantle; 11–altered rock-type gold deposit; 12–pyrite-bearing carbonate vein-type gold deposit; 13–stratum water and some meteoric water; 14–crust-mantle mixing-derived ore-forming fluids; 15–acidic ore-forming fluids; 16–alkaline ore-forming fluids.

Jiaolai Basin boast cumulative proven gold reserves of 223 t. Under the control of the dense fractures and the detachment structural system along basin margins, these deposits occur within the dominant detachment fault zone, as well as the secondary tectonic systems in the hanging wall of the dominant detachment fault zone, exhibiting two main mineralization types. The altered rock-type gold deposits, occurring in acidic fluid environments and undergoing mineralization dominated by metasomatism, show the development of silicification and phyllic alteration, with

pyrite and quartz acting as gold-bearing minerals. In contrast, the pyrite-bearing carbonate vein-type gold deposits occurred in alkaline fluid environments and experienced mineralization dominated by filling. They underwent carbonatization alteration, with gold-bearing minerals composed of pyrite and dolomite. Compared to the altered rock-type gold deposits, the pyrite-bearing carbonate vein-type gold deposits demonstrate larger scales, higher gold grades, and higher fineness.

(ii) The gold deposits experienced mineralization under the tectonic setting of crust-mantle interactions at 116–119 Ma. Their ore-forming fluids are both categorized as a CO_2-NaCl-H_2O fluid system rich in CO_2. The ore-forming fluids of the altered rock-type gold deposits are characterized by moderate to low temperatures, low salinity, and low density, whereas those of the pyrite-bearing carbonate vein-type gold deposits feature moderate to low temperatures, moderate salinity, and low density. The ore-forming fluids and materials were derived from the mantle and mixed with crustal materials in the early stage, mingled with formation water and some meteoric water participating in the late stage. Compared to the gold deposits in the basement uplift zone of Jiaodong, the ore-forming fluids of the gold deposits on the northeastern margin of the Jiaolai Basin were mixed with more formation water, exhibiting a certain basin affinity.

(iii) During the Late Mesozoic, the subduction of the Pacific Plate and the destruction of the North China Craton led to significant tectono-magmatic activity in Jiaodong. Consequently, a thermal uplifting-extension tectonic system was formed on the northeastern margin of the Jiaolai Basin, creating favorable conditions for the formation of gold deposits. During the Early Cretaceous, asthenospheric upwelling occurred. The resulting fluids, after metasomatizing the enriched mantle, differentiated and evolved into the C-H-O ore-bearing fluids. Subsequently, the ore-bearing fluids were mixed with crustal fluids as they ascended. Then, they were mingled with formation water and some meteoric water in the shallow crust, forming multi-source mixed fluids. Due to differences in the mixed crustal components or those in the surrounding rocks involved in water-rock reactions, alkaline and acidic ore-forming fluids were formed. These multi-source mixed fluids with different properties, after migrating to the basin-margin detachment fault system, were unloaded and experienced mineralization.

CRediT authorship contribution statement

Zheng-jiang Ding, Jun Deng and Feng-yue Sun conceived of the presented idea. Jun-wei Bo and Zheng-jiang Ding wrote the manuscript in consulation. Jun-wei Bo processed the data and drew all the figures. Jun-wei Bo, Zheng-jiang Ding, Feng-yue Sun, and Kun-feng Qiu participated in field investigation. Jun Deng and Ming-chun Song reviewed the draft. All authors discussed the results and contributed to the final manuscript.

Declaration of competing interest

The authors declare no conflicts of interest.

Acknowledgment

This study was supported by the Program of the National Natural Science Foundation of China (Nos. 41973048, U2006201), the Open Project of State Key Laboratory of Geological Processes and Mineral Resources (No. GPMR202203), the Key R&D Program of Shandong Province (No. 2023CXGC011001), the Taishan Scholars. Program (tstp20240847), and the Open Project of Shandong Engineering Research Center of Application and Development of Big Data for Deep Gold Exploration (No. SDK202207). The authors would like to extend their sincere gratitude to the reviewers of this manuscript for their valuable comments.

References

An W, Kuang HW, Liu YQ, Peng N, Xu KM, Xu H, Zhang P, Wang KB, Chen SQ, Zhang YX. 2016. Detrital zircon dating and tracing the provenances of dinosaur bone beds from the late Cretaceous Wangshi Group in Zhucheng, Shandong. Geological Review, 62(2), 453–471 (in Chinese with English abstract). doi: 10.16509/j.georeview.2016.02.017.

Bo JW, Ding ZJ, Song MC, Qiu KF, Sun FY, Ji P, Xu H, Zhang R. 2021. C, O, S and Pb isotopic compositions and genesis of the Liaoshang gold deposit in Jiaodong Peninsula. Acta Petrologica et Mineralogica, 40(2), 321–336 (in Chinese with English abstract).

Cai YC, Fan HR, Santosh M, Hu FF, Yang KF. 2018. Decratonic gold mineralization: Evidence from the Shangzhuang gold deposit, eastern North China Craton. Gondwana Research, 54, 1–22. doi: 10.1016/j.gr.2017.09.009.

Chai P, Hou ZQ, Zhang ZY. 2017. Geology, fluid inclusion and stable isotope constraints on the fluid evolution and resource potential of the Xiadian Gold Deposit, Jiaodong Peninsula. Resource Geology, 67(3), 341–359. doi: 10.1111/rge.12134.

Chen CX. 2015. Study on the geological characteristics and ore genesis of Tudui-Shawang gold deposit, Guocheng City, Shandong Province. Changchun, Jilin University, Master thesis, 1–86 (in Chinese with English abstract).

Chen GJ, Sun FY, Li YC, Liu K. 2014. U-Pb dating, geochemical characteristics and geological significance of Guojialing grandiorite in Jiaodong Peninsula. Global Geology, 33(1), 39–47 (in Chinese with English abstract). doi: 10.3969/j.issn.1004-5589.2014.01.004.

Chen JF, Xie Z, Li HM, Zhang XD, Zhou TX, Park YS, Ahn KS, Chen DG, Zhang X. 2003. U-Pb zircon ages for a collision-related K-rich complex at Shidao in the Sulu ultrahigh pressure terrane, China. Geochemical Journal, 37(1), 35–46. doi: 10.2343/geochemj.37.35.

Chen JZ, Jiang N. 2011. Petrogenesis of the Late-Triassic alkaline magmatism in the Jiaodong area: Evidence from U-Pb age, Hf-O isotopes of zircons. Acta Petrologica Sinica, 27(12), 3557–3574 (in Chinese with English abstract).

Chen Y. 2015. The geological characteristics and genesis research of Songjiagou gold deposit, Muping, Shandong Province. Changchun, Jilin University, Master thesis, 1–88 (in Chinese with English abstract).

Chen YJ, Franco P, Lai Y, Li C. 2004. Metallogenic time and tectonic setting of the Jiaodong gold province, eastern China. Acta Petrologica Sinica, 20(4), 907–922 (in Chinese with English abstract).

Chu H, Lu SN, Wang HC, Xiang ZQ, Liu H. 2011. U-Pb age spectrum of detrital zircons from the Fuzikuang Formation, Penglai Group in Changdao, Shandong Province. Acta Petrologica Sinica, 27(4),

1017–1028 (in Chinese with English abstract).

Deines P, Gold DP. 1973. The isotopic composition of carbonatite and kimberlite carbonates and their bearing on the isotopic composition of deep seated carbon. Geochimica et Cosmochimica Acta, 37(7), 1709–1733. doi: 10.1016/0016-7037(73)90158-0.

Deng J, Wang CM, Bages L, Carranza EJM. 2015a. Cretaceous-Cenozoic tectonic history of the Jiaojia Fault and gold mineralization in the Jiaodong Peninsula, China: Constraints from zircon U-Pb, illite K-Ar, and apatite fission track thermochronometry. Miner Deposita, 50, 987–1006. doi: 10.1007/s00126-015-0584-1.

Deng J, Liu XF, Wang QF, Pan RG. 2015b. Origin of the Jiaodong-type Xinli gold deposit, Jiaodong Peninsula, China: Constraints from fluid inclusion and C-D-O-S-Sr isotope compositions. Ore Geology Reviews, 65, 674–686. doi: 10.1016/j.oregeorev.2014.04.018.

Deng J, Wang CM, Bages L, Santosh M, Yao EY. 2018. Crustal architecture and metallogenesis in the south-eastern North China Craton. Earth-Science Reviews, 182, 251–272. doi: 10.1016/j.earscirev.2018.05.001.

Deng J, Yang LQ, Li RH, Groves DI, Santosh M, Wang ZL, Sai SX, Wang SR. 2019. Regional structural control on the distribution of world-class gold deposits: An overview from the Giant Jiaodong Gold Province, China. Geological Journal, 54(1), 378–391. doi: 10.1002/gj.3186.

Deng J, Qiu KF, Wang QF, Goldfarb R, Yang LQ, Zi JW, Geng JZ, Ma Y. 2020a. In situ dating of hydrothermal monazite and implications for the geodynamic controls on ore formation in the Jiaodong Gold Province, Eastern China. Economic Geology, 115(3), 671–685. doi: 10.5382/econgeo.4711.

Deng J, Yang LQ, Groves DI, Zhang L, Wang QF. 2020b. An integrated mineral system model for the gold deposits of the giant Jiaodong province, eastern China. Earth-Science Reviews, 208(2), 1–24. doi: 10.1016/j.earscirev.2020.103274.

Deng J, Wang QF, Santosh M, Liu XF, Liang YY, Yang LQ, Zhao R, Yang L. 2020c. Remobilization of metasomatized mantle lithosphere: A new model for the Jiaodong gold province, eastern China. Mineralium Deposita, 55(2), 257–274. doi: 10.1007/s00126-019-00925-0.

Deng J, Wang QF, Zhang L, Xue SC, Liu XF, Yang L, Yang LQ, Qiu KF, Liang YY. 2023. Metallogenetic model of Jiaodong-type gold deposits, eastern China. Science China Earth Sciences, 66(10), 2287–2310. doi: 10.1007/s11430-022-1136-4.

Deng JF, Su SG, Zhao HL, Mo XX, Xiao QH, Zhou S, Liu C, Zhao CG. 2003. Deep processes of Mesozoic Yanshanian lithosphere thinning in north China. Earth Science Frontiers, 10(3), 41–50 (in Chinese with English abstract).

Deng YH, Hu QH, Xu HQ, Yan YK, Qian MP. 1984. Study on Penglai Group and Fenzishan Group in eastern Shandong Province. Bulletin Nanjing Institute Geology Mineral Resources, Chinese Academy Geology Sciences, 5(2), 1–80 (in Chinese).

Ding ZJ, Sun FY, Liu FL, Liu JH, Liu DH, Zhang PJ, Du SX, Li B. 2013. U-Pb dating of zircons from the Weideshan molybdenum copper polymetallic deposits in Jiaodong Peninsula, China, and its geological significance. Acta Petrologica Sinica, 29(2), 607–618 (in Chinese with English abstract).

Ding ZJ, Sun FY, Liu FL, Liu JH, Peng QM, Ji P, Li BL, Zhang PJ. 2015. Mesozoic geodynamic evolution and metallogenic series of major metal deposits in Jiaodong Peninsula, China. Acta Petrologica Sinica, 31(10), 3045–3080 (in Chinese with English abstract).

Ding ZJ, Bo JW, Song MC, Wei XF, Li Y, Li GH. 2019. Rb-Sr and Sm-Nd isotopic ages and their geological significance for the pyrite carbonate vein type gold deposit in Guocheng gold deposit, Jiaodong Peninsula, China. Kunming, Proceedings of the 2019 Annual Conference, Geological Society of China, 880 (in Chinese).

Ding ZJ, Song MC, Deng J, Qiu KF, Chen J, Bo JW. 2021. Geological characteristics and Rb-Sr and Sm-Nd isotopic chronology of a new type of gold deposit: the Liaoshang pyrite carbonate vein type gold deposit in Jiaodong Peninsula, China. Hefei, Proceedings of the first National Mineral Exploration Conference of China, Topic 8, Gold mineralization models and exploration techniques, 15–16 (in Chinese).

Ding ZJ, Sun FY, Bo JW. 2022. Gold deposits in the northeastern margin of the Jiaolai Basin, Shandong Province. Beijing, Geological Publishing House, 1–156 (in Chinese).

Dong LL, Yang ZM, Liu YH, Song MC. 2023. Possible source of Au in the Jiaodong area from lower crustal sulfide cumulates: Evidence from oxygen states and chalcophile elements contents of Mesozoic magmatic suites. Ore Geology Reviews, 153, 1–16. doi: 10.1016/j.oregeorev.2022.105268.

Duan LA, Zhao MC, Wang ZJ. 2009. Metallogenic regularities and prospecting analysis of Xilaokou ore area in Rushan. Gold Science and Technology, 17(3), 31–34 (in Chinese with English abstract).

Duan LA, Guo YC, Han XM, Wang JT, Zhao PF, Wang LP, Wei YF. 2021. New understanding guiding the discovery of a medium-scale tectonic altered rock type gold deposit on the northeastern margin of Jiaolai Basin, Shandong Province, China. China Geology, 4(3), 1–3. doi: 10.31035/cg2021050.

Dunai TJ, Porcelli D. 2002. Storage and transport of noble gases in the subcontinental lithosphere. Reviews in Mineralogy and Geochemistry, 47(1), 371–409. doi: 10.2138/rmg.2002.47.10.

Fan HR, Zhai MG, Xie YH, Yang JH. 2003. Ore-forming fluids associated with granite-hosted gold mineralization at the Sanshandao deposit, Jiaodong gold province, China. Mineralium Deposita, 38(6), 739–750. doi: 10.1007/s00126-003-0368-x.

Fan HR, Hu FF, Yang JH, Shen K, Zhai MG. 2005. Fluid eveolution and large-scale gold metallogeny during Mesozoic tectonic transition in the eastern Shandong Province. Acta Petrologica Sinica, 21(5), 1317–1328 (in Chinese with English abstract).

Fan HR, Feng K, Li XH, Hu FF, Yang KF. 2016. Mesozoic gold mineralization in the Jiaodong and Korean peninsulas. Acta Petrologica Sinica, 32(10), 3225–3238 (in Chinese with English abstract).

Feng K, Fan HR, Groves DI, Yang KF, Hu FF, Liu X, Cai YC. 2020. Geochronological and sulfur isotopic evidence for the genesis of the post-magmatic, deeply sourced, and anomalously gold-rich Daliuhang orogenic deposit, Jiaodong, China. Mineralium Deposita, 55(2), 293–308. doi: 10.1007/s00126-019-00882-8.

Gao YJ, Zhang YM, Yan PK. 2006. Study of ore-controlling conditions and ore-forming type of Tudui gold deposit in Haiyang Shandong. Journal of Liaoning Institute of Technology, 26(4), 239–242 (in Chinese with English abstract). doi: 10.15916/j.issn1674-3261.2006.04.009.

Geng K, Wang RJ, Li HK, Liang TT, Zhang YB. 2016. Zircon SHRIMP U-Pb geochronology of Congjia granodiorite from northwest Jiaodong area. Acta Geoscientica Sinica, 37(1), 90–100 (in Chinese with English abstract). doi: 10.3975/cagsb.2016.01.09.

Geng K, Li DP, Hu BQ, Yan JY, Zou SY, Zhang Y, Wei PF, Liu Q, Cai N, Zhang C. 2020. 110 Ma hornblende gabbro dyke in deep part of Xilaokou gold deposit, Jiaodong and its constraints on metallogenic time. Mineral Deposits, 39(6), 974–994 (in Chinese with English abstract). doi: 10.16111/j.0258-7106.2020.06.002.

Guo CY. 2009. Tectonic setting, magmatic sequence and fluid of gold metallogenic system of the Sanshandao-Cangshang fault in Jiaodong, China. Beijing, China University of Geosciences, Ph. D. thesis, 1–196 (in Chinese with English abstract).

Guo JH, Chen FK, Zhang XM, Siebel W, Zhai MG. 2005. Evolution of syn- to post-collisional magmatism from north Sulu UHP belt, eastern China: Zircon U-Pb geochronology. Acta Petrologica Sinica, 21(4), 1281–1301 (in Chinese with English abstract).

Guo LN, Deng J, Yang LQ, Wang ZL, Wang SR, Wei JH, Chen BH. 2020. Gold deposition and resource potential of the Linglong gold deposit, Jiaodong Peninsula: Geochemical comparison of ore fluids. Ore Geology Reviews, 120, 1–17. doi: 10.1016/j.oregeorev.2020.103434.

Han XM, Guo YC, Duan LA, Wang JT, Zhao PF, Wang LP, Yu GM. 2023. S and Pb isotopic compositions of the Qianchuiliu gold deposit on the north-eastern margin of the Jiaolai basin: implication on the source of ore-forming material. Bulletin of Geological Science and Technology, 42(3), 210–221 (in Chinese with English abstract). doi: 10.19509/j.cnki.dzkq.tb20220659.

He DY, Qiu KF, Yu HC, Huang YQ, Ding ZJ, Shen Y. 2020. Petrogenesis of the early Cretaceous trachy-dacite from Mashan in the Jiaolai basin, North China Craton. Acta Petrologica Sinica, 36(12), 3705–3720 (in Chinese with English abstract). doi: 10.18654/1000-0569/2020.12.09.

Hou ML, Jiang SY, Jiang YH, Ling HF. 2006. S-Pb isotope geochemistry and Rb-Sr geochronology of the Penglai gold field in the eastern Shandong province. Acta Petrologica Sinica, 22(10), 2525–2533 (in Chinese with English abstract).

Hu FF. 2006. Magmatism, ore fluid evolution and gold mineralization of the Kunyushan area in the Jiaodong peninsula during the Mesozoic tectonic regime inversion in eastern China. Beijing, Institute of Geology and Geopgysics, Chinese Academy of Sciences, Ph. D. thesis, 1–183 (in Chinese with English abstract).

Hu FF, Fan HR, Jiang XH, Li XC, Yang KF, Mernagh T. 2013. Fluid inclusions at different depths in the Sanshandao gold deposit, Jiaodong Peninsula, China. Geofluids, 13, 528–541. doi: 10.1111/gfl.12065.

Hoefs J. 1997. Stable Isotope Geochemistry. Berlin, Springer Verlag, 1–260.

Huang DY. 1994. Sulfur isotope studies of the metallogenic series of gold deposits in Jiaodong (eastern Shandong) area. Mineral Deposits, 13(1), 75–87 (in Chinese with English abstract). doi: 10.16111/j.0258-7106.1994.01.008.

Huo TF, Yang DB, Xu WL, Wang F, Liu HB, Shi JP. 2015. U-Pb ages and Hf isotope compositions of detrital zircons from the Sanshandao in the early Cretaceous Wawukuang formation in the Jiaolai basin, Shandong Province and its tectonic implications. Geotectonica et Metallogenia, 39(2), 355–368 (in Chinese with English abstract). doi: 10.16539/j.ddgzyckx.2015.02.015.

Ji P. 2016. On geological characteristics and metallogenesis of Liaoshang gold deposit in Jiaodong Peninsula, Shandong Province. Changchun, Jilin University, Master thesis, 1–86 (in Chinese with English abstract).

Ji P, Ding ZJ, Li GH, Song MC, Qian Y. 2016. Geological characteristics of Liaoshang oversize gold deposit in Jiaodong Peninsula. Shandong Land and Resources, 32(6), 9–13 (in Chinese with English abstract).

Jiang XH, Fan HR, Hu FF, Yang KF, Lan TG, Zheng XL, Jin NX. 2011. Comparative studies on fluid inclusion in different depths and ore genesis of the Sanshandao gold deposit, Jiaodong Peninsula. Acta Petrologica Sinica, 27(5), 1327–1340 (in Chinese with English abstract).

Jiang YH, Du FG, Qing L, Ni CY. 2020. Elemental and multiple isotopic evidences of enriched lithospheric mantle origin of the Xiadian gold deposit in the Jiaodong Peninsula, East China. Ore Geology Reviews, 127, 1–13. doi: 10.1016/j.oregeorev.2020.103824.

Kong XC, Cheng RR, Sun JY, Lu WJ, Lu H. 2022. Zircon U-Pb age, geochemical characteristics and the geological significance of volcanic rocks of Cretaceous Qingshan Group at the Southwest margin of Jiaolai basin. Contributions to Geology and Mineral Resources Research, 37(1), 84–85 (in Chinese with English abstract). doi: 10.6053/j.issn.1001-1412.2022.01.012.

Kuang YS, Pang CJ, Luo ZY, Hong LB, Zhong YT, Qiu HN, Xu YG. 2012. ^{40}Ar-^{39}Ar geochronology and geochemistry of mafic rocks from Qingshan group, Jiaodong area: Implications for the destruction of the North China Craton. Acta Petrologica Sinica, 38(4), 1073–1091 (in Chinese with English abstract).

Li GH, Ding ZJ, Ji P, Li Y, Tang JZ, Liu LS. 2016. Features and prospecting direction of the gold deposits in the northeastern margin of the Jiaolai Basin. Geology and Exploration, 52(6), 1029–1036 (in Chinese with English abstract). doi: 10.13712/j.cnki.dzykt.2016.06.003.

Li GH, Ding ZJ, Song MC, Li JJ, Li XZ, Ji P, Zhang PJ, Wang ZX. 2017. The Liaoshang pyrite-carbonate veined deposit: A new type of gold deposit in Jiaodong peninsula. Acta Geoscientica Sinica, 38(3), 423–429 (in Chinese with English abstract). doi: 10.3975/cagsb.2017.03.12.

Li HK, Li DP, Geng K, Guo BK, Zhuo CY, Liang TT. 2017. The Mesozoic magmaticactivities framework in Jiaodong area: SHRIMP chronology recording of single particle zircon. Acta Geologica Sinica, 91(1), 163–179 (in Chinese with English abstract). doi: 10.19762/j.cnki.dizhixuebao.2017.01.010.

Li HM, Wei JH, Wang Q, Yu HT, Liu GC, Huang XZ. 2010. Isotopic composition features and ore-forming mechanism of the Tudui-Shawang gold deposit in Shandong Province. Acta Geoscientica Sinica, 31(6), 791–802 (in Chinese with English abstract).

Li J. 2012. The study on metallization and metallogenetic model of Mo-Cu-Pb-Zn complex deposits and comparison with gold metallization in Jiaodong area. Chengdu, Chengdu University Technology, PhD thesis, 1–142 (in Chinese with English abstract).

Li J, Zhang LP, Li CY, Jiang MY. 2020. Rb-Sr isochron age of the Guocheng gold deposit in the Jiaodong Peninsula, Shandong. Geology in China, 47(3), 894–895 (in Chinese). doi: 10.12029/gc20200330.

Li J, An MY, Song MC, Wang MY, Ding ZJ, Bao ZY, Wang SS. 2022. Sulfur isotopic composition and its source of Jiadong gold deposit. Geological Bulletin of China, 41(6), 993–1009 (in Chinese with English abstract). doi: 10.12097/j.issn.1671-2552.2022.06.008.

Li JJ, Zhang PP, Li GH, Liu WG, Zhao ZL, Li XZ, Ding ZJ, Fu C, Tang WL, Dang ZC, Tian JP. 2020. Formation of the Liaoshang gold deposit, Jiaodong Peninsula, eastern China: Evidence from geochronology and geochemistry. Geological Journal, 55(8), 5903–5913. doi: 10.1002/gj.3718.

Li MQ, Tang B. 2001. The geologic-geochemical characteristics of the ore-bearing rock series of Pengjiakuang gold deposit in east Shandong. Gold, 22(9), 1–4 (in Chinese with English abstract).

Li SR, Santosh M, Zhang HF, Luo JY, Zhang JQ, Li CL, Song JY, Zhang XB. 2014. Metallogeny in response to lithospheric thinning and craton destruction: Geochemistry and U-Pb zircon chronology of the Yixingzhai gold deposit, central North China Craton. Ore Geology Reviews, 56, 457–471. doi: 10.1016/j.oregeorev.2012.10.008.

Li SX, Liu CC, An YH. 2007. Geology of gold deposits in Jiaodong. Beijing, Geological Publishing House, 1–423 (in Chinese).

Li XF. 2011. The ore genesis and prospecting direction of Jinqingding gold deposit of the Muping-Rushan gold ore belt in Eastern Shandong. Xi'an, Chang'an University, Ph. D. thesis, 1–173 (in Chinese with English abstract).

Li XH, Chen FK, Guo JH, Li QL, Xie LW, Siebel W. 2007. South China provenance of the lower-grade Penglai Group north of the Sulu UHP orogenic belt, eastern China: Evidence from detrital zircon ages and Nd-Hf isotopic composition. Geochemical Journal, 41(1), 21–45. doi: 10.2343/geochemj.41.29.

Li ZL, Yang MZ, Li ZP. 1993. Geological geochemistry of Jiaodong gold deposit. Tianjin, Tianjin Science & Technology Press, 1–300 (in Chinese).

Li ZP. 1992. The genesis of the Rushan gold deposit in east Shandong. Mineral Deposits, 11(2), 165–178 (in Chinese with English abstract). doi: 10.16111/j.0258-7106.1992.02.008.

Liang H, Han ZZ, Wang LG, Tian RC, Wang LM, Wang JH, Zhi YB, Zhang W, Liu HD. 2022. The fluid inclusions, H-O-C-S-Pb isotopic characteristics and genesis of the Liaoshang gold deposit in Jiaodong Peninsula. Geological Bulletin of China, 41(6), 1053–1067 (in Chinese with English abstract). doi: 10.12097/j.issn.1671-2552.2022.06.012.

Ling WL, Xie XJ, Liu XM, Cheng JP. 2006. Zircon U-Pb age and its tectonic implication of Qingshan Group volcanic rock for Mesozoic standard section in eastern Shandong. Science in China (Series D), 36(5), 401–411 (in Chinese).

Liu JC, Wang JY, Liu Y, Tian JX, Li XZ, Zhang HD. 2017. Ore genesis of the Xiadian gold deposit, Jiaodong Peninsula, East China: Information from fluid inclusions and mineralization. Geological Journal, 53(51), 77–95. doi: 10.1002/gj.3042.

Liu JF, Tang ZL, Liu XH, Liu CX, Zhang ZC, Xie L, Zhao ZP. 2011. Test on different occurrence states of gold pyrite and its significance: An example of pyrite from gold mines in the Jiaolai basin. Geology and Exploration, 47(5), 823–827 (in Chinese with English abstract).

Liu JH, Liu FL, Liu PH, Wang F, Ding ZJ. 2011. Polyphase magmatic and metamorphic events from Early Precambrian metamorphic basement in Jiaobei area: Evidence from the zircon U-Pb dating of TTG and granitic gneisses. Acta Petrologica Sinica, 27(4), 943–960 (in Chinese with English abstract).

Liu JM, Liu JJ, Gu XX. 1997. Basin fluids and their related ore deposits. Acta Petrologica et Mineralogica, 16(4), 341–352 (in Chinese with English abstract).

Liu JY, Duan LA. 2006. The north edge of Jiao-Lai basin gold deposit fratures and analysis on ore-prospecting prospect. Gold Science and Technology, 14(2), 30–35 (in Chinese with English abstract).

Liu JY, Liu SL, Gao CX, Dun MX. 2012. Study on geochemical characteristics of Xilaokou gold deposit in Shandong Province. Gold Science and Technology, 20(4), 16–20 (in Chinese with English abstract).

Liu PH, Liu FL, Wang F, Liu JH. 2011a. U-Pb dating of zircons from Al-rich paragneisses of Jingshan Group in Shandong peninsula and its geological significance. Acta Petrologica et Mineralogica, 30(5), 829–843 (in Chinese with English abstract).

Liu PH, Liu FL, Wang F, Liu JH. 2011b. In-situ U-Pb dating of zircons from high-pressure granulites in Shandong Peninsula, Eastern China and its geological significance. Earth Science Frontiers, 18(1), 123–156 (in Chinese with English abstract).

Liu PH, Liu FL, Wang F, Liu JH. 2011c. Genetic characteristcs of the ultramafic rocks from the Early Precambrian high-grade metamorphic basement in Shandong Peninsula, China. Acta Petrologica Sinica, 27(4), 922–942 (in Chinese with English abstract).

Liu XD, Ding ZJ, Song MC, Zhou ML, Xu SH, Yang ZL, Xie TC, Cui T, Song YX, Gao XK, Li RX, Zhang LL, Zhang QB, Wang SS, Wang B. 2022. Geoloy and mineralization of the Dayin'gezhuang supergiant gold deposit (180 t) in the Jiaodong Peninsula, China: A review. China Geology, 5, 1–26. doi: 10.31035/cg2022058.

Liu XH, Sun XL, Zhu DQ. 2002. Elementary analysis of the mineralizing mechanism of the gold deposits in the northeast fringe of Jiaolai basin. Gold, 23(1), 10–13 (in Chinese with English abstract).

Liu Y, Deng J, Wang ZL, Zhang L, Zhang C, Liu XD, Zheng XL, Wang XD. 2014. Zircon U-Pb age, Lu-Hf isotopes and petrogeochemistry of the monzogranites from Xincheng gold deposit, northwestern Jiaodong Peninsula, China. Acta Petrologica Sinica, 30(9), 2559–2573 (in Chinese with English abstract).

Liu YQ, Liu DH, Yu ZC, Yu DB. 2000. Major types and propecting future of gold deposits in northeast Jiaolai basin. Shandong Geology, 16(1), 29–38 (in Chinese with English abstract).

Liu YW, Li HJ. 2002. Interlayer gliding structure and mineralization of Xilaokou gold fild, East Shandong. Gold, 23(10), 1–5 (in Chinese with English abstract).

Luo XD, Yang XY, Duan LA, Sun WD. 2014. Geochemical and geochronological study of the gold-related Guojialing Pluton and Shangzhuang Pluton in Jiaobei block. Acta Geologica Sinica, 88(10), 1874–1888 (in Chinese with English abstract). doi: 10.19762/j.cnki.dizhixuebao.2014.10.008.

Luo ZK, Miao LC. 2002. Granite and gold deposits in Zhaolai area, Jiaodong. Beijing, Metallurgical Industry Press, 1–157 (in Chinese).

Ma L, Jiang SY, Hofmann AW, Dai BZ, Hou ML, Zhao KD, Chen LH, Li JW, Jiang YH. 2014. Lithospheric and asthenospheric sources of lamprophyres in the Jiaodong Peninsula: A consequence of rapid lithospheric thinning beneath the North China Craton? Geochimica et Cosmochimica Acta 124, 250–271. doi: 10.1016/j.gca.2013.09.035.

Mao JW, Li HM, Wang YT, Zhang CQ, Wang RT. 2005. The relationship between mantle-derived fluid and gold ore-formation in the eastern Shandong Peninsula: Evidences from D-O-C-S isotopes. Acta Geologica Sinica, 79(6), 839–857 (in Chinese with English abstract).

Mamyrin BA, Tolstikhin IN. 1984. Helium Isotopes in Nature. Developments in Geochemistry. Amsterdam, Elsevier Science Publishers, 1–248.

Mao JW, Wang YT, Li HM, Franco. 2008. The relationship of mantle-derived fluids to gold metallogenesis in the Jiaodong Peninsula: Evidence from D-O-C-S isotope systematics. Ore Geology Reviews, 33, 361–381. doi: 10.1016/j.oregeorev.2007.01.003.

Men YK, Wang ED, Wu MG, Zhao CF. 2013. The ore-controlling mechanism of lattice structures in Guocheng goldfield of Eastern China. Journal of Northeastern University (Natural Science), 34(6), 880–883 (in Chinese with English abstract).

Meng FC, Li TF, Xue HM, Liu FL, Xu ZQ. 2006. Two serials of basic magmas from different mantle sources of Late Cretaceous in east Shandong procince, China: A comparative study on basalts from Zhucheng and Jiaozhou. Acta Petrologica Sinica, 22(6), 1644–1656 (in Chinese with English abstract).

Qi JJ, Yu BB. 2009. Preliminary analysis types and genesis of typical gold deposit in peripheral of Jiao-Lai basin. Gold Science and Technology, 17(4), 25–30 (in Chinese with English abstract).

Ren TL, Wang LM, Zhu XQ, Yu XW, Yang ZY, Liu HD, Guo RP, Tao YB. 2021. Early Cretaceous Weideshan Period granite in Jiaodong area. Shandong Land and Resources, 37(10), 1–12 (in Chinese with English abstract). doi: 10.12128/j.issn.1672-6979.2021.10.001.

Shen JF, Li SR, Santosh M, Meng K, Dong GC, Wang YJ, Yin N, Ma GG, Yu HJ. 2013. He-Ar isotope geochemistry of iron and gold deposits reveals heterogeneous lithospheric destruction in the North China Craton. Journal of Asian Earth Sciences. 78(15), 237–247. doi: 10.1016/j.jseaes.2013.04.004.

Shen YC, Zeng QD, Liu TB, Li GM, Zhang LC, Zou WL, Yang JZ. 2002. Ore-forming isotope chronology studies on interlayer sliding breccia gold deposits along north margin of Jiaolai basin. Mineral Deposits, 21(s1), 658–661 (in Chinese). doi: 10.16111/j.0258-7106.2002.s1.173.

Shen YK, Guo T, Yang YQ, Chen ZL, Wei CS, Sun HS. 2016. Discovery of biotite monzolite and Ar-Ar thermochronology significance in Linglong gold field. Journal of Geomechanics, 22(3), 778–793 (in Chinese with English abstract).

Shui P. 2019. Study on geological characteristics and genetic mechanism of the Guocheng-Liaoshang gold deposits in northeast margin of the Jiaolai basin. Beijing, China University of Geosciences, Master thesis, 1–88 (in Chinese with English abstract).

Song MC, Yi PH, Cui SX, Xue JX, Zhou ML, Jiang HL, Huang TL, Jiao XM, Wang GP, Cao CG. 2013. Thermal uplifting-extension ore-forming theory and its prospecting significance in Jiaodong gold

deposit. Shandong Land and Resources, 29(7), 1–12 (in Chinese with English abstract).

Song MC, Song YX, Li J, Li SY. 2015. Metallogenic series of gold and nonferrous metal deposits related to Cretaceous granites in eastern Shandong Peninsula, China. Geotectonica et Metallogenia, 39(5), 828–843 (in Chinese with English abstract). doi: 10.13278/j.cnki.jjuese.2017145.

Song MC, Li J, Li SY, Ding ZJ, Tan XF, Zhang ZL, Wang SJ. 2018. Late Mesozoic thermal upwelling-extension structure and its dynamics background in eastern Shandong province. Journal of Jilin University (Earth Science Edition), 48(4), 941–946 (in Chinese with English abstract). doi: 10.13278/j.cnki.jjuese.20170145.

Song MC, Zhou JB, Song YX, Wang B, Li SY, Li J, Wang SS. 2020a. Mesozoic Weideshan granitoid suite and its relationship to large-scale gold mineralization in the Jiaodong Peninsula, China. Geological Journal, 55(8), 5703–5724. doi: 10.1002/gj.3607.

Song MC, Li J, Zhou JB, Song YX, Li SY, Wang B, Ding ZJ, Zhang ZL. 2020b. The discovery and tectonic setting of the Early Cretaceous high-Mg diorites in the Jiaodong Peninsula. Acta Petrologica Sinica, 36(1), 279–296 (in Chinese with English abstract). doi: 10.18654/1000-0569/2020.01.22.

Song MC, Ding ZJ, Zhang JJ, Song YX, Bo JW, Wang YQ, Liu HB, Li SY, Li J, Li RX, Wang B, Liu XD, Zhang LL, Dong LL, Li J, He CY. 2021. Geoloy and mineralization of the Sanshandao supergiant gold deposit (1200 t) in the Jiaodong Peninsula, China: A review. China Geology, 4(4), 686–719. doi: 10.31035/cg2021070.

Song MC, Song YX, Li J, Liu HB, Li J, Dong LL, He CY, Wang RS. 2023. Thermal doming-extension metallogenic system of Jiaodong type gold deposits. Acta Petrologica Sinica, 39(5), 1241–1260 (in Chinese with English abstract). doi: 10.18654/1000-0569/2023.05.02.

Stuart FM, Turner G, Duckworth RC, Fallick AE. 1994. Helium isotopes as tracers of trapped hydrothermal fluids in ocean-floor sulfides. Geology, 22(9), 823–826. doi: 10.1130/0091-7613(1994)022<0823:HIATOT>2.3.CO;2.

Stuart FM, Burnard PG, Taylor RP, Turner G. 1995. Resolving mantle and crustal contributions on ancient hydrothermal fluids: He-Ar isotopes in fluid inclusions from Dae Hwa W-Mo mineralization, South Korea. Geochimica et Cosmochimica Acta, 59(22), 4663–4673. doi: 10.1016/0016-7037(95)00300-2.

Sun FY, Shi ZL, Feng BZ. 1995. Gold ore geology, lithogenesis and metallogenesis related to the differentiaion of mantle-derived C-H-O fluids in Jiaodong peninsula, Eastern China. Changchun, Jilin People's Publishing House, 1–184 (in Chinese).

Sun LW. 2015. The study of the geological characteristics and enrichment regularities of mineralization of Pengjiakuang deposit in Rushan County, Shandong province. Changchun, Jilin University, Master thesis, 1–86 (in Chinese with English abstract).

Sun XL. 2013. Geological characteristics and genesis of the Xilaokou gold deposit in the margin of the Jiaolai basin, Jiaddong Gold Province. Beijing, China University of Geosciences, Ph. D. thesis, 1–168 (in Chinese with English abstract).

Tam PY, Zhao GC, Liu FL, Zhou XW, Sun M, Li SZ. 2011. Timing of metamorphism in the Paleoproterozoic Jiao-Liao-Ji Belt: New SHRIMP U-Pb zircon dating of granulites, gneisses and marbles of the Jiaobei massif in the North China Craton. Gondwana Research, 19(1), 150–162. doi: 10.1016/j.gr.2010.05.007.

Tan J, Wei JH, Guo LL, Zhang KQ, Yao CL, Lu JP, Li HM. 2008. LA-ICP-MS zircon U-Pb dating and phenocryst EPMA of dikes, Guocheng, Jiaodong Peninsula: Implications for North China Craton lithosphere evolution. Science in China Series D: Earth Sciences, 51(10), 1483–1500. doi: 10.1007/s11430-008-0079-3.

Tan J. 2009. Magmatic evolution process of dikes in Guocheng fault zone, Jiaodong peninsula: Implications for North China craton lithosphere thinning and gold ore formation. Wuhan, China University of Geosciences, Ph. D. thesis, 1–138 (in Chinese with English abstract).

Tan J, Wei J H, Audeta A, Pettke T. 2012. Source of metals in the Guocheng gold deposit, Jiaodong Peninsula, North China Craton: Link to early Cretaceous mafic magmatism originating from Paleoproterozoic metasomatized lithospheric mantle. Ore Geology Reviews, 48, 70–87. doi: 10.1016/j.oregeorev.2012.02.008.

Tan J, Wei JH, Li YJ, Fu LB, Li HM, Shi WJ, Tian N. 2015. Origin and geodynamic significance of fault-hosted massive sulfide gold deposits from the Guocheng-Liaoshang metallogenic belt, eastern Jiaodong Peninsula: Rb-Sr dating, and H-O-S-Pb isotopic constraints. Ore Geology Reviews, 65, 687–700. doi: 10.1016/j.oregeorev.2014.06.007.

Tan J, Wei JH, He HY, Su F, Li YJ, Fu LB, Zhao SQ, Xiao GL, Zhang F, Xu JF, Liu Y, Stuart FM, Zhu RX. 2018. Noble gases in pyrites from the Guocheng-Liaoshang gold belt in the Jiaodong province: For a mantle source of gold. Chemical Geology, 480, 105–115. doi: 10.1016/j.chemgeo.2017.09.027.

Tang J, Zheng YF, Wu YB, Zha XP, Zhou JB. 2004. Zircon U-Pb ages and oxygen isotope of high-grade metamorphic rocks in the eastern part of the Shandong Peninsula. Acta Petrologica Sinica, 20(5), 1039–1062 (in Chinese with English abstract).

Wan YS, Song B, Liu D Y, Simon A Wilde, Wu J S, Shi Y R, Yin X Y, Zhou HY. 2006. SHRIMP U-Pb zircon geochronology of Palaeoproterozoic metasedimentary rocks in the North China Craton: Eidence for a major Late Palaeoproterozoic tectonothermal event. Precambrian Research, 149(3–4), 249–271. doi: 10.1016/j.precamres.2006.06.006.

Wang B, Song MC, Huo G, Zhou ML, Xu ZH, Jiang L, Song YX, Li J. 2021. Source characteristics and tectonic evolution of Late Mesozoic granites in Jiaodong and their implications of gold mineralization. Acta Petrologica et Mineralogica, 40(2), 288–320 (in Chinese with English abstract).

Wang CM, Deng J, Santosh M, Carranza EJM, Gong QJ, Guo CY, Xia R, Lai XR. 2015. Timing, tectonic implications and genesis of gold mineralization in the Xincheng gold deposit, China: C-H-O isotopes, pyrite Rb-Sr and zircon fission track thermochronometry. Ore Geology Reviews, 2015, 65,659–673. doi: 10.1016/j.oregeorev.2014.04.022.

Wang DR, Wang L, Chen Y. 2015. Study on fluid inclusions of Songjiagou gold deposit in Muping, Shandong province. Gold, 36(5), 21–26 (in Chinese with English abstract). doi: 10.11792/hj20150506.

Wang HC, Xiang ZQ, Ren YW, Kang JL, Chu H, Wang Z, Teng F, Tong X. 2022. The northern margin of the Yangtze Craton or the southeastern margin of the North China Craton: New insights on the tectonic attribution of Neoproterozoic granitic gneisses in Jiaodong Peninsula. Acta Geologica Sinica, 96(9), 3012–3033 (in Chinese with English abstract). doi: 10.19762/j.cnki.dizhixuebao.2022167.

Wang LM, Ren TL, Liu HD, Ning ZG, Yu XW, Guo RP, Hou JH, Zhu XQ. 2021. Division of mesozoic granites in Jiaodong area. Shandong Land and Resources, 37(8), 1–14 (in Chinese with English abstract). doi: 10.12128/j.issn.1672-6979.2021.08.001.

Wang M, Sun FY, Wang L, Chen CX, Wang XY. 2016. Study on ore-forming fluid inclusions of Tudui gold deposit in Haiyang, Shandong. Gold, 37(6), 24–30 (in Chinese with English abstract). doi: 10.11792/hj20160606.

Wang QF, Yang L, Zhao HS, Groves DI, Weng WJ, Xue SC, Li HJ, Dong CY, Yang LQ, Li DP, Deng J. 2022. Towards a universal model for orogenic gold systems: A perspective based on Chinese examples with geodynamic, temporal, and deposit-scale structural and geochemical diversity. Earth-Science Reviews, 224, 1–31. doi: 10.1016/j.earscirev.2021.103861.

Wang SJ, Wang LM, Wan YS, Zhang CJ, Song ZY, Wang JG. 2009. Study on intrusive rocks forming period and stages division in Ludong area. Shandong Land and Resources, 25(12), 8–20,25 (in Chinese with English abstract).

Wang SJ, Wan YS, Wang W, Song ZY, Wang JG, Dong CY, Xie HQ,

Liu QD. 2010. Forming ages of granites in Laoshan area of Shandong province: Zircon SHRIMP U-Pb dating. Shandong Land and Resources, 26(10), 1–5,10 (in Chinese with English abstract).

Wang YW, Zhu FS, Gong RT. 2002. Tectonic isotope geochemistry: Further study on Sulphur isotope of Jiaodong gold concentration area. Gold, 23(4), 1–16 (in Chinese with English abstract).

Wang ZC, Cheng H, Zong K, Geng X, Liu Y, Yang J, Wu F, Becker H, Foley S, Wang CY. 2020. Metasomatized lithospheric mantle for Mesozoic giant gold deposits in the North China Craton. Geology, 48(2), 169–173. doi: 10.1130/G46662.1.

Wang ZC, Xu Z, Cheng H, Zou Y, Guo JH, Liu YH, Yang JH, Zong KQ, Xiong L, Hu Z. 2021. Precambrian metamorphic crustal basement cannot provide much gold to form giant gold deposits in the Jiaodong Peninsula, China. Precambrian Research, 354, 1–10. doi: 10.1016/j.precamres.2020.106045.

Wang ZJ, He YH. 2009. The analysis of geological characteristics and metallogenic potential of Xilaokou gold deposit. Gold Science and Technology, 17(1), 29–33 (in Chinese with English abstract).

Wang ZX, Jiao XM, Ding ZJ, Liu XM, Li GH, Ji XB, Tang JZ. 2017. Feature of ore-controlling structure and prospecting direction for the Liaoshang-type gold deposit in the northeast margin of Jiaolai basin, Shandong Province. Gold Science and Technology, 25(3), 61–69 (in Chinese with English abstract). doi: 10.11872/j.issn.1005-2518.2017.03.061.

Wei YJ, Yang LQ, Feng JQ, Wang H, Lv GY, Li WC, Liu SG. 2019. Ore-fluid evolution of the Sizhuang orogenic gold deposit, Jiaodong Peninsula, China. Minerals, 9(3), 1–20. doi: 10.3390/min9030190.

Wen BJ, Fan HR, Hu FF, Liu X, Yang KF, Sun ZF, Sun ZF. 2016. Fluid evolution and ore genesis of the giant Sanshandao gold deposit, Jiaodong gold Province, China: Constrains from geology, fluid inclusions and H-O-S-He-Ar isotopic compositions. Journal of Geochemical Exploration, 171, 96–112. doi: 10.1016/j.gexplo.2016.01.007.

Wu FY, Ge WC, Sun DY, Guo CL. 2003. Discussions on the lithospheric thinning in eastern China. Earth Science Frontiers, 10(3), 51–60 (in Chinese with English abstract).

Xie SW, Wu YB, Zhang ZM, Qin YC, Liu XC, Wang H, Qin ZW, Liu Q, Yang SH. 2012. U-Pb ages and trace elements of detrital zircons from Early Cretaceous sedimentary rocks in the Jiaolai Basin, north margin of the Sulu UHP terrane: Provenances and tectonic implications. Lithos, 154, 346–360. doi: 10.1016/j.lithos.2012.08.002.

Xiong L, Zhao XF, Wei JH, Jin XY, Fu LB, Lin ZW. 2020. Linking Mesozoic lode gold deposits to metal-fertilized lower continental crust in the North China Craton: Evidence from Pb isotope systematics. Chemical Geology, 533, 1–17. doi: 10.1016/j.chemgeo.2019.119440.

Xu WL, Wang QH, Wang DY, Pei FP, Gao S. 2004. Processes and mechanism of Mesozoic lithospheric thinning in eastern North China Craton: Evidence from Mesozoic igneous rocks and deep-seated xenoliths. Earth Science Frontiers, 11(3), 309–317 (in Chinese with English abstract).

Xu YG, Huang XL, Ma ZL, Wang YB, Lizuka Y, Xu JF, Wang Q, Wu XY. 2004. Crust-mantle interaction during the tectono-thermal reactivation of the North China Craton: Constraints from SHRIMP zircon U-Pb chronology and geochemistry of Mesozoic plutons from western Shandong. Contrib Mineral Petrol, 147(6), 750–767. doi: 10.1007/s00410-004-0594-y.

Xu YW, Mao GZ, Geng HY, He TL, Xu QL, Meng YK, Cao MP, Yang FJ, An PR, Song LG, Dou YX, Wang Y, Yu XW, Shen Y. 2023. Ore-forming materials and fluids and ore-conteolling factors of the Liaoshang gold deposit in Jiaodong Peninsula, NE China. Ore Geology Reviews, 154, 105330. doi: 10.1016/j.oregeorev.2023.105330.

Xu ZQ, Liu FL, Qi XX, Zhang ZM, Zeng LS, Liang FH. 2006. Deep subbuction erosion model for continent-continent collision of the Sulu HP-UHP metamorphic terrain. Earth Science, 31(4), 427–436 (in Chinese with English abstract).

Xue JL, Li SR, Sun WY, Zhang YQ, Zhang X, Liu CL. 2013. Helium and argon isotopic composition in fluid inclusions and the source of ore-forming materials of Denggezhuang gold deposit in Jiaodong Peninsula. Journal of Jilin University (Earth Science Edition), 43(2), 400–414 (in Chinese with English abstract). doi: 10.13278/j.cnki.jjuese.2013.02.003.

Yan J, Chen JF, Xie Z, Gao S, Foland KA, Zhang XD, Liu MW. 2005. Studies on petrology and geochemistry of the later Cretaceous basalts and mantle-derived xenoliths from eastern Shandong. Acta Petrologica Sinica, 21(1), 99–112 (in Chinese with English abstract).

Yan J, Chen JF. 2007. Geochemistry of Qingshan formation volcanic rocks from Jiaolai basin, eastern Shandong province: petrogenesis and geological significance. Geochimica, 36(1), 1–10 (in Chinese with English abstract). doi: 10.19700/j.0379-1726.2007.01.001.

Yan YT. 2012. Genetic and prospecting mineralogy studies of quartz-type and altered-type gold deposit in Jiaodong Region. Beijing, China University of Geosciences, Ph. D. thesis, 1–232 (in Chinese with English abstract).

Yang CF. 2010. Mineralization characteristics of gold deposit in the Guocheng region, Haiyang, Shandong province. Geology and Exploration, 46(3), 462–469 (in Chinese with English abstract).

Yang JH, Chung SL, Wilde SA, Wu FY, Chu MF, Lo CH, Fan HR. 2005. Petrogenesis of post-orogenic syenites in the Sulu Orogenic Belt, East China: Geochronological, geochemical and Nd-Sr isotopic evidence. Chemical Geology, 214(1–2), 99–125. doi: 10.1016/j.chemgeo.2004.08.053.

Yang JZ, Shen YC, Liu TB, Zhang LC, Zou WL, Li GM, Zeng QD. 2001. Geological and geochemical characteristics of Pengjiakuang gold deposit, east Shandong. Chinese Journal of Geology, 36(1), 51–63 (in Chinese with English abstract).

Yang LQ, Deng J, Wang ZL, Zhang L, Guo LN, Song MC, Zheng XL. 2014. Mesozoic gold metallogenic system of the Jiaodong gold province, eastern China. Acta Petrological Sinica, 30(9), 2447–2467 (in Chinese with English abstract).

Yang MZ, Lv GX. 1996. The Geology and Geochemistry of Gold Deposits in Jiaodong Greenstone Belt. Beijing, Geological Publishing House, 1–228 (in Chinese).

Yang QY, Santosh M. 2015. Early Cretaceous magma flare-up and its implication on gold mineralization in the Jiaodong Peninsula, China. Ore Geology Reviews, 65(3), 626–642. doi: 10.1016/j.oregeorev.2014.01.004.

Yang Y, Fu WZ, Yu JF, Ning ZG, Cui JJ, Li Q, Zhuo XZ, Chen JP. 2021. Cyclostratigraphical analysis of continental red beds below K/Pg boundary in the Jiaolai basin. Acta Sedimentologica Sinica, 942–952 (in Chinese with English abstract). doi: 10.14027/j.issn.1000-0550.2020.046.

Ying HL. 1994. Isotopic compositions and their geological significance of Jinqingding and Denggezhuang gold depsoits, Jiaodong. Journal of Precious Metallic Geology, 3(3), 201–207 (in Chinese with English abstract). doi: 10.13686/j.cnki.dzyzy.1994.03.06.

Yu XF, Yang DP, Li DP, Shan W, Xiong YX, Chi NJ, Liu PR, Yu LH. 2019. Mineralization charcateristics and geological significance in 3000 m depth of Jiaojia gold metallogenic belt, Jiaodong Peninsula. Acta Petrologica Sinica, 35(9), 2893–2910 (in Chinese with English abstract). doi: 10.18654 /1000-0569/2019.09.18. doi: 10.18654/1000-0569/2019.09.18.

Zartman RE, Doe BR. 1981. Plumbotectonics: The model. Tectonophysics, 75(1–2), 135–162. doi: 10.1016/0040-1951(81)90213-4.

Zeng QD, Shen YC, Liu TB, Zhang LC. 2002. Sulfur and lead isotopic studies of Fayunkuang gold deposit in north-east margin of Jiaolai basin, eastern Shandong. Mineral Deposits, 21(s1), 759–762 (in Chinese). doi: 10.16111/j.0258-7106.2002.s1.199.

Zhai MG, Zhu RX, Liu JM, Meng QR, Hou QL, Hu SB, Li Z, Zhang HF,

Liu W. 2003. Key time limits for the transition of the mesozoic structural system in eastern north China. Science in China (Series D), 33(10), 913–920 (in Chinese).

Zhai MG, Fan HR, Yang JH, Miao LC. 2004. Large-Scale cluster of gold deposits in east Shandong: Anorogenic metallogenesis. Earth Sciences Frontiers, 11(1), 85–98 (in Chinese with English abstract).

Zhang C, Liu Y, Liu XD, Feng JQ, Huang T, Zhang Q, Wang XD. 2014. Characteristics of sulfur isotope geochemistry of the Xincheng gold deposit, Northwest Jiaodong, China. Acta Petrologica Sinica, 30(9), 2495–2506 (in Chinese with English abstract).

Zhang HF, Lu FX, Zhao L, Menzies MA, Mattey DP, Liang SY. 2009. Carbon isotopes in China natural diamonds. Earth Science, 3(1), 37–42 (in Chinese with English abstract).

Zhang HQ, Zhu HL. 2006. Geological features and its prospecting direction of Xilaokou gold deposit in Yushan City, Shandong Province. Gold Science and Technology, 14(6), 24–28 (in Chinese with English abstract).

Zhang L, Weinberg RF, Yang LQ, Groves DI, Sai SX, Matchan E, Phillips D, Kohn BP, Miggins DP, Liu Y, Deng J. 2020. Mesozoic orogenic gold mineralization in the Jiaodong Peninsula, China: A focused event at 120±2 Ma during cooling of pregold granite intrusions. Economic Geology, 115(2), 415–441. doi: 10.5382/econgeo.4716.

Zhang LC, Shen YC, Zeng QD, Zou WL. 2001. Sulfur and lead isotopic geochemistry of gold deposits at the northern margin of Jiaolai basin, east Shandong. Bulletin of Mineralogy, Petrology and Geochemistry, 20(4), 380–384 (in Chinese with English abstract).

Zhang LC, Shen YC, Liu TB, Zeng QD, Li GM, Li HM. 2002a. $^{40}Ar/^{39}Ar$ and Rb-Sr isochron dating of the gold deposits on northern margin of the Jiaolai basin, Shandong, China. Science in China (Series D), 46(7), 708–718.

Zhang LC, Shen YC, Liu TB, Yang JZ, Zou WL, Li HM. 2002b. Sulfur lead, carbon, and oxygen isotope geochemistry of Pengjiakuang gold deposit in Shandong Province. Acta Mineralogica Sinica, 22(3), 255–260 (in Chinese with English abstract). doi: 10.16461/j.cnki.1000-4734.2002.03.012.

Zhang LC, Liu TB, Shen YC, Zeng QD, Li GM. 2003. Structure, Isotopes, and $^{40}Ar/^{39}Ar$ Dating of the Pengjiakuang Gold Deposit, Mesozoic Jiaolai Basin, Eastern China. International Geology Review, 45(8), 691–711. doi: 10.2747/0020-6814.45.8.691.

Zhang LX, Liu PH, Wang YL, Zhou WP, Zhang YJ, Zhang CH. 2021. Depositional timing and provenance characteristics of the Cretaceous Linsishan formation in the Shewopo area, Jiaolai basin: New evidence from detrital zircon U-Pb Dating and REE composition. Earth Science, 46(3), 1119–1132 (in Chinese with English abstract). doi: 10.3799/dqkx.2020.403.

Zhang PJ, Liu DH, Li GH, Ding ZJ, Li Y, Yang GF, Li P. 2015. Gold metallogenic features and prospecting in the margin of the Mesozoic basins, Jiaodong peninsula. Geological Survey and Research, 38(4), 273–283 (in Chinese with English abstract).

Zhang PP, Li JJ, Tian JP, Tang WL, Dang ZC, Fu C, He JT. 2018. Geological and geochemical characteristics of gold deposits in the Guocheng region, Jiaodong. Gold, 39(3), 7–14 (in Chinese with English abstract). doi: 10.11792/hj20180303.

Zhang RZ, Wang ZL, Wang SR, Liu Y, Qin WK. 2016. Metallognic mechanism of Dayingezhuang gold deposit northwestern Jiaodong Peninsula: Geochemistry constrains from the gold bearing pyrite typomorph and sulfur isotope. Acta Petrologica Sinica, 32(8), 2451–2464 (in Chinese with English abstract).

Zhang T, Zhang YQ. 2007. Geochronological sequence of Mesozoic intrusive magmatism in Jiaodong peninsula and its tectonic constraints. Geological Journal of China Universities, 13(2), 323–336 (in Chinese with English abstract). doi: 10.16108/j.issn1006-7493.2007.02.015.

Zhang YQ, Li JL, Zhang T, Yuan JY. 2007. Late Mesozoic kinematic history of the Muping-Jimo fault zone in Jiaodong peninsula, Shandong province, east China. Geological Review, 53(3), 289–300 (in Chinese with English abstract). doi: 10.16509/j.georeview.2007.03.001.

Zhang YQ, Li JL, Zhang T, Dong SW, Yuan JY. 2008. Cretaceous to Paleocene tectono-sedimentary evolution of the Jiaolai basin and the contiguous areas of the Shandong peninsula (North China) and its geodynamic implications. Acta Geologica Sinica, 82(9), 1229–1257 (in Chinese with English abstract).

Zhang YQ, Li SR, Chen HY, Zhang XB, Zhou QF, Cui JC, Song YB, Guo J. 2012. Trace element and He-Ar isotopic evidence of pyrite for the source of ore-forming fluids in the Jinqingding gold deposit, eastern Shandong province. Geology in China, 39(1), 195–204 (in Chinese with English abstract).

Zhang ZC, Liu XH, Liu JF, Fan LQ, Zhang RS, Liu SL. 2012. Characteristics of pyrites in Jiaolai basin gold deposits and its prospecting significance. Gold, 33(12), 14–19 (in Chinese with English abstract).

Zhang ZR, Chen SZ. 1999. Superlarge gold deposit exploration perspective in Jiaolai basin of Jiaodong gold metallogenetic domain. Geochimica, 28(3), 203–212 (in Chinese with English abstract). doi: 10.19700/j.0379-1726.1999.03.001.

Zhao YL, Yang JZ, Shen YC. 2000. The geological and geochemical characteristics of Pengjiakuang gold deposit, Shandong Province. Journal Mineral Petrol, 20(4), 19–24 (in Chinese with English abstract). doi: 10.19719/j.cnki.1001-6872.2000.04.004.

Zhou JB, Han W, Song MC. 2016. The exhumation of the Sulu Terrane and the forming of the Tancheng-Lujiang Fault: Evidence from detrital zircon U-Pb dating of the sediments of the Laiyang Basin, Central China. Acta Petrologica Sinica, 32(4), 1171–1181 (in Chinese with English abstract).

Zhou XH. 2006. Major transformation of subcontinental lithosphere beneath eastern China in the Cenozoic-Mesozoic: Review and prospect. Earth Science Frontiers, 13(2), 50–64 (in Chinese with English abstract).

Zhou XW, Zhao GC, Wei CJ, Geng YS, Sun M. 2008. EPMA U-Th-Pb monazite and SHRIMP U-Pb zircon geochronology of high-pressure politic granulites in the Jiaobei massif of the North China Craton. American Journal of Science, 308(3), 328–350. doi: 10.2475/03.2008.06.

Zhou YQ, Zhou TF, Ma CQ, Zhang ZK, Dong SH, Gu YJ, Yin XC, Li MJ, Liang WD. 2018. Transcrustal magmatic system of early Cretaceous (Qingshan stage) in eastern Shandong and the basin formation related to “thermal upwelling-detachment”. Earth Science, 43(10), 3373–3390 (in Chinese with English abstract). doi: 10.3799/dqkx.2018.998.

Zhu FS. 1980. Preliminary study on mineralization of migmatitization hydrothermal gold deposits: A case study of gold deposits in Zhaoye Area. Geology and Exploration, (7), 1–10 (in Chinese).

Zhu G, Xu JW, Fitches WR, Fletcher CJN. 1994. Isotopic ages of the Penglai Group in the Jiaobei Belt and their geotectonic implications. Acta Geologica Sinica, 68(2), 158–172 (in Chinese with English abstract). doi: 10.19762/j.cnki.dizhixuebao.1994.02.005.

Zou J, Tang WL, Ding ZJ, Bo JW, Li ZQ, Yu S. 2021. Zircon U-Pb dating of the Yuangezhuang pluton in Muping of Shandong Province and its constraints on mineralization of Cu-Mo deposits. Geology in China, 48(3), 883–889 (in Chinese with English abstract). doi: 10.12029/gc20210316.

Zou WL, Yang JZ, Zeng QD, Li GM, Zhang LC. 2010. Geological characteristics and metallogenic geodynamic setting of interlayer-sliding tectonic breccia-type gold deposit in the margin of the Jiaolai basin, Shandong province. Acta Geologica Sinica, 84(4), 508–517 (in Chinese with English abstract). doi: 10.19762/j.cnki.dizhixuebao.2010.04.008.